A Geochemical Model for the Magmatic History of the Carrizozo Basalt Field, South Central New Mexico

by

Kathleen B. Faris

Submitted in Partial Fullfillment
of the Requirements for the Degree of
Master of Science in Geochemistry

New Mexico Institute of Mining and Technology

Socorro, New Mexico

April, 1980

Table of Contents

List of Illustrations

Tables

Figures

Appendices

ABSTRACT

The Carrizozo Basalt Field is associated with the central portion of the Rio Grande rift and consists of three Quaternary flows of subalkaline olivine basalt; in order of decreasing age, these are the Broken Back Crater, lower Carrizozo, and upper Carrizozo Flows. Analyses for 20 trace elements were made using x-ray fluorescence and neutron activation analysis and were combined with previously determined major element analyses to develop a geochemical model for the magmatic history of the field.

Several compositional trends were identified at statistically significant levels. The concentrations of LIL elements decrease with decreasing age of the flows. Significant light REE enrichment relative to chondrites is observed, ranging from 80X in the oldest flow to 60X in the youngest flow. Concentrations of transition metals increase from the Broken Back Crater Flow to the lower Carrizozo Flow and decrease from the lower to the upper Carrizozo flow.

The observed decrease in K_2O concentration with time is inconsistent with a simple differentiation model; concentrations of LIL elements are observed at levels 2-3X higher than can be expected to result from enrichment by fractional crystallization. Several lines of geochemical evidence, supported by geophysical data, suggest that these basalts were derived by 4-6% melting of a spinel peridotite parent which was itself derived from a previous partial

melting episode(s). It is proposed that continuing melting of spinel peridotite at depths of 40-50 km produced a compositionally-zoned magma chamber; successively deeper levels of this chamber, with average compositions representing greater degrees of partial melting, were tapped to produce the three major flows. Up to 5% fractional crystallization of olivine $\pm$ pyroxene seem to be required to account for the decrease in transition metal concentrations from the lower to the upper Carrizozo Flows.

ACKNOWLEDGEMENTS

I would like to thank the members of my thesis committee for their guidance throughout this project. Jacques Renault provided the blend of direction, insight, and thoughtful criticism that made working on this project interesting and enjoyable. Kent Condie offered many suggestions which proved useful in the development of the proposed model. Marc Bodine carefully reviewed the manuscript.

I would also like to thank Ashok Singh for his advice on the statistical evaluation of the data, John Wright for his field assistance, and many student colleagues for helpful discussions along the way.

The New Mexico Bureau of Mines and Mineral Resources provided the financial support for this project.

INTRODUCTION

Purpose and Methods of Investigation

The purpose of this study is to determine the distribution of selected trace elements in the Carrizozo Basalt Field and to evaluate these data, along with previously determined major element data, in order to propose possible geochemical models for the magmatic history of this field. Particular emphasis is placed on suggesting possible sources of these lavas, and the processes which operated to produce them. Relationships between the three major flows of this field are also explored.

Methods of investigation include the determination of trace element concentrations using x-ray fluorescence and neutron activation analysis; the examination of thin sections and aerial photographs; and the use of computer programs to process analytical data, classify basalt samples, and to aid in geochemical modeling studies.

The Rio Grande Rift and its Basaltic Associations

The Carrizozo Basalt Field is associated with the southern portion of the Rio Grande rift (Figure 1) (Chapin and others, 1978). The rift is a tectonic feature which dominates the north-south trending structural elements from

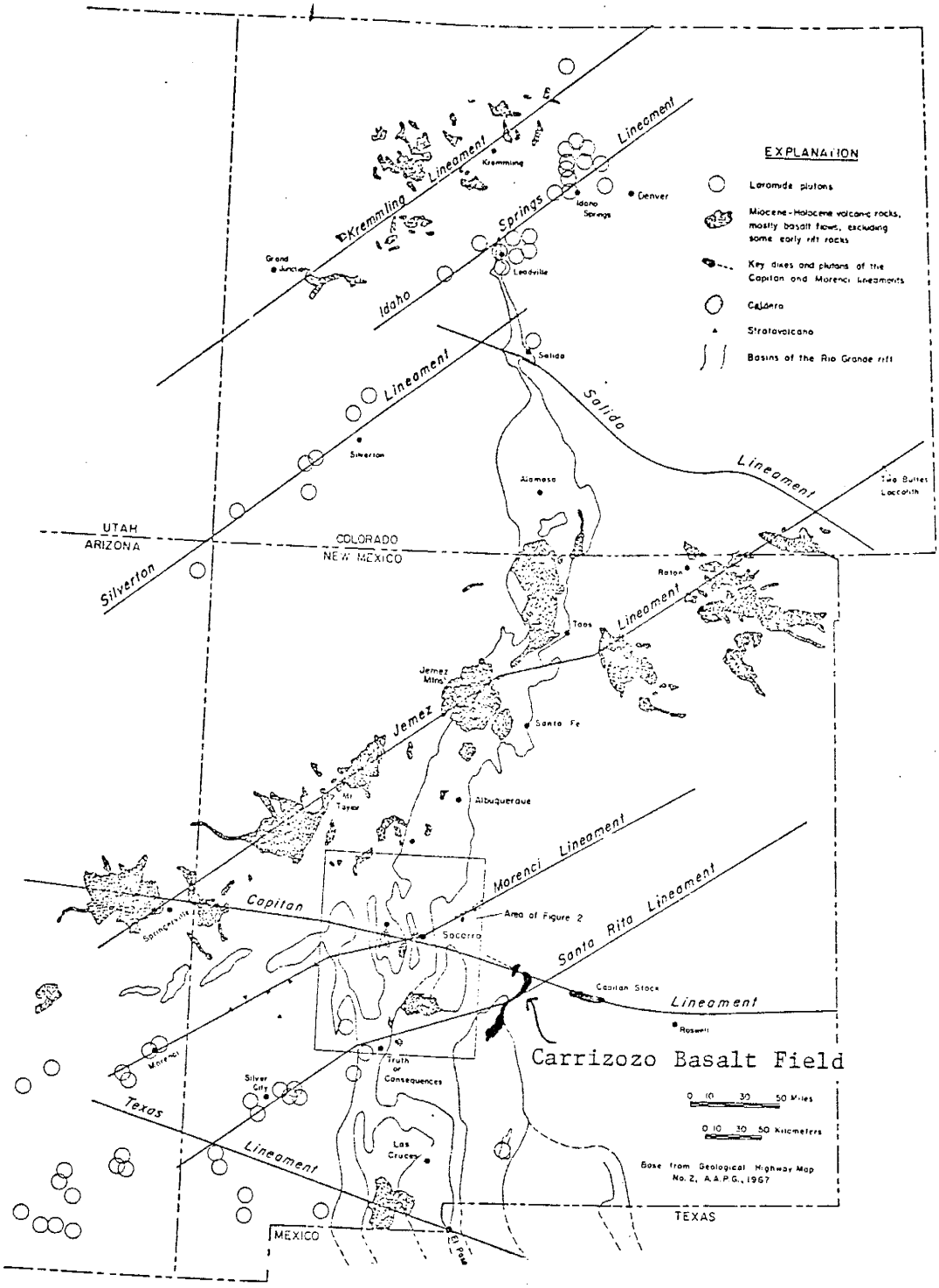

Figure 1. Generalized map of the Rio Grande rift and major crustal lineaments (after Chapin and others, 1978).

central Colorado southward to southern New Mexico (Woodward and others, 1978). It has been characterized as a graben or complex series of grabens with a broad axial structure (Cordell, 1978b) and widens irregularly southward. Extensional strain has been involved, increasing in magnitude southward; extensional faulting along the rift began in the Neogene and continues into Quaternary time (Cordell, 1978a). Relative to adjacent, more stable areas, the Rio Grande rift is a tectonically active, thermally anomalous region (Seager and Morgan, 1979) characterized by:

1) high regionally averaged heat flow values of 2.56 ± 0.65 HFU (Reiter and others, 1979);
2) thinned continental crust (Keller and others, 1978);
3) extensive faulting, recent volcanism (Reiter and others, 1979; Seager and Morgan, 1979).

A summary of field, geophysical, and geochemical information regarding the evolution of the rift is provided by Chapin (1979); the regional geophysical setting of the Rio Grande rift is described by Cordell (1978a). Cook and others (1979) and Seager and Morgan (1979) discuss the evolution of the southern portion of the rift.

The mantle beneath the rift is characterized by high electrical conductivity and p-wave velocities (Cordell, 1978a; Shankland, 1978), geomagnetic (Jiracek and others,

1979) and gravity (Woolard and Joesting, 1964) anomalies. Cordell (1978b), summarizing geophysical data, suggests that heat and mass were supplied convectively by the upper mantle concurrent with crustal extension, and further that anomolously hot or partially melted mantle rock occurs within the upper mantle beneath the rift. Other workers (Schmucker, 1964; Decker and Smithson, 1975; Eaton, 1978; Seager and Morgan, 1979) speculate that these rift characteristics are shallow manifestations of an asthenosphere upwarp or diapiric ridge of mantle material beneath the rift.

There is also geophysical evidence to indicate that shallow magma chambers occur along the Rio Grande rift. Interpretation of magnetotelluric data implies that a zone of melt accumulation exists at a depth of 15 km beneath the north-central rift and at a depth of 27 km beneath the southern rift (Hermance and Pedersen, 1978). A magma body at mid-crustal depths beneath Socorro, NM, has been delineated by Rinehart and others (1979). Reiter and others (1979) suggest that high heat flow values in the southern portion of the rift may be caused by secondary crustal intrusions originating from a primary, deeper source.

Alkali olivine basalts first appeared in the southern portion of the Rio Grande rift 13 m.y. ago, after a 7 m.y. mid-Miocene lull in rift volcanism (Cook and others, 1979) and after 13-15 m.y. of crustal extension (Seager and

Morgan, 1979). Although basalts have formed sporadically during the last 13 m.y., two periods of extensive mafic volcanism in the rift have been identified, one from 13-9 m.y., and another at 5 m.y. (Cook and others, 1979). The first period has been related to weakening and critical stretching of the continental crust, and to thermal activity at depth, such as emplacement of a mantle diapir (Cook and others, 1979) or appearance of an incipient mantle bulge (Seager and Morgan, 1979). Basaltic volcanism at 5 m.y. has been related to a major period of rifting 8-3 m.y. ago (Chapin and Seager, 1975), which was accompanied by an accelerated rate of crustal extension and/or an increase in heat flow and emplacement of shallow magma bodies (Seager and Morgan, 1979).

Much interest in Rio Grande rift basalts has developed within recent years. Aoki and Kudo (1976) and Renault (1978) summarize the major element geochemistry and provide an overview of Rio Grande rift basalts; Baldridge (1979) discusses the petrology and petrogenesis of basaltic lavas of the central Rio Grande rift. Specialized geochemical investigations of basalts from the southern portion of the rift are beginning to ~~to~~ emerge. These include strontium (Stinnett, 1976) and lead (Everson and Silver, 1978) isotopic studies, and studies of mafic inclusions (Padovani, 1978; Reid, 1978; Warren, 1979).

Basalts of the southern rift are relatively undifferentiated (Renault, 1970) and have low $^{87}Sr/^{86}Sr$ ratios (Stinnett, 1976); accidental zenoliths lack evidence for reaction with host magmas (Seager and Morgan, 1979). This information indicates relatively rapid transport of these magmas to the surface, with little or no contamination from crustal materials.

GENERAL ASPECTS OF THE CARRIZOZO BASALT FIELD

Location

The Carrizozo Basalt Field is located in Socorro and Lincoln Counties, south central New Mexico, between north latitudes 33°15′ and 34°00′, and west longitudes 105° 45′ and 106°30′. The following 15-minute quadrangles include portions of the basalt field: Broken Back Crater, Little Black Peak, Chihuahua Ranch, Carrizozo, Capitol Peak, and Three Rivers. Figure 2 shows the location of these quadrangles in New Mexico and the extent of the field within these quadrangles. The "Valley of Fires" New Mexico State Park is located on the eastern edge of the flow, approximately 3.5 miles northwest of the town of Carrizozo, on U.S. 380.

Geologic Setting

Broken Back Crater and Little Black Peak (Figure 3) are the probable vents for the flows of the Carrizozo Basalt Field and lie on a west-northwest axis defined by the linear intrusions of Capitan Mountain and Jones Dike (Renault, 1970). Chapin and others (1978) show that these features, along with some Miocene or younger volcanic rocks, define the Capitan Lineament, which is thought to extend from eastern Arizona to eastern New Mexico (Figure 1).

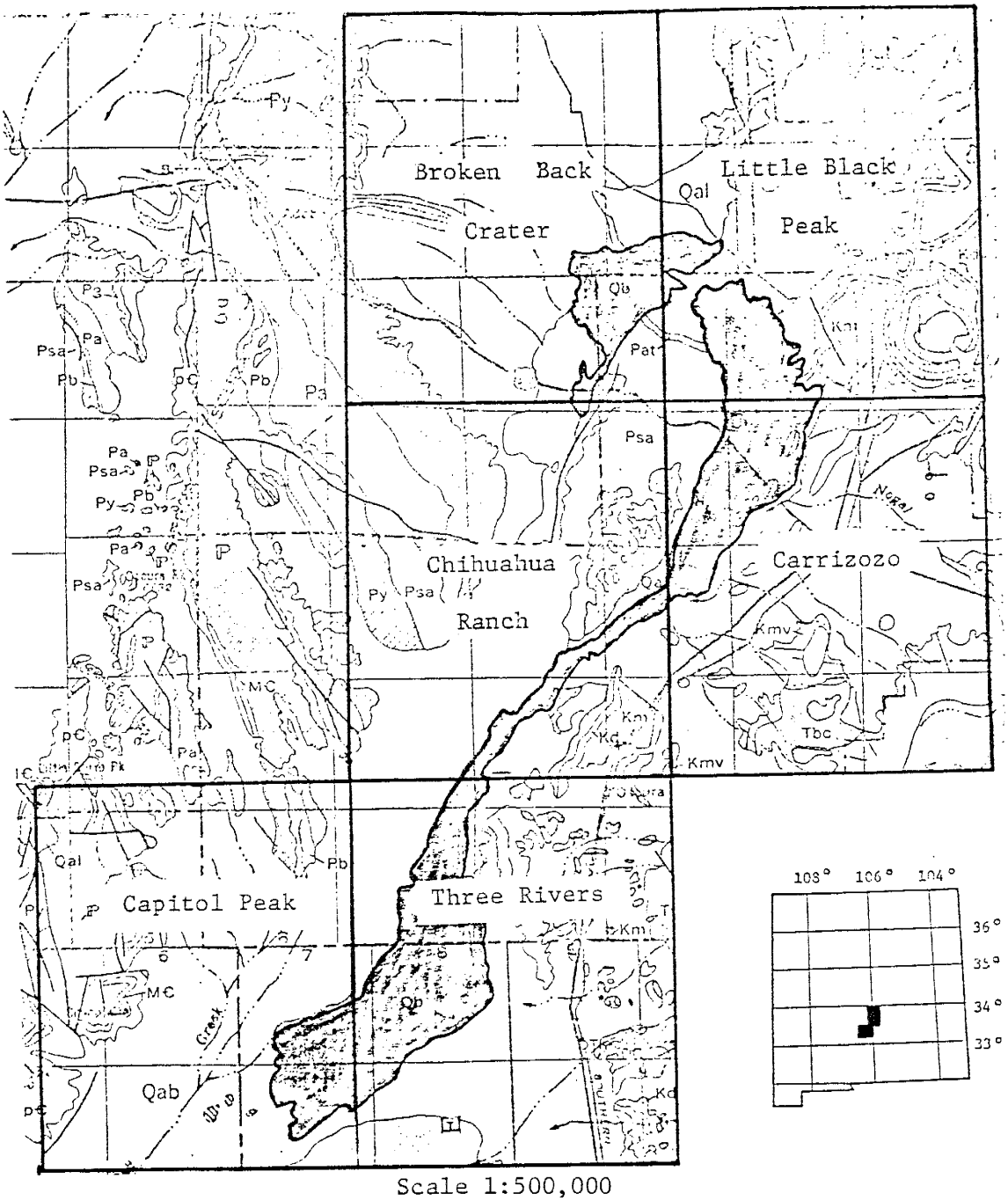

Scale 1:500,000
1 inch equals approximately 8 miles

10 0 10 miles

10 0 10 kilometers

Figure 2. Location of the Carrizozo Basalt Field on the Geologic Map of New Mexico (Dane and Bachman, 1965).

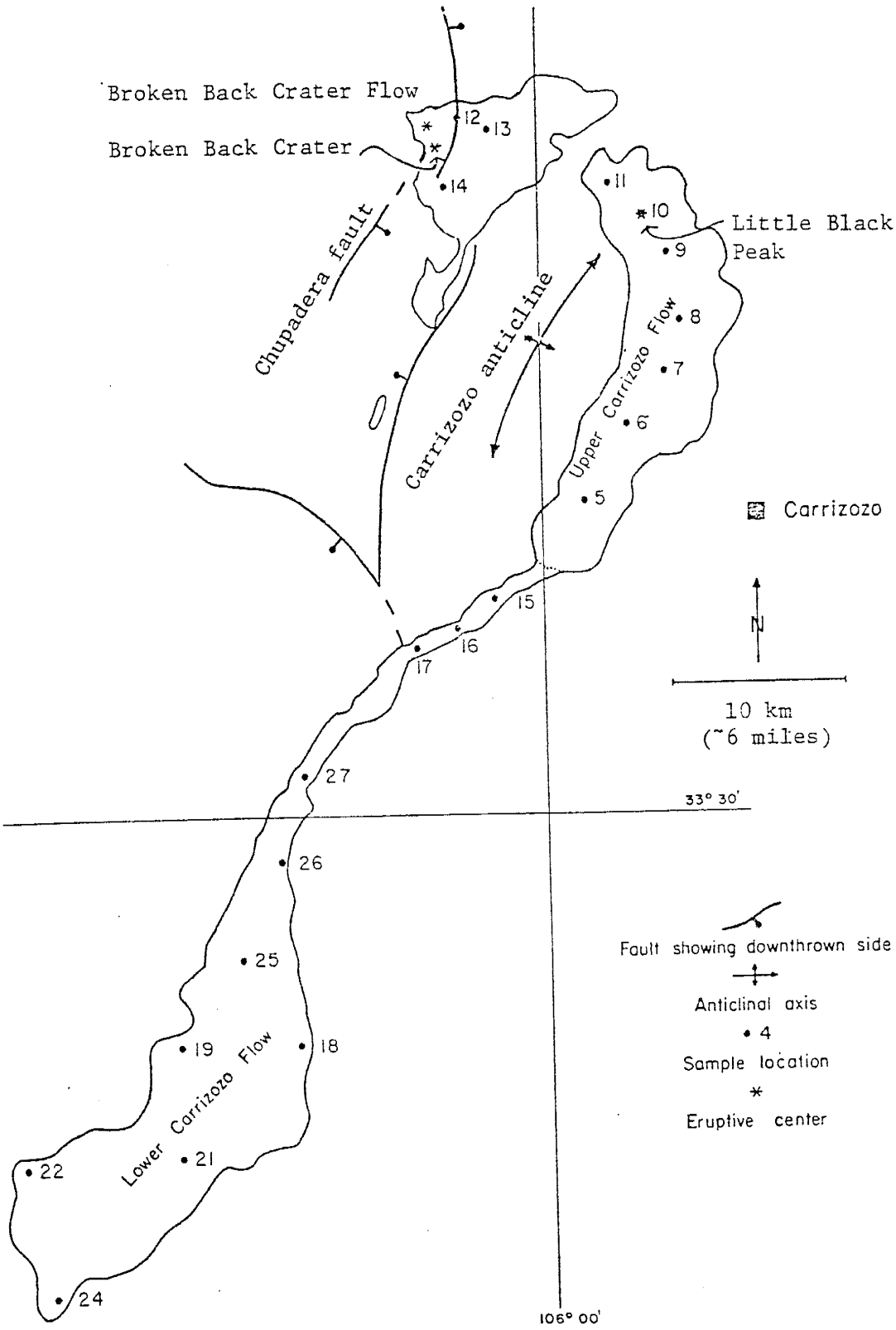

Figure 3. Map of the Carrizozo Basalt Field showing structural features, boundaries of major flows, and sample locations (after Renault, 1970).

Chapin and others (1978) suggest that the Capitan Lineament is a deeply penetrating flaw in the lithosphere that tends to "leak" magma and influence deformation in the brittle near-surface rocks.

The following paragraph regarding the geological setting is a summary provided by Renault (1970). The Broken Back Crater Flow erupted through Permian sediments, and the Carrizozo Flows through Triassic sediments (Dane and Bachman, 1965), on the west flank of a north-south trending basin. A north-northeastward trending normal fault, crossing U.S. 380 in T.6S., R.9E., projects midway between the Broken Back Crater and the Little Black Peak vent areas; it is down to the west (Figure 3). The main trend of the Chupadera fault, down to the east, passes one mile east of the Broken Back Crater vent area; the southernmost branch of the Chupadera fault, also down to the east, projects north-northeastward between the two cinder cones of the Broken Back Crater Flow (Figure 3). Little Black Peak, the probable vent of the Carrizozo Flows, lies near the crest of the Carrizozo anticline defined by Kelley and Thompson (1964) (Figure 3) at the top of Permian beds.

Allen (1951) provided a physical description, including estimates of volume and areal extent, of the Carrizozo Flows. Smith and Budding (1959) published a reconnaissance geologic map of the eastern half of the Little Black Peak quadrangle. Dane and Bachman (1958, 1961)

published preliminary geologic maps of southern New Mexico, including the Carrizozo Basalt Field, and indicated its boundaries on the Geologic Map of New Mexico (1965). The geology of the Carrizozo and Little Black Peak quadrangles was published by Weber (1964) and Smith (1964) respectively.

Stratigraphy

The Carrizozo Basalt Field consists of two informally named, topographically separated basalt fields: the older Broken Back Crater Flow, and the younger Carrizozo Flows (Renault, 1970) (Figure 3). The Carrizozo Flows, also called the Little Black Peak Flow (Smith, 1964) and the Carrizozo Malpais (Weber, 1964), have been subdivided into the lower and upper Carrizozo Flows using chemical criteria (Renault, 1970). Weber (1964) recognized the contact between the upper and lower Carrizozo Flows, exposed in the wall of a karst sinkhole. Although morphological differences between the two flows can be identified in air photos, the lower and upper Carrizozo Flows are generally indistinguishable in the field (Renault, 1970). The Broken Back Crater, lower, and upper Carrizozo Flows contain secondary flow bands which will not be considered further.

The Broken Back Crater Flow

The Broken Back Crater Flow consists of a dense, gray to black, vesicular olivine basalt. It is fine-grained to aphanitic in texture and weathers to a dark brown color. The vesicles are round to ovoid in shape, and range in size from 1 mm to several cm in the longest dimension. They are usually found in sub-parallel orientation and are occasionally filled with light brown weathering products. Olivine phenocrysts are sparse to abundant and measure 1 mm in average diameter; feldspar and pyroxene phenocrysts are not visible in hand specimen.

The Broken Back Crater Flow lies unconformably on the Permian San Andreas Limestone and Bernal Formations, and on the Triassic Santa Rosa Formation. It is topographically separated from the Carrizozo Flows by a valley containing the Triassic sediments (Smith and Budding, 1959). From the flow boundaries indicated by Dane and Bachman (1965), the areal extent of the flow is estimated to be slightly less than 65 sq. km (25 sq. miles). The Broken Back Crater Flow probably issued from a vent marked by two cinder cones at Broken Back Crater (Weber, 1964) (Figure 3). Smith (1964) and Weber (1964) note that the Broken Back Crater Flow is distinctly older than the Carrizozo Flows: the thin soil cover and the weathered surface of the Broken Back Crater Flow is contrasted with the lack of soil and effects of weathering and erosion on the Carrizozo Flows.

Consideration of these geomorphological data have led to late Holocene or Pleistocene age estimates for the Broken Back Crater Flow (Weber, personal communication, 1979; Smith, 1964).

The Carrizozo Flows

The Carrizozo Flows are composed of a dense, gray to black, vesicular olivine basalt, with a fine-grained to aphanitic texture. Vesicles range in size from 0.25 mm to several cm in the longest dimension and are round to ovoid in shape; irregular ovoid-shaped vesicles occur in samples taken from the vicinity of the vent. Vesicles almost always occur in sub-parallel orientation. Olivine phenocrysts are sparse to abundant and measure 1 mm or less in average diameter. Plagioclase laths measuring less than 2 mm in length are seen in some specimens; pyroxene phenocrysts are not visible in hand specimen. The basalt weathers to a gray or light brown color; occasionally vesicles are filled with weathered material.

Weber (1964) observed two major flows totaling approximately 49 m (162 feet) in thickness, exposed in the walls of a sinkhole formed by the solution of the underlying gypsum, 3.2 km (2 miles) south of U.S. 380 and approximately 3.2 km (2 miles) west of the eastern edge of the flows; these represent the lower and upper Carrizozo Flows (Figure 4).

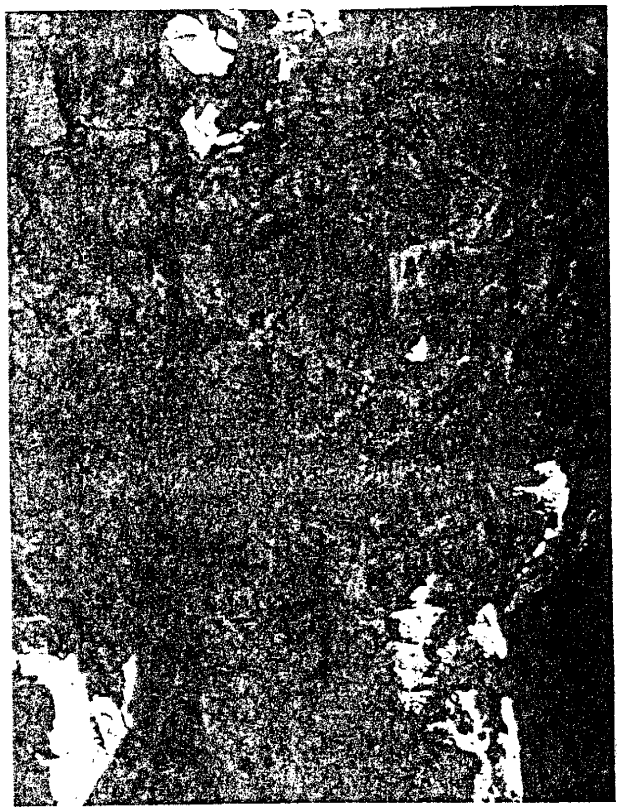

Figure 4. Contact between the upper and lower Carrizozo Flows showing a zone of brecciation.

Weber describes the lower flow as a gray, massive, fine-grained olivine basalt, with a thin, vesicular to scoriaceous zone at the top, and a thickness of approximately 18 m (60 feet). He describes the upper flow as lithologically similiar, but having a thicker vesicular zone at the top; its thickness was measured as approximately 31 m (102 feet).

The uneroded surface of the Carrizozo Flows shows many features characteristic of young, fluidal basalts. These include highly vesicular, ropy flow surfaces (pahoehoe texture) sometimes occurring with a glassy crust; flow bands (Allen, 1951); collapse structures, including lava tunnels (Allen, 1951) and sinkholes (Weber, 1964); pressure domes; and pressure ridges, most prominently developed along the margins of the central portion of the flow (Ulvog and Thompson, 1964). A kipuka (island surrounded by lava) of Dakota Sandstone is found within the boundaries of the "Valley of Fires" State Park. The vegetation growing on the flow is supported by soil blown in by wind, as the basalt has not weathered sufficiently to produce its own soil cover.

The Carrizozo Flows are among the youngest basalt flows in the continental United States: other flows of comparable age include the Craters of the Moon Flow, Idaho; the McKenzie Pass and Bend Flow, Oregon; the Modoc Lava Fields, California; and the McCarty's, Jornado, and Capulin

Mountain Flows, New Mexico (Allen, 1951). Observation of the fresh surficial flow features and the intact conditions of the youngest cinder cone, Little Black Peak, has lead to age estimates of 1000-1500 years (Allen, 1951; Weber, 1964). The effects of weathering and erosion are negligible in both flows.

The Carrizozo Flows were erupted from one or more vents in the vicinity of Little Black Peak at the northern end of the field (Allen, 1951) and flowed in a southwestward direction along the floor of the Tularosa Valley (Ulvog and Thompson, 1964). Weber (1964) provides the following description of the vent area. A cluster of small cinder cones in the vicinity of Little Black Peak marks the vent for the Carrizozo Flows. Little Black Peak, the most prominent of these, is located near the northern edge of the field (Figure 3), stands approximately 26 m (85 feet) high, and contains an intact crater approximately 10 m (32 feet) deep; it probably acted as a vent for the upper Carrizozo Flow, and possibly also for the lower Carrizozo Flow (Renault, 1970). A cinder cone containing a small crater lies at the north-northwestern foot of Little Black Peak, and in addition, remnants of a still older cone lie further to the north and northeast. The flows disconformably mantle Permian (San Andreas Limestone, Bernal Formation), Triassic (Santa Rosa Formation), and Cretaceous (Dakota Sandstone) rocks, Tertiary intrusive rocks, and Quaternary alluvial valley fill (Dane and Bachman, 1965).

Allen (1951) and Weber (1964) provide the following estimates of the extent of these flows:

Length	: 72 km (44 miles)
Average width	: 5 km (3.0 miles)
Width range	: 0.8 to 8 km (0.5 to 5 miles)
Average thickness	: 13 m (42 feet)
Volume of lava	: 4.2 cu. km (1 cu. mile)

Major element data (Renault, 1970) and observation of a contact between the two flows (Weber, 1964) indicate that at least two Recent basalt flows have issued from the Little Black Peak vent area.

Petrography

All of the basalts examined are fresh, porphyritic, olivine basalts. Point counts of constituent phases provide the following estimated modal analyses:

	Ground-mass	Olivine phenocrysts	Plagioclase phenocrysts	Vesicles	Zeolites
upper Carrizozo Flow	74	2	3	20	< 1
lower Carrizozo Flow	76	5	1	17	< 1
Broken Back Crater Flow	78	5	3	14	1

More than 1500 points were counted for each flow (300 points per slide) on slides representing more than half the number of samples of each flow.

The groundmass is composed of plagioclase, olivine, augite, glass, and zeolites; magnetite and ilmenite are finely distributed throughout. Groundmass plagioclase has average compositions of An55 in the Broken Back Crater Flow, An57 in the lower Carrizozo Flow, and An52 in the upper Carrizozo Flow (labradorite), as determined by the Michel-Levy method (Kerr, 1959, p. 257-260). The average length of observed groundmass plagioclase laths is 0.05 mm in the Broken Back Crater Flow, 0.25 mm in the lower Carrizozo Flow, and 0.32 mm in the upper Carrizozo Flow (Figures 5-7). A fluidal texture is displayed in the lower and upper Carrizozo Flows.

Olivine, plagioclase and rare augite phenocrysts are present in all three flows. Olivine phenocrysts are Fa20 in composition (Smith, 1964; Renault, 1970), contain inclusions of magnetite and spinel, and very frequently show embayments and magmatically corroded edges in contact with the groundmass (Figures 5-7); iddingsite rims are occasionally present. Plagioclase phenocrysts have compositions of An62 in the Broken Back Crater Flow, An58 in the lower Carrizozo Flow, and An64 in the upper Carrizozo Flow (labradorite). They are very rare in the lower Carrizozo Flow. A very few plagioclase phenocrysts show zonation and oscillatory extinction; more commonly, plagioclase phenocrysts show corroded edges. Augite occurs primarily in the groundmass, although rare phenocrysts are

Figure 5. Photomicrograph of the Broken Back Crater Flow (25X, crossed-nicols).

A glomeroporphyritic aggregate of olivine phenocrysts shows corrosion and invasion by groundmass material.

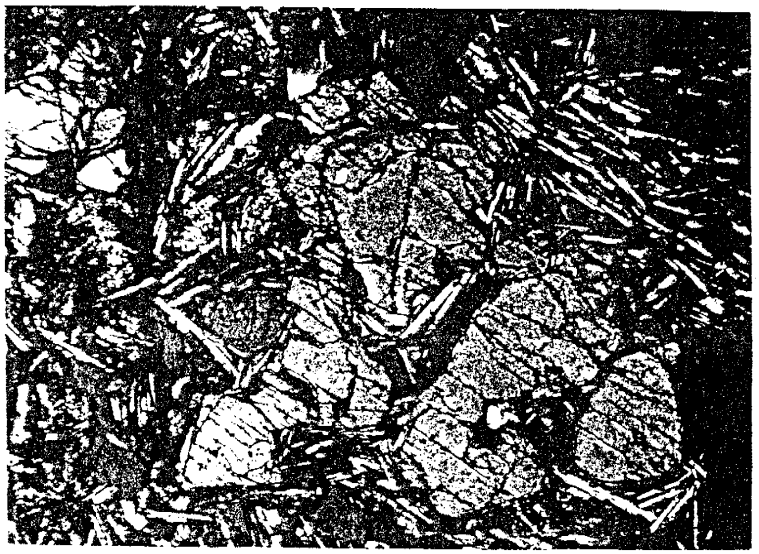

Figure 6. Photomicrograph of the lower Carrizozo Flow (25X, crossed-nicols).

A rounded olivine phenocrysts showing invasion and digestion by groundmass material. Note the presence of vesicular cavities and their control of the arrangement of groundmass components. The groundmass plagioclase laths are 4-5X larger than those in the Broken Back Crater Flow.

Figure 7. Photomicrograph of the upper Carrizozo Flow (25X, crossed-nicols).

A cluster of olivine phenocrysts has been corroded and embayed by the surrounding groundmass. The groundmass plagioclase laths are larger than those in the Broken Back Crater or lower Carrizozo Flows.

observed; it has a brown color in thin section and shows slight pleochroism.

The anorthite content of the groundmass plagioclase increases from the Broken Back Crater to the lower Carrizozo Flows, and decreases from the lower to the upper Carrizozo Flows, as does the whole-rock CaO content in these intervals. The anorthite content of the plagioclase phenocrysts shows an inverse trend.

Zeolites occur as irregularly-shaped amygdules and are most abundant in the Broken Back Crater Flow; their petrogenesis is probably related to deposition by the action of meteoritic waters (Nockolds and others, 1978, p.131). Little devitrification of matrix glass is observed.

Several petrographically observed characteristics of these basalts indicate that the magmas representing the flows of the Carrizozo Basalt Field may have been able to cool slowly in a subsurface chamber prior to eruption. The first is the observed porphyritic texture: relatively large olivine and plagioclase phenocrysts are set in fine-grained groundmass (Figures 5-7). The most common genetic interpretation for this texture is that phenocrysts develop during a period of slow, subsurface cooling; following eruption, rapid cooling and loss of volatiles causes the remaining liquid to solidify as a fine-grained aggregate or glass (Nockolds and others, 978, p. 5).

Secondly, observation of rounded and embayed edges of olivine and plagioclase phenocrysts (Figures 5-7) indicates that a disequilibrium condition between crystals and magma has existed. Cox and others (1979, p. 183-184) sugggest that resorption may be caused by changes in temperature-pressure conditions as the magma moves toward the surface, or by changes in the temperature-pressure-composition conditions as the crystal moves about the magma chamber. Thirdly, the anorthite content of the plagioclase phenocrysts and microcrysts is consistent with normal crystallization trends yielding more sodic plagioclase with time.

The term "porphyritic" describes the texture of an igneous rock in which larger crystals (phenocrysts) are set in a fine-grained groundmass which may be crystalline or glassy or both (American Geological Institute, 1972, p. 558). In this study, no genetic interpretation, except that of igneous origin, has been implied by the use of the terms "phenocryst" and " porphyritic". Because xenocrysts commonly display the same resorptional features as do the phenocrysts in the basalts of this study, the origin of the phenocrysts is uncertain. However, some chemical evidence indicates that the observed olivine phenocrysts were formed by crystallization of the cognate magma. In their study of the partitioning of Mg and Fe^{2+} between olivine and basaltic magma, Roeder and Emslie (1970) concluded that the

composition of olivine is independent of temperature and depends only on the Mg/Fe^{2+} ratio in the liquid from which it is crystallizing. Therefore, the Mg/Fe^{2+} ratio in an olivine crystal can be used to determine the Mg/Fe^{2+} ratio in the liquid from which it crystallized. Based on the experimental data of Roeder and Emslie (1970), if olivine phenocrysts in the lavas of the Carrizozo Basalt Field are approximately Fa20 in composition (Smith, 1964; Renault, 1970), they would be expected to form from a liquid having a Mg/Fe^{2+} molar ratio of ~ 1.2; the Broken Back Crater Flow has such an average composition.

Some olivine phenocrysts have edges which have been altered to iddingsite; olivine crystals in the groundmass appear to be unaltered. These observations indicate that the melt was hydrous prior to eruption, but that groundmass olivine crystallized in an anhydrous environment (Renault, personal communication, 1979).

GEOCHEMISTRY OF THE CARRIZOZO BASALT FIELD

Previous Geochemical Studies

Renault (1970) analyzed 21 samples from the Carrizozo Basalt Field using x-ray fluorescence for SiO_2, Al_2O_3, FeO, MgO, CaO, Na_2O, K_2O, TiO_2 and MnO (Table 1).

The Broken Back Crater and Carrizozo Flows represent separate and distinct episodes in the history of the Carrizozo Basalt Field (Weber, 1964; Smith, 1964). However, the distinction between the lower and upper Carrizozo Flows is less obvious, as these two flows are continuous and generally indistinguishable in the field (Renault, 1970). Based on results from major chemical analyses and differences in flow morphology detectable in aerial photographs (Renault, personal communication, 1979), Renault (1970) estimated the location of a contact between these two flows to be at the northern edge of the narrow neck area (Figure 3).

Statistical comparisons of major element chemical data were made between the sample groups of Renault's lower and upper Carrizozo Flows using the Wilcoxon rank-sum test. This test is appropriate for the comparison of two groups of data when a normal population distribution is not assumed and when sample sizes are small (Bhattacharyya and Johnson, 1977, p. 505-509); for further discussion of this test, see Appendix A. The mean concentrations of SiO_2, MgO, CaO,

Table 1. Major element chemical analyses and statistics of the Carrizozo Basalt Field.

Broken Back Crater Flow

	SiO2	Al2O3	FeO	MgO	CaO	Na2O	K2O	TiO2	MnO
CAR-12	51.75	17.51	9.20	6.73	8.06	3.53	1.52	1.75	0.15
CAR-13	51.15	17.05	8.95	7.31	8.21	3.23	1.51	1.67	0.15
CAR-14	52.12	18.76	9.04	5.94	8.09	3.44	1.60	1.85	0.15
MEAN	51.67	17.78	9.06	6.66	8.12	3.40	1.54	1.76	0.15
STD DEV	0.49	0.89	0.12	0.69	0.08	0.15	0.05	0.09	0.00
STD ERR	0.28	0.51	0.07	0.40	0.05	0.09	0.03	0.05	0.00
95% CI	1.21	2.20	0.30	1.71	0.20	0.38	0.13	0.23	0.10
MG-VALUE	0.66								

lower Carrizozo Flow

	SiO2	Al2O3	FeO	MgO	CaO	Na2O	K2O	TiO2	MnO
CAR-15	50.32	16.92	9.68	5.93	8.71	3.58	1.34	1.76	0.16
CAR-16	48.16	17.03	9.70	6.81	9.11	3.14	1.58	1.93	0.17
CAR-17	50.51	17.17	9.59	6.78	8.34	3.37	1.38	1.69	0.15
CAR-18	50.09	17.47	9.85	6.66	8.46	3.45	1.33	1.71	0.16
CAR-19	50.28	17.26	9.93	6.32	8.57	3.47	1.30	1.75	0.16
CAR-21	49.31	17.07	9.47	6.92	9.32	3.59	1.39	1.75	0.16
CAR-22	50.46	16.56	9.96	7.12	8.75	3.46	1.28	1.69	0.17
CAR-24	48.80	16.14	9.57	7.25	8.90	3.49	1.46	1.75	0.16
CAR-25	50.83	16.46	9.59	6.71	8.53	3.90	1.32	1.69	0.16
CAR-26	50.42	16.58	9.96	7.46	8.79	3.60	1.21	1.65	0.17
CAR-27	49.12	16.58	9.51	7.15	8.94	3.60	1.64	1.90	0.16
MEAN	49.85	16.84	9.71	6.83	8.77	3.51	1.38	1.75	0.16
STD DEV	0.86	0.40	0.18	0.44	0.29	0.19	0.13	0.09	0.01
STD ERR	0.26	0.12	0.06	0.13	0.09	0.06	0.04	0.03	0.00
95% CI	0.58	0.27	0.12	0.29	0.20	0.12	0.09	0.06	0.00
MG-VALUE	0.64								

upper Carrizozo Flow

	SiO2	Al2O3	FeO	MgO	CaO	Na2O	K2O	TiO2	MnO
CAR-5	51.06	17.70	9.11	7.21	8.44	3.80	1.41	1.69	0.14
CAR-6	51.66	17.24	9.69	6.43	8.34	3.89	1.28	1.72	0.15
CAR-7	50.78	17.03	9.81	6.08	8.25	3.85	1.29	1.73	0.15
CAR-8	51.11	16.75	9.83	5.82	8.23	3.46	1.30	1.71	0.15
CAR-9	51.01	17.78	9.83	6.62	8.29	3.60	1.18	1.59	0.15
CAR-10	52.72	16.33	9.96	5.63	8.12	3.73	1.30	1.82	0.16
CAR-11	52.86	17.61	9.86	6.28	8.13	3.66	1.19	1.74	0.16
MEAN	51.60	17.21	9.66	6.30	8.26	3.71	1.28	1.71	0.15
STD DEV	0.86	0.54	0.31	0.53	0.11	0.15	0.18	0.07	0.01
STD ERR	0.32	0.20	0.12	0.20	0.04	0.06	0.07	0.03	0.00
95% CI	0.79	0.50	0.29	0.49	0.11	0.14	0.17	0.07	0.01
MG-VALUE	0.62								

STD DEV = standard deviation
STD ERR = standard error and 95% confidence interval
95% CI = 95% confidence interval (mean $\pm$ 95% CI)
MG-VALUE= Mg/(Mg+Fe) molar ratio

Analyses from Renault (1970).
Statistical parameters are defined in Appendix A.

Na_2O, and K_2O in the two flows show significant differences at the 95% confidence level. These results are summarized in Table 2 and justify Renault's location of the contact.

Classification

Several schemes for the classification of basalts are currently in use; a historical review is provided by Irving and Barager (1971). All are based on the concentrations of major element oxides, and some make use of the relative abundances of minerals represented in standard CIPW norms. CIPW norms for the basalts of this study (Table 3) were calculated by means of a computer program (Bingler and others, 1976) using the major element data of Renault (1970). Because the total iron concentration is expressed as FeO in the analyses, and because both Fe_2O_3 and FeO abundances are necessary for the calculation of CIPW norms, the upper limit of Fe_2O_3 in the these basalts has been estimated by the equation:

$$\text{weight \% } Fe_2O_3 = \text{weight \% } TiO_2 + 1.5$$

This equation is based on the observation that Fe_2O_3 and TiO_2 generally have similiar trends of variation in unaltered rocks (Irvine and Barager, 1971). It must be kept in mind that the Fe_2O_3/FeO ratio can appreciably affect the calculated norm, particularly with respect to olivine and hypersthene, and so classification schemes involving

Table 2. Major element concentration differences at the 95% confidence level.

SiO_2	BB > LC	LC < UC
Al_2O_3	BB > LC	
FeO	BB < LC	
MgO		LC > UC
CaO	BB < LC	LC > UC
Na_2O		LC < UC
K_2O	BB > LC	LC > UC

BB = mean concentration of the Broken Back Crater Flow

LC = mean concentration of the lower Carrizozo Flow

UC = mean concentration of the upper Carrizozo Flow

Statistical comparisons were made using the Wilcoxon rank-sum test described in Appendix A.

Table 3. CIPW normative minerals.

Broken Back Crater Flow

	Or	Ab	An	Di	Hy	Ol	Mt	Il	Ne	Q
CAR-12	8.94	29.71	27.30	10.02	10.83	5.21	4.69	3.31		
CAR-13	8.97	27.46	27.69	10.60	12.76	4.73	4.62	3.19		
CAR-14	9.33	28.73	30.62	7.23	13.93	1.91	4.79	3.47		

lower Carrizozo Flow

	Or	Ab	An	Di	Hy	Ol	Mt	Il	Ne	Q
CAR-15	8.02	30.69	26.48	13.98	5.56	7.09	4.79	3.39		
CAR-16	9.53	26.39	28.28	14.35		12.24	5.08	3.74	0.40	
CAR-17	8.21	28.72	27.84	11.14	9.22	6.97	4.66	3.23		
CAR-18	7.90	29.34	28.40	11.13	5.76	9.53	4.68	3.26		
CAR-19	7.73	29.55	27.86	12.08	7.00	7.70	4.74	3.35		
CAR-21	8.27	27.49	26.54	16.10		11.82	4.75	3.35	1.68	
CAR-22	7.58	29.34	25.93	14.19	5.31	9.79	4.64	3.22		
CAR-24	8.82	28.01	24.59	16.51		12.68	4.82	3.40	1.18	
CAR-25	7.84	33.16	23.62	15.24	0.73	11.53	4.65	3.23		
CAR-26	7.14	30.41	25.46	14.57	1.99	12.75	4.56	3.13		
CAR-27	9.80	26.77	24.50	16.31		11.83	4.98	3.65	2.18	

upper Carrizozo Flow

	Or	Ab	An	Di	Hy	Ol	Mt	Il	Ne	Q
CAR- 5	8.26	31.87	26.84	11.77	0.93	12.56	4.58	3.18		
CAR- 6	7.51	32.68	25.61	12.49	5.37	8.46	4.64	3.24		
CAR- 7	7.68	32.82	25.48	12.74	4.50	8.74	4.72	3.31		
CAR- 8	7.79	29.67	26.68	11.91	14.31	1.64	4.72	3.29		
CAR- 9	6.98	30.50	28.90	9.90	9.18	7.03	4.49	3.02		
CAR-10	7.68	31.53	23.95	13.21	14.95		4.81	3.45		0.43
CAR-11	6.91	30.42	27.61	9.71	16.10	1.40	4.61	3.25		

Ol	olivine	Or	orthoclase
Mt	magnetite	Ab	albite
Il	ilmenite	An	anorthite
Ne	nepheline	Di	diopside
Q	quartz	Hy	hypersthene

CIPW normative analyses of these two minerals must be evaluated with particular care.

Yoder and Tilley (1962) suggested two primary basaltic magma types, tholeiitic and alkali olivine basalts, and proposed a classification whereby basalts with quartz (Q) and hypersthene (Hy) in the CIPW norm are called tholeiites, those with olivine (Ol) and hypersthene (Hy) are called olivine tholeiites, and those with olivine (Ol) and nepheline (Ne) are called alkali basalts. Based on this scheme, the basalts in this study would be termed olivine tholeiites, except for one sample from the upper Carrizozo Flow which would be termed a tholeiite and four samples from the lower Carrizozo Flow which would be termed alkali basalts.

Chayes (1966) reviewed the history of the term "tholeiite", suggested that it be replaced by "subalkaline", and proposed a means by which olivine basalts lacking normative Ne and Q could be classified as either dominantly alkaline or subalkaline. Following this classification, the basalts in this study would be termed subalkaline, except for the four samples from the lower Carrizozo Flow which would be termed alkaline.

Irvine and Barager (1971) proposed three main series of basalts: tholeiitic, calc-alkaline, and alkali olivine basalts; their use of the term subalkaline includes the calc-alkaline and alkali olivine basalt series.

According to their method of classification, the basalts of this study are termed subalkaline based on discriminant functions in the ol-opx-cpx ternary system, and belong to the tholeiite series, based on plots of normative plagioclase composition against Al_2O_3 concentration; they are termed "average rocks" with respect to their potassium concentrations. Irvine and Barager (1971) contend that members of the tholeiite series can be distinguished petrographically but not chemically, although according to Yoder and Tilley's (1962) scheme, most of the basalts in this study may be called olivine tholeiites.

The samples fromm the Carrizozo Basalt Field are compositionally transitional between the typical tholeiitic and typical alkalic basalt series. Lowder (1973) noted similiar compositions is his study of late Cenozoic basalts of southwest Utah and used the total alkalies vs. silica diagram of McDonald and Katsura (1964) to show this transitional nature. Figure 8 is such a diagram for the basalts of this study, and shows that most samples plot in the alkaline field but lie very close to the boundary between the alkaline and tholeiitic fields.

It is interesting to note that the composition of basaltic lavas varies regularly along the axis of the rift. Aoki and Kudo (1976) remarks that volcanism predominantly consisted of aluminous olivine tholeiite in the northern portion of the rift (north of Santa Fe), of tholeiite and

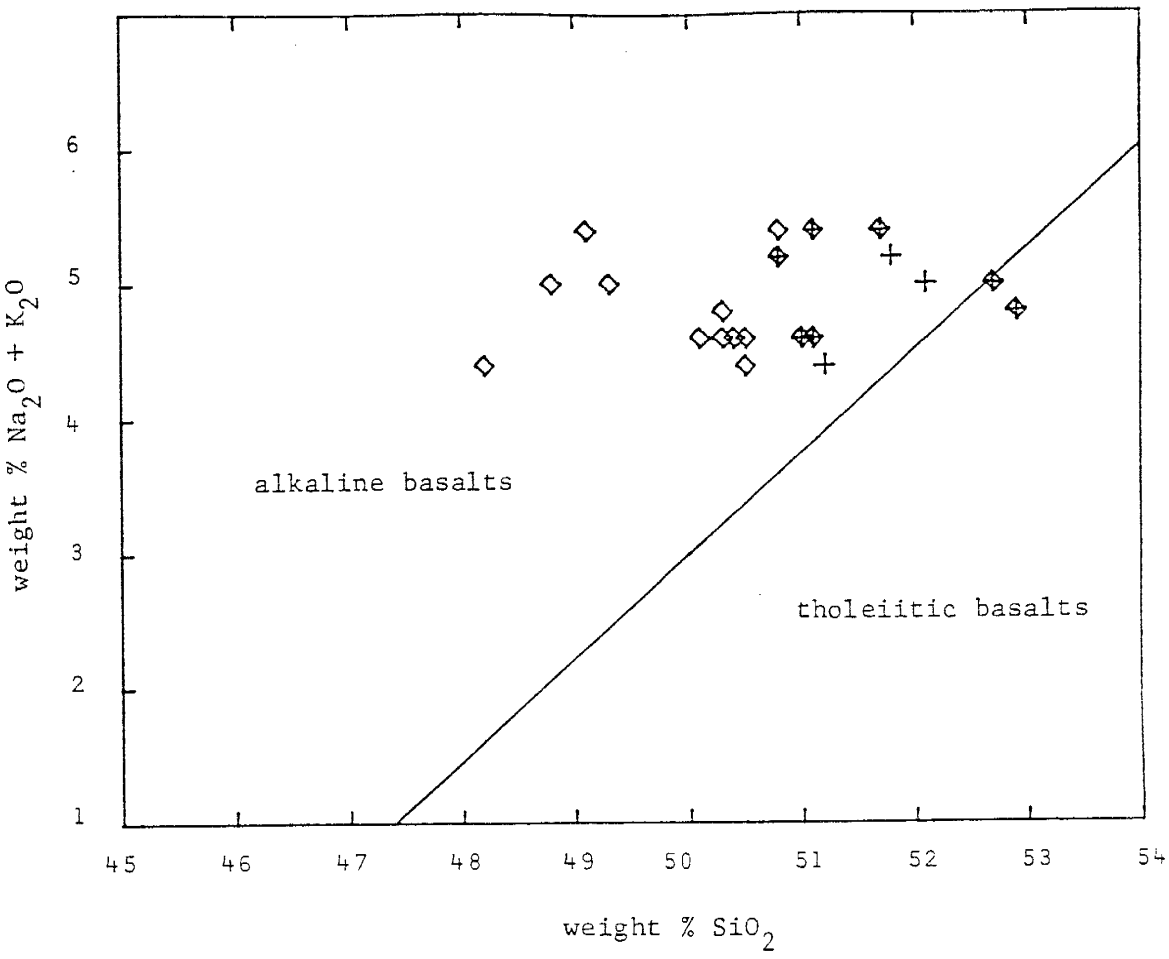

+ Broken Back Crater Flow

◇ lower Carrizozo Flow ⊕ upper Carrizozo Flow

The solid line dividing the alkaline and tholeiitic fields is an empirical one based on data from Hawaiian rocks (McDonald and Katsura, 1973). Yoder (personal communication to McDonald and Katsura, 1973) has suggested that the line approximates the critical plane of silica undersaturation and so corresponds with Yoder and Tilley's (1962) criterion of the presence or absence of hypersthene to distinguish between these two groups of basalts.

Figure 8. Total alkalies vs. silica diagram for the samples from the Carrizozo Basalt Field.

alkali olivine basalt in the central portion of the rift (Santa Fe to Socorro), and of alkali olivine basalt in the southern portion of the rift (south of Socorro). Thus the transitional nature of the basalts of the Carrizozo Basalt Field appears to reflect the larger picture of varying basaltic compositions along the Rio Grande rift.

Analytical Methods

Sampling

Field sampling was done by J.R. Renault as a part of his study of major element concentration variations in some Rio Grande rift basalts. A summary of his procedures follows (Renault, 1970). Locations of the 21 samples (Figure 3) were selected prior to field work and modified in the field to obtain fresh, representative material. As much as possible, samples were taken from the base of the upper zone of vesiculation at each site to avoid compositional variations due to possible differentiation during extrusion or subsequent surficial processes. Sample locations on the Broken Back Crater Flow occupy grid positions with approximately 2.6 miles between samples. The sinuous shape of the Carrizozo Flows suggested serial sampling; the average sample interval is approximately 2.7 miles.

The number of samples required to characterize the mean compositions of sampling units at the 95% confidence

Table 4. Number of samples required to characterize the mean compositions of sampling units at the 95% confidence level.

	SiO_2	Al_2O_3	FeO	MgO	CaO	Na_2O	K_2O	TiO_2	MnO
BBC	4.42	58.12	1.11	35.16	0.47	10.68	2.24	3.82	0.27
LC	3.64	3.23	0.67	3.80	1.68	4.23	3.72	0.94	0.13
UC	4.37	6.92	2.32	6.71	0.31	3.33	1.57	0.73	0.24
Tolerance Values	1.00	0.50	0.50	0.50	0.50	0.20	0.15	0.20	0.03

Broken Back Crater Flow : 3 samples taken
lower Carrizozo Flow :11 samples taken
upper Carrizozo Flow : 7 samples taken

Calculations are based on analyses by Renault (1970).
See Appendix A for a discussion of the statistical method used to determine sample size.

level was determined (Table 4); a discussion of the statistical method used to determine sample size can be found in Appendix A. The acceptable deviations from the mean, or tolerance values, are those used by Renault (1970), and are also the class intervals used by Manson (1967) in his study of the major element composition of basalts. These tolerance values are generally greater than the observed standard deviations.

The number of samples taken from the lower and upper Carrizozo Flows is sufficient to characterize the mean composition as lying within the tolerance values, with 95% confidence for all major oxides. The Broken Back Crater Flow appears to be undersampled, in that less than half of the major oxides can be said to have mean compositions which lie within the specified tolerance values at the 95% confidence level. However, Renault (1970) notes that, as a consequence of the statistics of small sample size, some of the calculated numbers of samples required are unrealistically high. For example, the calculated required number of samples for the Al_2O_3 analysis of the Broken Back Crater Flow is 59; if the actual number of samples taken was 6 instead of 3, then even if the standard deviation remained the same, the required number of samples would become 21. Therefore, the Broken Back Crater Flow may not have been seriously undersampled.

Sample preparation

Preparation of rock samples for chemical analysis was accomplished by the procedure outlined below:

1. The sample was reduced to pieces measuring less than 75 mm in maximum dimension using a sledge and stainless steel plate.
2. 500-1000 grams of this material was fed through two jaw-crushers, equipped steel plates, with aperatures at the discharge opening of 20 and 6 mm.
3. 10 grams of this material was hand-picked to eliminate pieces containing vesicle filling or those showing any signs of weathering.
4. The sample was reduced in size to particles measuring less than 2 mm in average diameter using a Diamet mortar and pestle.
5. Final grinding was done using a Fisher automatic mortar-grinder, equipped with a fused alumina mortar and pestle. The sample was ground in distilled water for 30 minutes, then filtered and air-dried. A grain size analysis showed that greater than 95% of the resulting material measured less than 62 microns in average particle diameter, an acceptable size for the analytical work to follow.

6. Undiluted pellets of the sample material were prepared for x-ray fluorescence analysis with the following specifications:

    Amount per pellet : 3 grams

    Backing material : Buehler Bakelite powder

    Pressure : 20 tons

    The die used follows the description of Baird (1961), but was modified to include a polished carbide (SiC) anvil. Pellets were prepared in duplicate for each sample.

7. Samples for neutron activation analysis were prepared by sealing 0.5 grams of ground sample from step #5, weighed to the nearest 0.0001 gram, in a small polyethylene vial.

During the entire sample preparation procedure, care was taken to prevent contamination by carefully cleaning all equipment between samples.

Trace element determination methods

X-ray Fluorescence Analysis (XRF)

The 21 samples from the Carrizozo Basalt Field were analyzed for Cr, Mn, Ni, Cu, Rb, Sr, and Zr using a wavelength dispersive Philips Universal vacuum spectrometer, equipped with a Harshaw scintillation counter. The primary

source unit components, measuring electronics, and display equipment are specified in Table 5.

Standard rocks used to construct calibration curves included the U.S. Geological Survey standards PCC-1 (peridotite), BCR-1 (basalt), AGV-1 (andesite), and GSP-1 (granodiorite) (Flanigan, 1976), the Tanganyikan tonalite standard T-1 (Tanganyikan Geological Survey, 1963), and the New Mexico Tech standard basalts BCLR and BR (Condie, unpublished data, 1978). The accepted chemical analyses of the non-USGS standard rocks are given in Appendix B.

Instrumental parameters for the XRF analyses are given in Table 5 and were determined using a pellet composed of 50% BCR-1 and 50% Spex Mix. A choice was made between available Cr, Mo, and W x-ray tubes so as to provide maximum excitation of the analyte. The use of a LiF(200) analyzing crystal and a scintillation counter were suited to the dispersion and detection of the range of desired analytical wavelengths, respectively.

It is seen from Table 5 that the position of the pulse height analysis (PHA) window is shifted towards higher voltages with increasing atomic number of the analyte if the potential on the counter's anode wire (HV) remains constant; this happens beause the high voltage (HV) plateau of the scintillation counter occurs at lower voltages as the atomic number of the analyte and the energy of the analytical wavelength increases. The interested reader is referred to

Table 5. Instrumental parameters for x-ray fluorescence analyses.

Element	Target	KV	MA	HV	Gain	E	ΔE	FT
Cr	W	50	30	950	16	0.17	0.50	10
Mn	W	50	35	900	16	0.12	0.36	10
Ni	W	50	40	900	16	0.20	0.44	10
Cu	Mo	50	30	850	16	0.09	0.24	10
Rb	Mo	40	20	850	16	0.27	0.32	20
Sr	Mo	40	20	800	16	0.16	0.24	10
Zr	W	54	40	800	16	0.22	0.24	10

For all elements:

Crystal = LiF (200)
Detector = Scintillation counter
Path = Air
Collimator = Fine
Analytical Peak = Kα

E = Base volts PHA
ΔE = Window volts PHA
FT = Fixed time in seconds

Primary source unit:

stabilized Philips high voltage generator
selection of Philips x-ray tubes with Cr, Mo, and W targets

Measuring electronics: Tennelec modules including

dual counter/timer
ratemeter
linear amplifier
single channel analyzer
high voltage bias supply

Recording equipment:

Teletype simultaneous output printer
Honeywell Electronik 19 strip chart recorder

discussions by Jenkins (1976) and Jenkins and DeVries (1967) for further information regarding the determination of XRF instrumental settings.

In order to monitor changing instrumental conditions and correct for the effects of long term drift, a "ratio method" of data reduction was used. Accordingly, the value correlated with concentration is the net intensity of a sample's analytical peak divided by that of a reference "drift pellet". For each element, one of the standards was chosen as a drift pellet and was counted with each trayload of samples.

A correction was made for the effects of sample absorption on the intensity of measured wavelengths by multiplying the value of the mass absorption coefficient by the intensity ratio. For all the samples and standards, values of the mass absorption coefficent at desired analytical wavelengths were calculated by means of a computer program (CHEM2 by J.R. Renault) using major element chemical analyses and Victoreen (1949) parameters, and are tabulated in Appendix C.

The concentration of Rb in samples from the Carrizozo Basalt Field is below the lower level of determination (defined in Appendix A) for the instrumental settings listed in Table 5.

For the Cr analysis, a correction was made for enhancement effects by iron, as the FeKα line lies just to

the short wavelength side of chromium's K absorption edge. A linear multiple regression analysis was performed, where Cr concentration was assumed to be proportional to the intensity ratio, mass absorption coefficient, and total iron concentration expressed as FeO. For all other elements analyzed for by XRF, calibration curves were constructed by simple linear regressions, with elemental concentrations correlated with the intensity ratio corrected for absorption effects. Calibration curve statistics are given in Table 6.

Instrumental Neutron Activation Analysis (INAA)

Due to restriction placed on the number of samples which could be submitted for irradiation, nine samples representing the three major flows were selected to be irradiated at Sandia Laboratories, Albuquerque, NM. These samples were chosen because they appeared to define differentiation trends within the various flows, based on Fe vs. Fe/Mg diagrams. A Canberra 4,096 channel gamma-ray spectrometer with a high-resolution Li-drifted germanium detector system was used for the analysis of 14 trace elements: Ba, La, Ce, Sm, Eu, Tb, Yb, Lu, U, Th, Sc, Co, Hf, and Ta. Instrumental parameters for the INAA analyses are given in Table 7.

The method described by Gordon and others (1968) was used for the determinations. Briefly, the amount of a given element in a sample is computed by comparing the

Table 6. X-ray fluorescence calibration curve statistics.

Element	Correlation coefficient	Regression equation	% Relative RMS Error	Standards used to construct calibrative curve
* Cr	0.99	$Y = -65.46\ [FeO_T] + 7.72\ (I \cdot \mu) - 770.55$	0.10	BCR-1,BLCR,BR
Mn	0.99	$Y = 0.02 + 0.01\ I$	0.66	PCC-1,BCR-1,AGV-1
Ni	0.99	$Y = -11.30 + 0.32\ I$	1.85	BCR-1,BLCR,AGV-1
Cu	0.99	$Y = -37.37 + 1.35\ I$	2.73	BCR-1,AGV-1,GSP-1
Sr	0.99	$Y = -6.37 + 23.56\ I$	0.56	BCR-1,AGV-1,GSP-1
Zr	0.99	$Y = 87.68 + 16.80\ I$	0.20	AGV-1,GSP-1

I = Intensity ratio = net counts sample/net counts drift pellet
Y = Concentration in ppm (except for MnO, whose concentration is given in oxide weight percent)
μ = Mass absorption coefficient
FeO_T = Total iron concentration expressed as FeO

Statistical parameters are defined in Appendix A.

* Multiple regression analysis performed due to enhancement effects by iron.

Table 7. Neutron activation analysis analytical parameters.

Radionuclide	Peak (Kev)	Cooling period (days)	Counting time (secs)	Coarse gain	Fine gain
153 Sm	103	4	4000	4	2.80
239 Np (U)	278	4	4000	4	2.80
140 La	1575	4	4000	4	2.80
177 Lu	208	7	4000	8	5.10
175 Yb	396	7	4000	8	5.10
131 Ba	496	7	4000	8	5.10
141 Ce	145	28	5000	4	2.86
169 Yb	177	28	5000	4	2.86
233 Pa (Th)	312	28	5000	4	2.86
181 Hf	482	28	5000	4	2.86
160 Tb	879	28	5000	4	2.86
46 Sc	889	28	5000	4	2.86
182 Ta	1222	28	5000	4	2.86
60 Co	1333	28	5000	4	2.86
152 Eu	1408	28	5000	4	2.86

Samples were irradiated for 1 hour at 300 kwatts.

System calibrated with ^{60}Co, ^{137}Cs, and ^{152}Eu.

gamma-ray intensities due to the element in a sample to those emitted by a standard which has been irradiated simultaneously with the rock samples. The spectrum over a window of 7-11 channels around the peak maximum is integrated; the backround, taken as an average of several channels on both sides of the window is subtracted to obtain a net peak area. The USGS basalt BCR-1 was used as the standard; BCLR and additional counts of BCR-1 were used as internal standards. Corrections were applied for radioactive decay occurring between sample and standard counting times, and for differences in weights of irradiated material, with the aid of simple computer programs (NUTDAT and NUTRON at New Mexico Tech).

Because of the limited number of analyses, precision and accuracy tests were not performed. However, the percent counting error and the percent difference between the calculated concentration values of the internal standards and accepted values for these standards are given in Table 8.

Table 8 . Neutron activation analysis errors.

Element	% CE	% Diff IS
Ba	4.7	15.2
La	4.8	6.0
Ce	2.7	7.3
Sm	0.7	4.0
Eu	8.6	10.7
Tb	5.0	4.4
Yb	4.5	6.4
Lu	3.5	3.2
U	6.3	8.9
Th	2.9	3.9
Sc	1.0	2.8
Co	2.4	2.0
Hf	3.7	5.3
Ta	5.5	14.4

% CE = percent counting error defined in Appendix A

% Diff IS = percent difference between calculated concentration values of internal standards and accepted values for these standards

Analytical Results

Alkali and alkaline earth elements

The concentrations of Sr and Ba in the basalts of this study are given in Table 9; the concentrations of K_2O (Renault,1970) are given in Table 1. Wilcoxon rank-sum tests were applied to compare mean concentration differences between the Broken Back Crater, lower, and upper Carrizozo Flows. These results are also summarized in Table 9 and show that the absolute concentration of alkali and alkaline earth trace elements tends to decrease with decreasing age of the flows: at the 95% confidence level, the mean concentration of K_2O decreases with decreasing age of the flows, and the mean concentration of Sr in the lower Carrizozo Flow is greater than that of the upper Carrizozo Flow.

For the Carrizozo Flows, the concentrations of K_2O and Sr as a function of distance from the vent are shown in Figures 9 and 10, respectively. For both K_2O and Sr, it is seen that the trend of decreasing concentration with distance from the vent can be expressed by a straight line approximation in the upper Carrizozo Flow: the correlation coefficient of this line is 0.72 for K_2O and 0.83 for Sr, indicating that a linear model is reasonable. When a linear regression analysis is applied to the K_2O and Sr data from the lower Carrizozo Flow, the calculated correlation

Table 9 . Alkali and alkaline earth trace element concentrations.

	ppm Sr	ppm Ba
Broken Back Crater Flow		
CAR-12	484	
CAR-13	456	
CAR-14	499	468
Mean	479.7	468
Std Dev	21.8	
lower Carrizozo Flow		
CAR-15	457	
CAR-16	560	
CAR-17	468	
CAR-18	417	
CAR-19	424	
CAR-21	522	284
CAR-22	434	
CAR-24	515	397
CAR-25	428	324
CAR-26	415	
CAR-27	516	
Mean	468.7	335.0
Std Dev	53.9	57.3
upper Carrizozo Flow		
CAR-5	441	359
CAR-6	444	
CAR-7	432	390
CAR-8	411	
CAR-9	418	
CAR-10	351	344
CAR-11	373	337
Mean	410.0	357.5
Std Dev	35.4	23.5

Mean concentration differences between flows at the 95% confidence level:

K	BB > LC	LC > UC
Sr		LC > UC

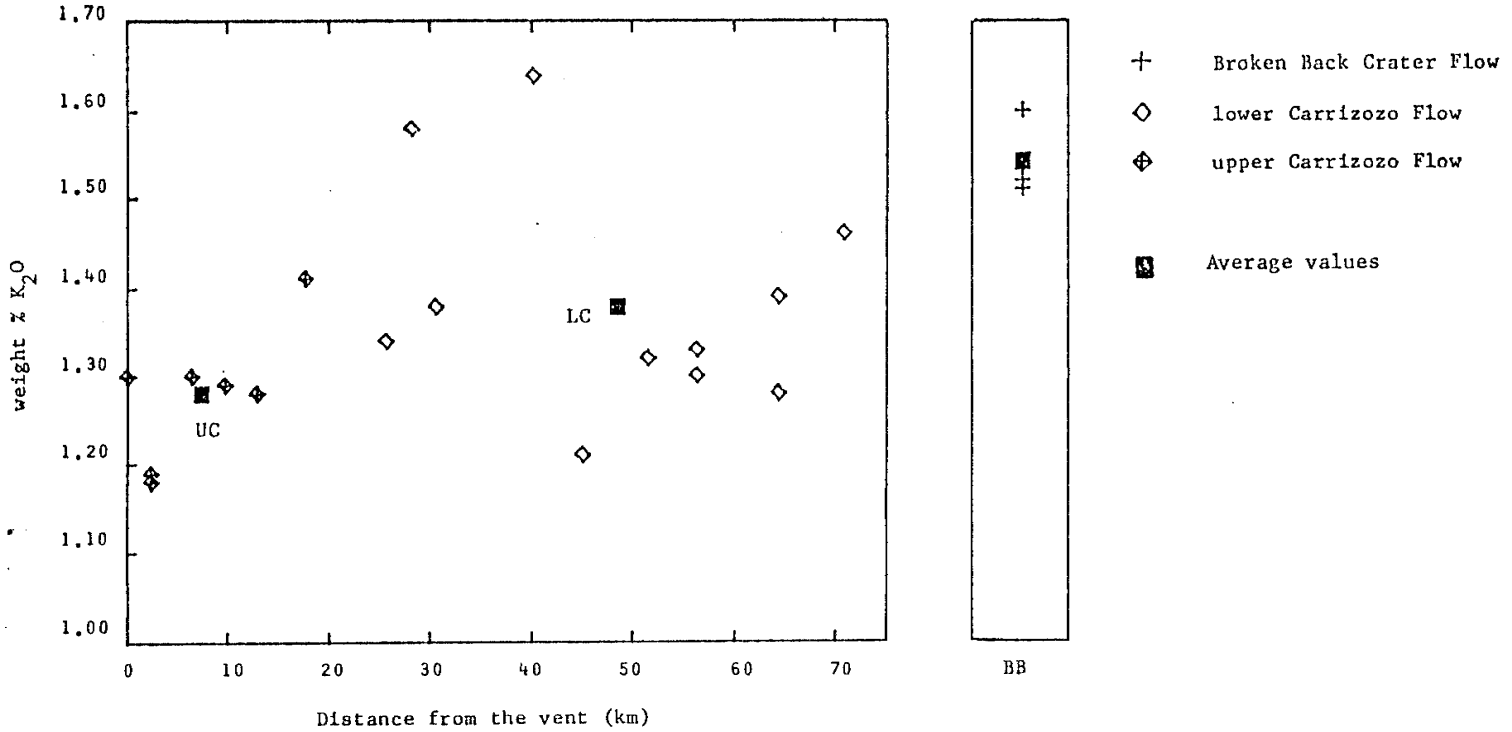

Figure 9. K_2O variation in the flows of the Carrizozo Basalt Field.

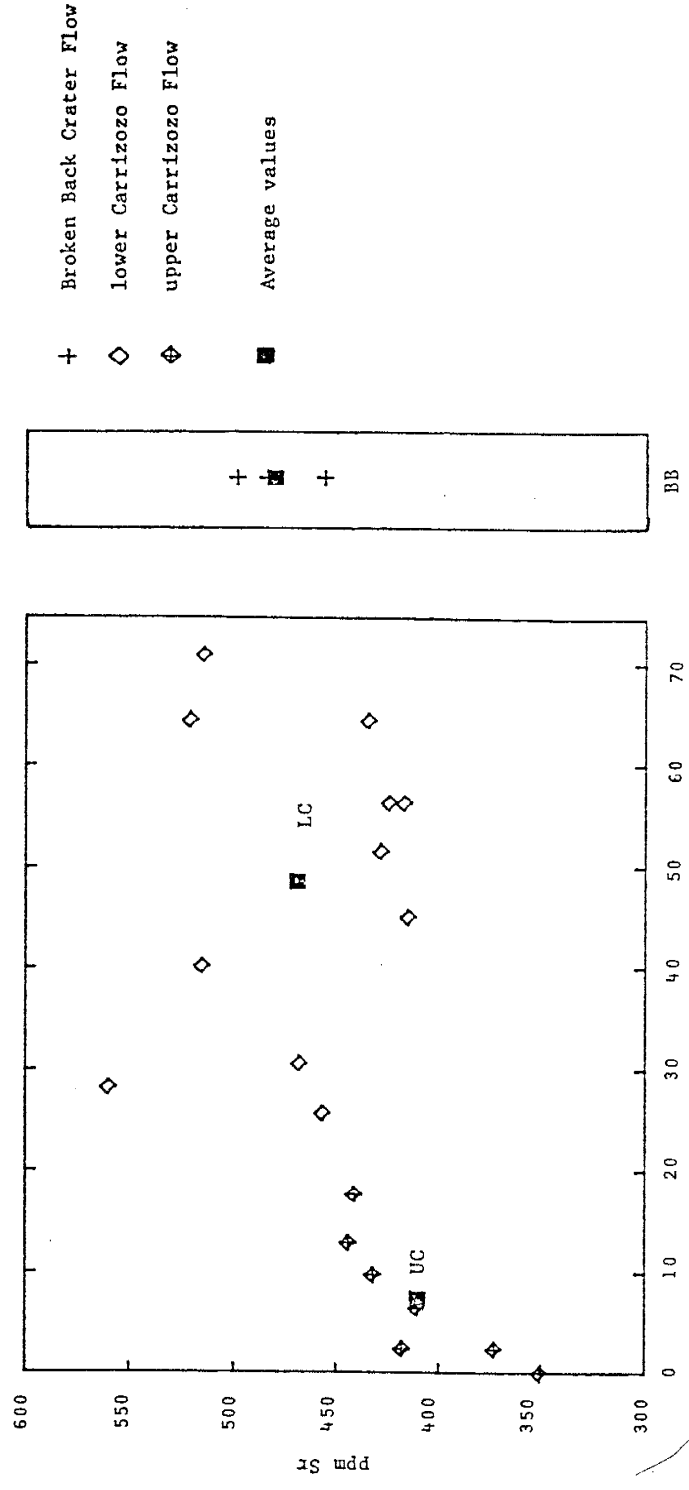

Figure 10. Sr variation in the flows of the Carrizozo Basalt Field.

coefficients are approximately equal to zero, indicating that no linear relationship exists between the data points.

However, if the four samples from the narrow neck area of the lower Carrizozo Flow (CAR-15, CAR-16, CAR-17, and CAR-27; Figure 3) are grouped with the samples from the upper Carrizozo Flow, two reasonably well-defined linear trends are observed. For K_2O, the correlation coefficients for the lines defining these trends in the "new" lower and upper Carrizozo Flow sample groups are 0.81 and 0.85, respectively; similiarly, for Sr they are 0.76 and 0.86.

These observations are not sufficient to justify a new location for the contact between the lower and upper Carrizozo Flows, but rather, they may indicate a compositional change within the lower Carrizozo Flow not detectable from major element chemistry, and/or a closer relationship between the lower and upper Carrizozo Flows, an alternative which will be developed in a following section. Also, the assumption that compositional trends within a complex natural system such as a basalt flow are ideally represented by linear models itself requires a number of assumptions such as compositional homogeneity of the parent rock or magma, a specific shape of the magma chamber, and regular eruption and flow sequences. These assumptions and thus the expectation of linear compositional trends may not be realistic.

Rare earth elements, uranium, and thorium

The concentrations of rare earth elements (REE) in the basalts of this study are given in Table 10; the concentrations of U and Th are given in Table 11. Wilcoxon rank-sum tests were applied to compare mean concentration differences between the Broken Back Crater, lower, and upper Carrizozo Flows. Due to the necessity of limiting the number of samples for neutron activation analysis, it is difficult to establish mean concentration differences between the three flows for this group of elements. However, differences existing at the 80% or greater confidence level are given in Table 12.

Plots of La, Ce, Sm, Yb, and Th concentrations vs. relative ages of the flows are shown in Figure 11. Trends of decreasing average concentrations of these elements with decreasing age of the flows are probably present, even though these trends are not easily statistically documented due to the small number of analyses, and only three points, representing the three major flows, can be plotted.

In the chondrite-normalized REE diagram (Figure 12), it is seen that the light REE are more enriched with respect to chondrites than are the heavy REE: light REE concentrations range from approximately 80-25X chondrite values; heavy REE concentrations range from approximately 20-12X chondrite values. Also, the light REE appear to be fractionated between the three flows, with the level of

Table 10. Rare earth element concentrations.

	La		Ce		Sm		Eu		Tb		Yb *		Lu	
	PPM	CN	PPM	CN	PPM	CN	PPM	CN	PPM	CN	PPM	CN	PPM	CN
Broken Back Crater Flow														
CAR-13	24	73	51	58	5.9	32.6	1.6	23.6	0.7	14.9	2.3	11.3	0.5	13.5
CAR-14	29	88	58	66	6.1	33.7	1.4	19.7	1.0	21.3	3.5	17.6	0.4	12.9
MEAN	26.5	80.5	54.5	62.0	6.00	33.15	1.51	21.65	0.85	18.10	2.90	14.45	0.45	13.20
STD DEV	3.5	10.6	4.9	5.7	0.14	0.78	0.14	2.76	0.21	4.53	0.85	4.45	0.07	0.42
lower Carrizozo Flow														
CAR-21	26	79	51	58	5.7	31.5	1.5	21.9	1.0	21.3	2.7	13.7	0.5	14.4
CAR-24	23	70	50	57	5.7	31.5	1.9	27.5	0.8	17.0	2.7	13.4	0.5	14.4
CAR-25	19	58	44	50	5.7	31.5	1.7	24.2	1.2	25.5	2.4	12.1		
MEAN	22.7	69.0	48.3	55.0	5.70	31.50	1.70	24.53	1.00	21.27	2.60	13.07	0.50	14.40
STD DEV	5.0	10.5	3.8	4.4	0.00	0.00	0.20	2.81	0.20	4.25	0.17	0.85	0.00	0.00
upper Carrizozo Flow														
CAR-5	21	64	41	46	5.3	29.3	2.0	29.1	0.7	14.9	2.0	10.1	0.4	11.8
CAR-7	20	61	46	53	5.5	30.4	1.5	22.2	0.7	14.9	2.6	12.9	0.4	10.9
CAR-10	23	70	45	51	5.9	32.6	1.7	25.1	1.0	21.3	3.1	15.3	0.5	13.5
CAR-11	17	52	32	36	5.3	29.3	1.4	20.7	0.9	19.1	2.2	11.1	0.4	12.7
MEAN	20.3	61.8	41.0	46.5	5.50	30.40	1.65	24.28	0.83	17.55	2.48	12.35	0.43	12.23
STD DEV	2.5	7.5	6.4	7.6	0.28	1.56	0.26	3.70	0.15	3.19	0.49	2.28	0.05	1.12

CN = concentrations normalized to chondritic values listed in Appendix D

* average results from analyses of ^{175}Yb and ^{169}Yb

Table 11. Uranium and thorium concentrations.

	ppm U	ppm Th
Broken Back Crater Flow		
CAR-13	1.2	3.6
CAR-14	1.2	3.9
Mean	1.20	3.75
Std Dev	0.00	0.21
lower Carrizozo Flow		
CAR-21	1.4	3.4
CAR-24	1.3	3.2
CAR-25	1.5	3.2
Mean	1.30	3.27
Std Dev	0.10	0.12
upper Carrizozo Flow		
CAR-5	1.4	3.1
CAR-7	1.0	3.0
CAR-10		3.5
CAR-11		2.7
Mean	1.20	3.08
Std Dev	0.28	0.33

Table 12. Rare earth element, uranium, and thorium mean concentration differences between flows.

	BB > LC	LC > UC
La	√√	√
Ce	√√	√√
Sm	√√	√√
Tb		√√
Yb	√	√
Lu		√√
U		√
Th	√√	√√

√√ = difference exists at the ≥ 80% confidence level

√ = difference exists, but is not established at a statistically significant level

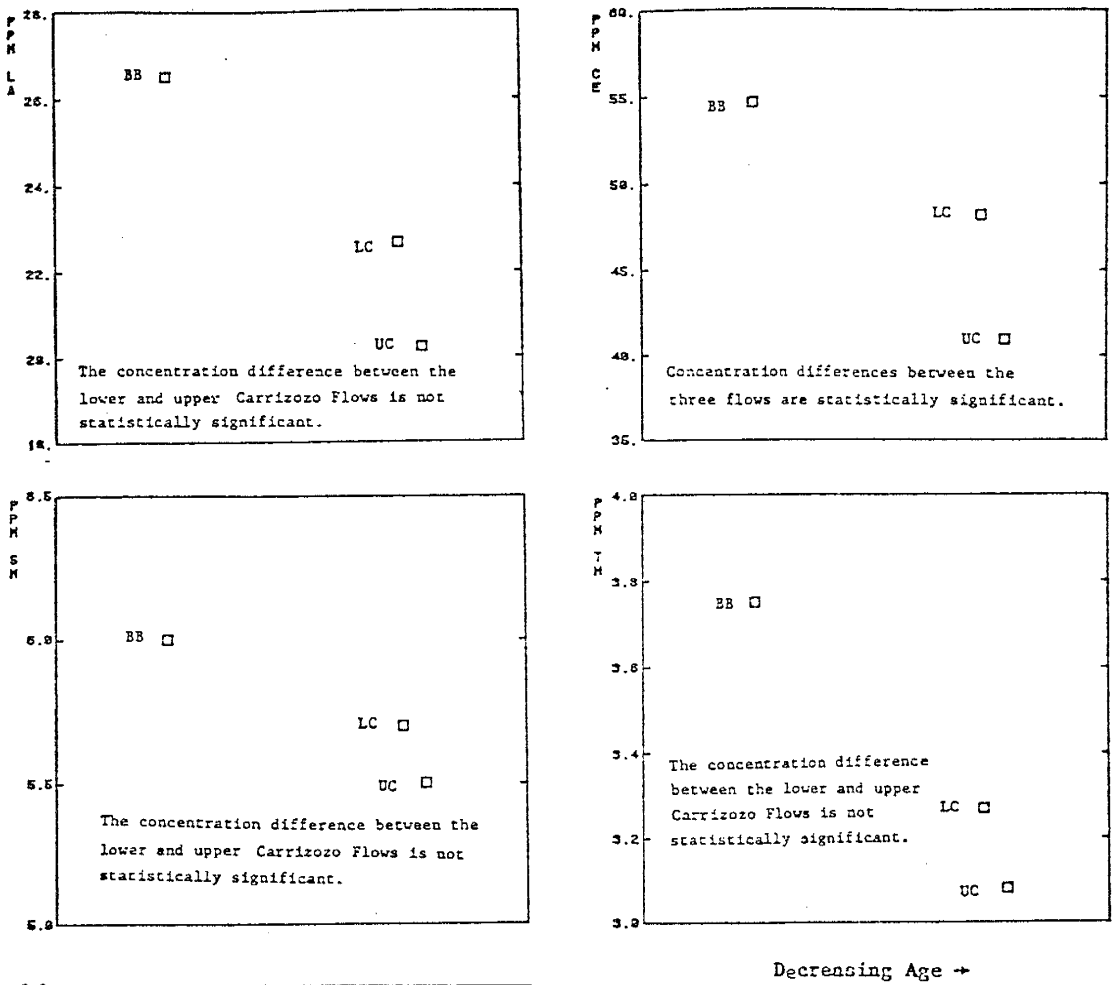

Figure 11. La, Ce, Sm, Yb, and Th concentrations vs. relative ages of the flows.

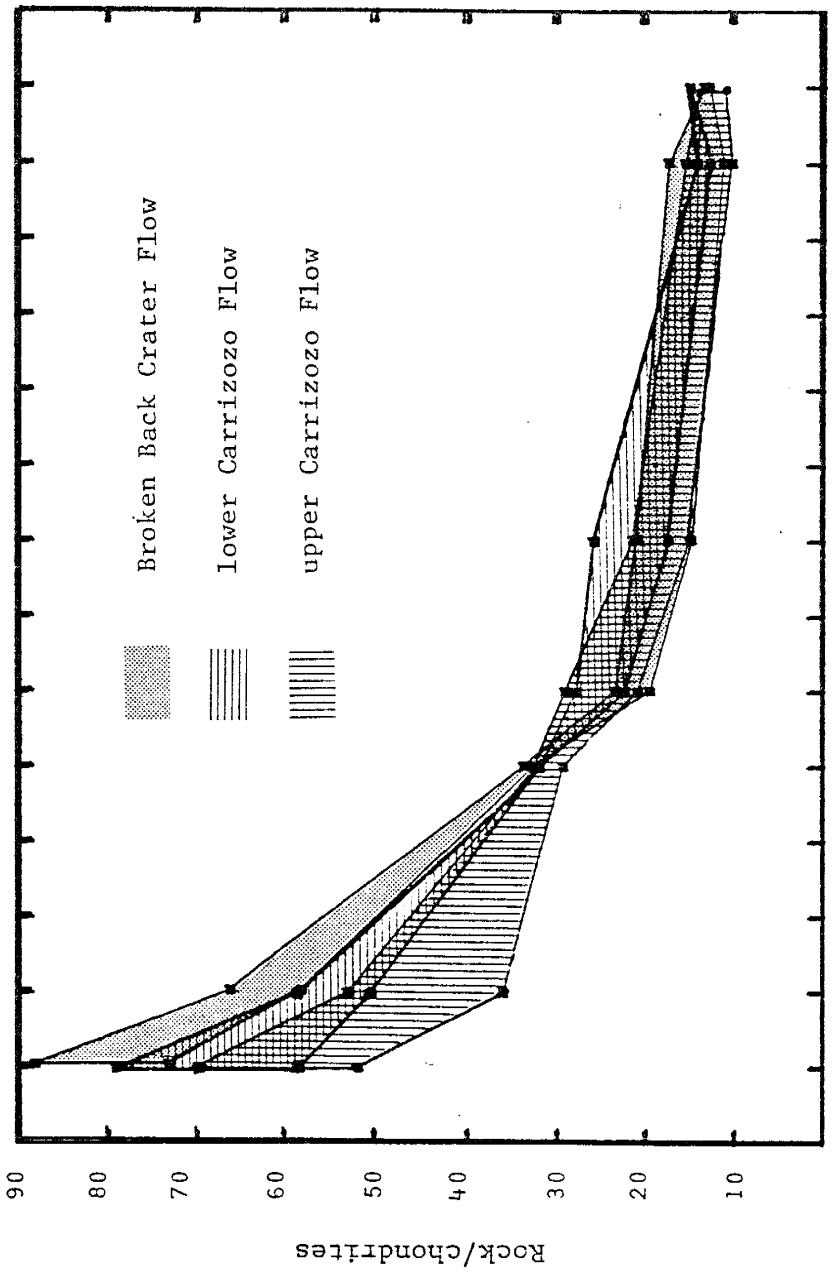

Figure 12. Chondrite-normalized REE patterns for the flows of the Carrizozo Basalt Field. Patterned area represents the range of observed values for each flow.

light REE enrichment decreasing with decreasing age of the flows. The heavy REE exhibit more uniform behavior in the three flows. No Eu anomalies are present. Assumed chondrite values are given in Appendix D.

Transition metals

The concentrations of nine transition metals in the samples from the Carrizozo Basalt Field are given in Table 13. Wilcoxon rank-sum tests were applied to compare mean concentration differences between the Broken Back Crater, lower, and upper Carrizozo Flows; these results are summarized in Table 14.

Due to the limited number of analyses, it is difficult to establish mean concentration differences between the three flows for those elements whose concentrations were determined using neutron activation analysis. However, at the 95% confidence level, the mean concentrations of Ni and Cu are greater in the lower Carrizozo Flow than in the Broken Back Crater Flow; the same relationship is seen for Sc, Co, Hf, and Ta, but not at statistically significant levels. Also at the 95% confidence level, the mean concentrations of Sc, Co, Ni, and Cu are greater in the lower than in the upper Carrizozo Flow; the same relationship is seen with Cr, Zr, Hf, and Ta, but again, not at statistically significant levels. The concentrations of TiO_2 (Renault, 1970) and MnO show no mean concentration differences between the three flows.

Table 13. Transition metal concentrations.

	Sc	Cr	MnO	Co	Ni	Cu	Zr	Hf	Ta
Broken Back Crater Flow									
CAR-12		274	0.15		114	38	191		
CAR-13	23	250	0.15	42	114	25	186	3.4	2.0
CAR-14	24	313	0.15	41	95	29	192	4.3	2.2
MEAN	23.5	279.0	0.15	41.5	107.7	30.7	190.0	3.85	2.10
STD DEV	0.7	31.8	0.00	0.7	11.0	6.7	3.2	0.64	0.14
lower Carrizozo Flow									
CAR-15		255	0.16		122	49	190		
CAR-16		203	0.16		139	62	199		
CAR-17		263	0.15		133	50	186		
CAR-18		273	0.16		162	58	179		
CAR-19		274	0.16		136	60	183		
CAR-21	25	311	0.16	49	166	64	190	4.6	2.1
CAR-22		295	0.16		172	72	184		
CAR-24	24	237	0.16	44	158	59	194	3.6	2.2
CAR-25	23	294	0.16	43	121	52	187	4.9	1.6
CAR-26			0.16		115	47	185		
CAR-27			0.16		126	52	197		
MEAN	24.0	267.1	0.16	45.3	140.9	56.8	188.5	4.37	1.97
STD DEV	1.0	32.9	0.00	3.2	20.2	7.6	6.2	0.68	0.32
upper Carrizozo Flow									
CAR-5	21		0.16	40	120	50	184	3.6	1.7
CAR-6		290	0.16		80	48	187		
CAR-7	22	277	0.16	41	72	48	185	3.5	1.9
CAR-8		214	0.16		83	47	191		
CAR-9		191	0.15		75	40	182		
CAR-10		188	0.15	38	43	47	187	4.6	1.7
CAR-11	21	224	0.16	36	73	48	180	3.3	1.6
MEAN	21.3	230.7	0.16	38.8	78.0	46.9	185.1	3.75	1.73
STD DEV	0.6	43.3	0.00	2.2	22.7	3.2	3.6	0.58	0.13

All concentrations are expressed in ppm, except for MnO which is expressed in weight percent.

Table 14. Transition metal mean concentration differences between flows.

	BB < LC	LC > UC
Sc	√	√√
Cr		√
Co	√	√√
Ni	√√	√√
Cu	√√	√√
Zr		√
Hf	√	√
Ta	√	√

√√ = difference exists at the 95% confidence level

√ = difference exists, but is not established at a statistically significant level

For the Carrizozo Flows, plots of Sc, Cr, Co, Ni, and Cu concentrations vs. distance from the vent are shown in Figures 13-17, respectively. Transition metal concentrations tend to increase with distance from the vent, although irregularities exist. For example, in the case of Ni, the four samples from the narrow neck area of the lower Carrizozo Flow (CAR-15, CAR-16, CAR-17, and CAR-27; Figure 3) might be grouped with the samples of the upper Carrizozo Flow in order to define two linear trends having approximately the same slope (Figure 16). For Cu, two linear trends can be defined for samples from the the lower and upper Carrizozo Flows; the samples from the narrow neck area of the lower Carrizozo Flow could be grouped with samples from the upper rather than the lower Carrizozo Flow (Figure 17). For Cr , two fairly well-defined linear trends are observed for the lower and upper Carrizozo Flows based on Renault's (1970) sample groups (Figure 14); here, the slope for samples from the upper Carrizozo Flow is much steeper than that for samples from the lower Carrizozo Flow.

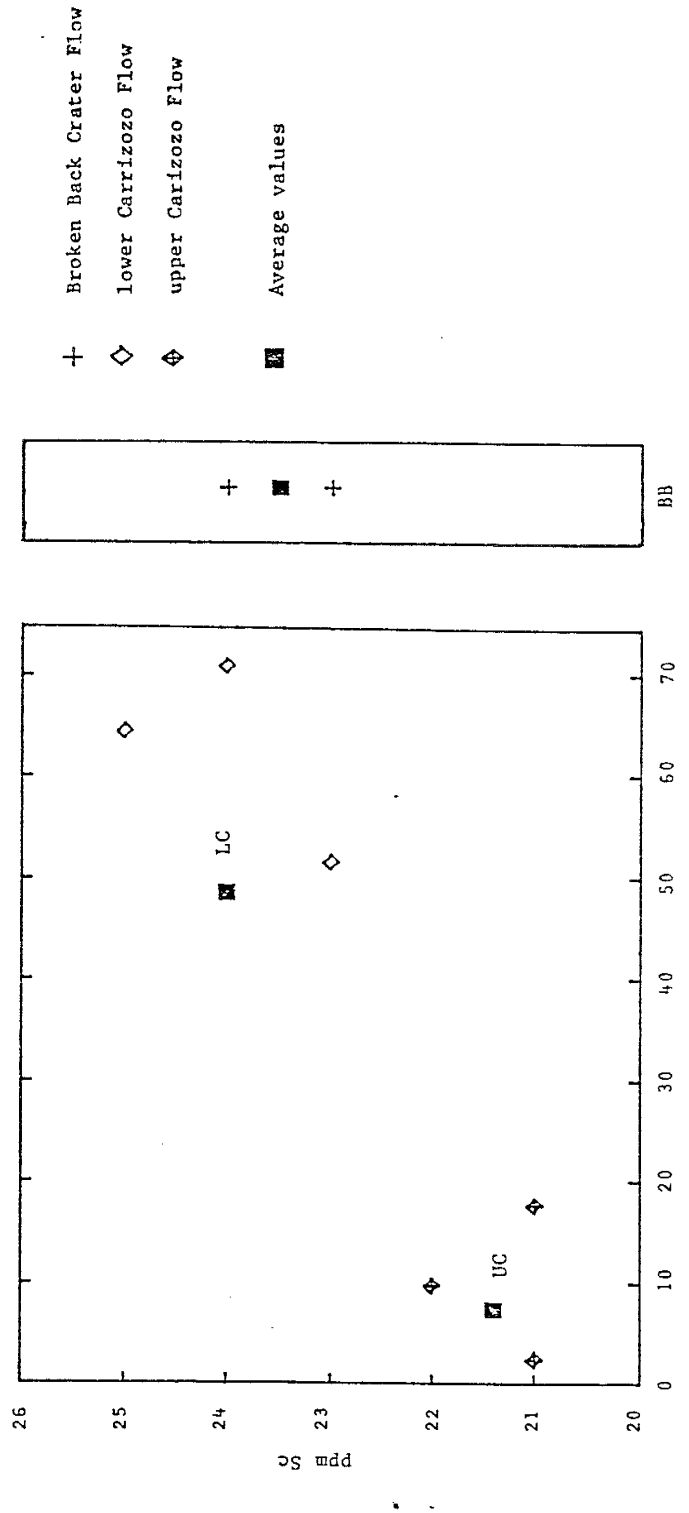

Figure 13. Sc variation in the flows of the Carrizozo Basalt Field.

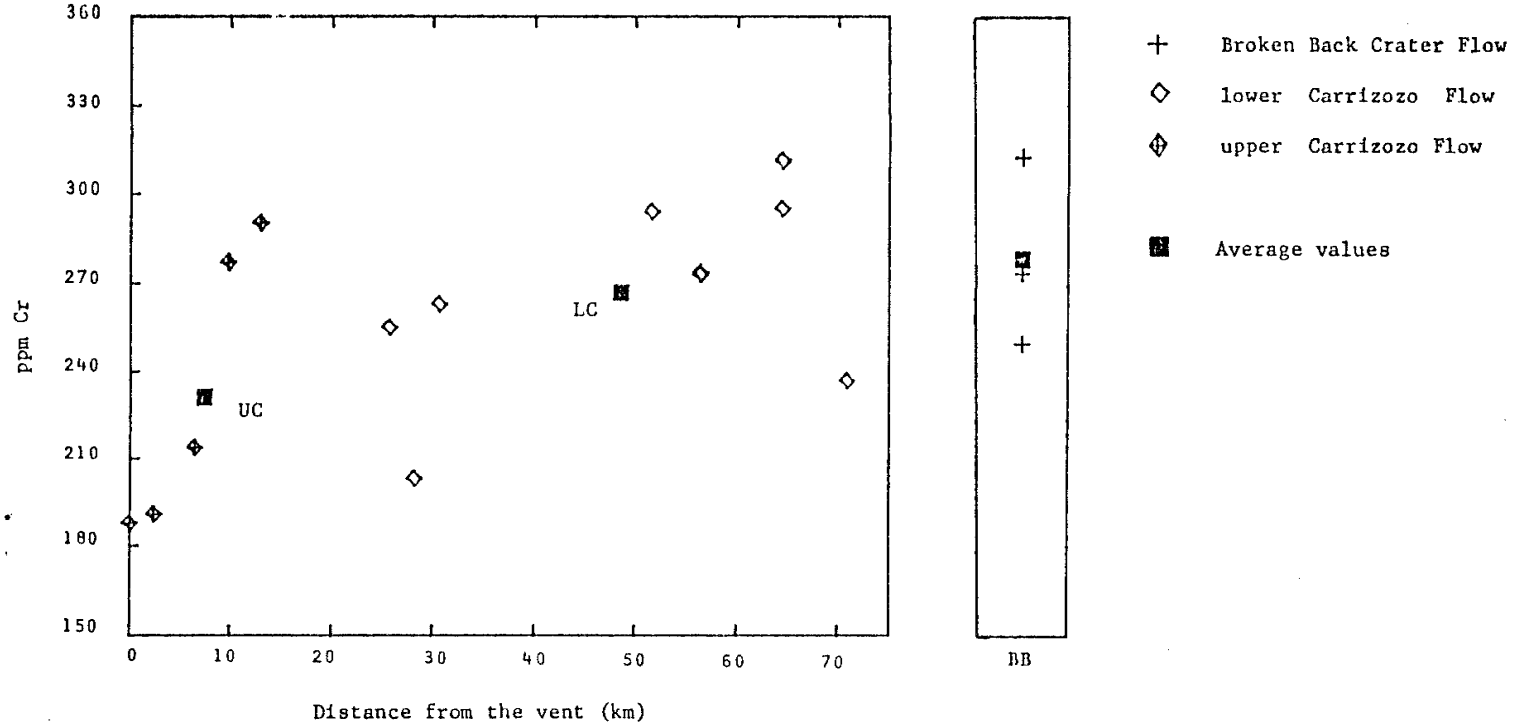

Figure 14. Cr variation in the flows of the Carrizozo Basalt Field.

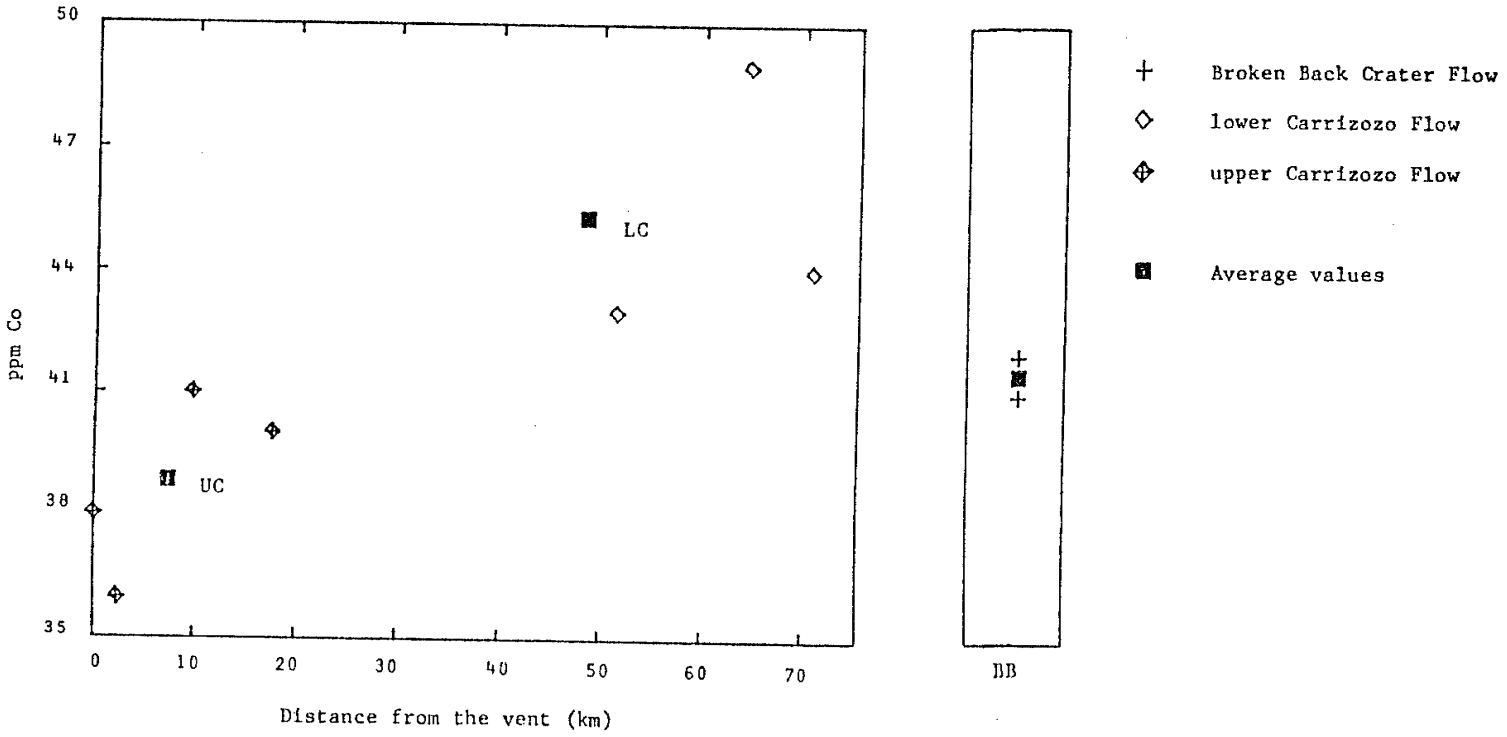

Figure 15. Co variation in the flows of the Carrizozo Basalt Field.

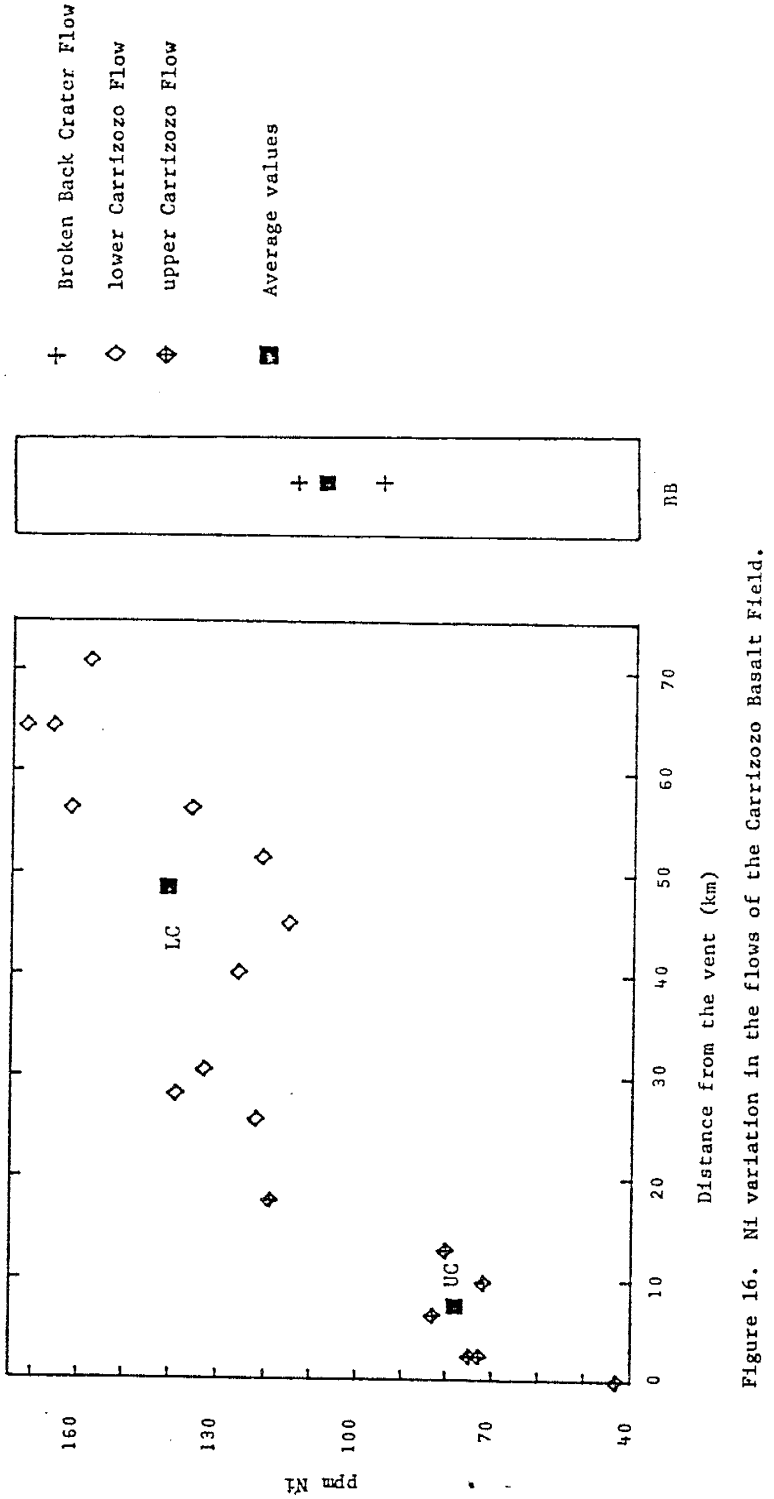

Figure 16. Ni variation in the flows of the Carrizozo Basalt Field.

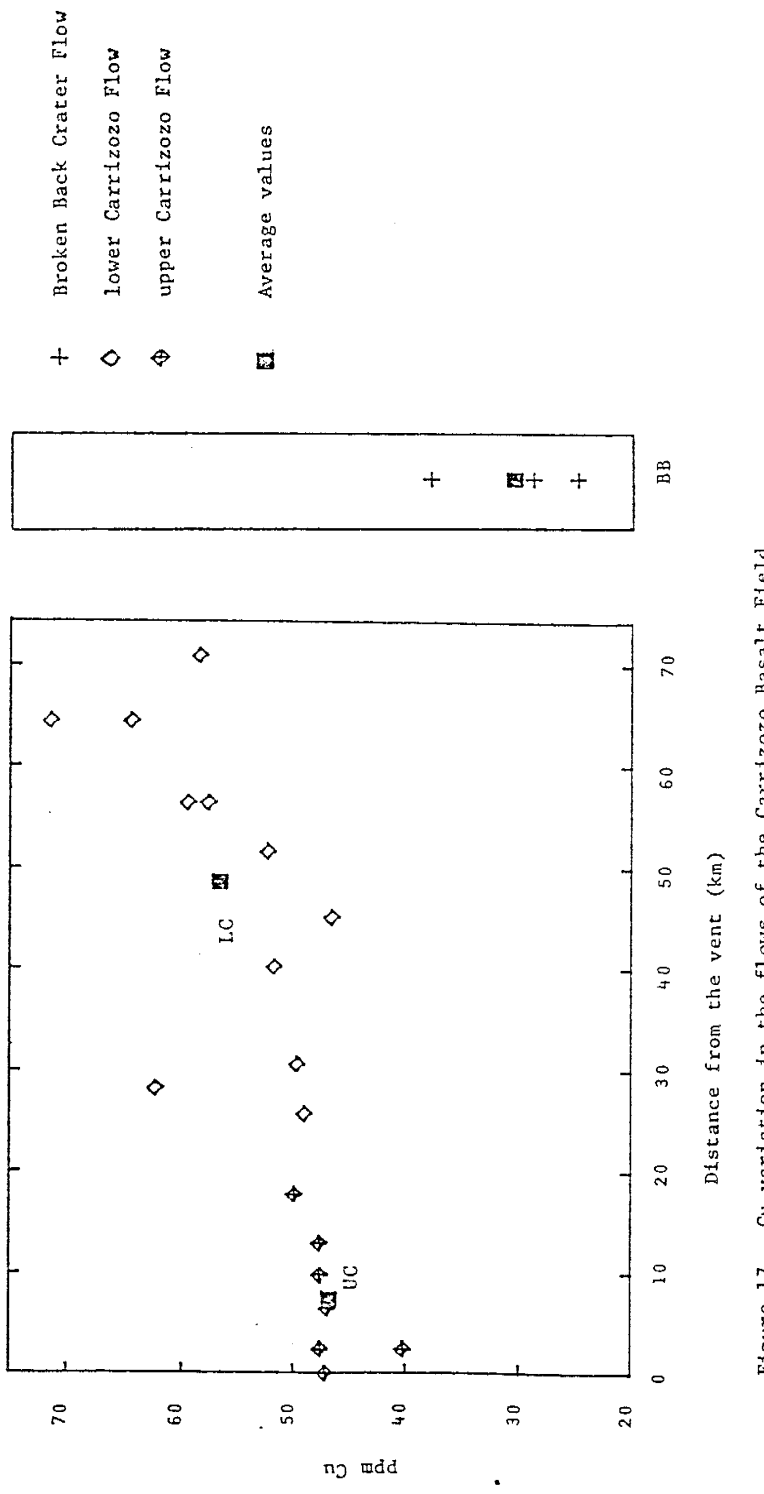

Figure 17. Cu variation in the flows of the Carrizozo Basalt Field.

GEOCHEMICAL MODELS FOR A MAGMATIC HISTORY

Fractional Crystallization and Partial Melting Processes

The concentration of a given element in a magma depends on the concentration of the element in the source of the liquid and the extent of chemical fractionation which occurs during melting and crystallization processes (Gast, 1968). Although it has been generally accepted that melting of an ultramafic mineral assemblage must be involved in the formation of basaltic liquids, there has been debate as to the relative importance of partial melting and fractional crystallization processes in controlling the chemical composition of basaltic lavas.

A number of writers (Engel and others, 1975; Green and Ringwood, 1967; O'Hara and Yoder, 1967) have proposed that fractional crystallization may be the dominant process controlling compositional variations in basalts, and that alkali- or potassium-rich liquids are derived by fractional crystallization from subalkaline or tholeiitic parent liquids.

However, following further studies of basalt genesis, with particular attention given to the concentration of large-ion lithophile (LIL) elements in alkalic basalts, many workers (Yoder and Tilley, 1962; Gast, 1968; Ringwood, 1975; Schilling, 1975) now believe that the composition of basalts is controlled in the region

of magma generation. Variations in basalt compositions can be accounted for by reasonable variation in the extent of partial melting of upper mantle sources; subsequent minor diversification may occur by fractional crystallization, oxidation or reduction, gas fluxing, or contamination.

Partial melting and fractional crystallization will be investigated as two possible processes involved in the evolution of the lavas of the Carrizozo Basalt Field. Evaluation of major and trace element data can place constraints on the nature of these processes, and the extent to which they may have operated in the production of these basalts.

Methods of Model Testing

Major elements

In order to estimate, on the basis of major element oxides, whether a proposed daughter liquid such as a flow of the Carrizozo Basalt Field could be derived from a proposed solid or liquid parent, a two-stage computer-based calculation developed by Wright and Doherty (1970) (called "MIXING" in the New Mexico Tech Computer Library) was used. In addition to other applications, this program was originally developed to solve a set of simultaneous scalar equations for "liquid line of descent" petrologic models. Given the composition of a differentiate, the suitability of

various magma types parental to that differentiate can be evaluated. For a fractional crystallization model the equations to be solved are of the form:

$$X_{par} = x_n y_n + \sum_{i=1}^{n-1} x_i y_i$$

where:

x = a chemically analyzed constituent of the system given as a weight fraction of the the oxide

X_{par} = the weight fraction of constituent x in the parent magma

x_i = the weight fraction of constituent x in the mineral i

y_i = the weight fraction of mineral i which is removed from the parent magma during fractional crystallization

x_n = weight fraction of constituent x in the differentiate (liquid produced as a result of removing minerals i to n-1)

y_n = the weight fraction of the liquid differentiate

Equations are formed for as many oxides as are needed to describe the composition of the system. In this study, equations are formed for nine oxides: SiO_2, TiO_2, Al_2O_3, FeO, MgO, MnO, CaO, Na_2O, and K_2O. A linear regression analysis can be applied to this overdetermined system (system having more equations than unknowns) to obtain a set of solution values. In petrologic problems, it is desirable to constrain solution variables to take only

non-negative values. Negative solution values cannot be prevented using a conventional linear regression analysis, so linear programming is used to circumvent this limitation.

Linear programming is designed to solve underdetermined linear systems (systems having more unknowns than equations). It is used when there are a large number of potentially negative solution values and it is only meaningful to accept non-negative values, such as the case where it is not known beforehand which magma types and minerals are relevent to a particular fractionation process. A linear programming model of the least squares problem is created by treating the residuals (the amount by which the equations of the system fail to be satisfied by the solution set for any given variable) as unknowns. An underdetermined system has an infinite number of solutions; linear programming is used to identify and reject negative solution values, which are called "prohibited solution values" in the computer output, then select from among the remaining solution sets the one that will minimize the sum of the squares of the residuals, i.e., provide the best fit in the least squares sense. The approximate solution provided is always followed by a conventional least-squares calculation in the computer program, which uses the analyses represented by non-negative solution values as input to yield an optimum set of solution values.

The results of the MIXING program can also be interpreted in terms of a partial melting model. The equations to be solved are of the same form as for the ractional crystallization model but in this case:

X_{par} = the weight fraction of constituent x in the parent rock

x_n = the weight fraction of constituent x in the daughter liquid (the liquid produced by melting of the parent rock)

y_i = the weight fraction of mineral i in the residue

y_n = the weight fraction of the daughter liquid

An example of the computer output is given in Figure 18 where "SP-1" is tested as a possible parent for a magma called "BB". The first part of the output is an echo of the input data which includes the chemical compositions of the proposed parent, daughter, and minerals which constitute the residue. Also, a set of weighting factors may be included as input data. Wright and Doherty (1970) use weighting factors which are proportional to the absolute standard deviation of the chemical analyses. The choice of weighting factors generally makes a small difference in the final result.

The echo of the input data is followed by the set of approximate solution values determined by linear programming. In this example, there are no negative solution values. The results of the linear regression analysis follow under the heading of "CALCULATED DATA". The

Figure 18. Sample of computer output from the "MIXING" program.

SP-1 >>> BB

INPUT DATA ACCEPTED

OXIDE	WEIGHT	SP-1	BB	+ oliv	+ opx	+ cpx	+ SPNL
SIO2	10.0	44.70	51.70	39.40	54.50	49.70	0.00
TIO2	5.0	0.16	1.76	0.00	0.26	0.55	0.00
AL2O	10.0	2.46	17.80	0.00	3.29	6.60	57.70
FEO	8.0	8.15	9.06	9.73	6.23	3.47	8.54
MNO	1.0	0.18	0.15	0.14	0.16	0.13	0.10
MGO	8.0	41.00	6.67	50.00	32.10	16.10	2.38
CAO	5.0	2.42	8.12	0.04	2.94	21.90	0.00
NA2O	4.0	0.29	3.40	0.00	0.03	0.21	0.00
K2O	4.0	0.09	1.54	0.00	0.00	0.00	0.00
TOTAL		99.45	100.20	99.31	99.51	98.66	68.72

SUM= 0.9815, SOLUTIONS= 0.06158 0.71182 0.13585 0.06651 0.00573

CALCULATED DATA

OXIDE	WEIGHT	CALC	DIFF	SP-1	BB	oliv	opx	cpx	SPNL
SIO2	10.0	43.00	-4.3%	44.95	51.60	39.67	54.77	50.38	0.00
TIO2	5.0	0.18	14.5%	0.16	1.76	0.00	0.26	0.56	0.00
AL2O	10.0	2.52	1.7%	2.47	17.76	0.00	3.31	6.69	83.96
FEO	8.0	8.85	8.0%	8.20	9.04	9.80	6.26	3.52	12.43
MNO	1.0	0.14	-20.6%	0.18	0.15	0.14	0.16	0.13	0.15
MGO	8.0	42.52	3.1%	41.23	6.66	50.35	32.26	16.32	3.46
CAO	5.0	2.45	0.7%	2.43	8.10	0.04	2.95	22.20	0.00
NA2O	4.0	0.23	-20.6%	0.29	3.39	0.00	0.03	0.21	0.00
K2O	4.0	0.10	6.5%	0.09	1.54	0.00	0.00	0.00	0.00
SOLUTIONS ARE					6.27%	72.52%	13.84%	6.78%	0.58%
SENSITIVITY					-1.38	0.31	-0.80	-1.14	1.05

column titled "CALC" shows the calculated composition of the parent, and the column titled "SP-1" shows the proposed composition of the parent (input data) recalculated to 100%; the column titled "DIFF" shows the percent difference between the two. The columns titled "oliv", "opx", "cpx", and "spnl" show the proposed compositions of the minerals expected to constitute the residue (input data) recalculated to 100%, from which the bulk composition of the residue can be calculated. The solution values can be interpreted as follows:

1) For a partial melting model: daughter liquid "BB" can be produced by ~6% melting of parent rock "SP-1"; residual minerals are olivine, ortho- and clinopyroxene, and spinel, occurring in the proportions of 72.5 : 14 : 7 : 0.5, respectively.

2) For a fractional crystallization model: daughter liquid "BB" can be produced by crystallizing ~94% of the parent magma "SP-1" (differentiate "BB" represents ~6% by weight of the parent magma); the residue has the same modal composition as for the partial melting model.

The error attached to each solution value is estimated by an empirical procedure which tests the

sensitivity of the residuals to small changes in the calculated solution values. "Sensitivity" values approaching zero indicate the least error.

The results of these calculations can be used to determine if various proposed processes and parents could have been involved in the production of various magmas based on major element chemical analyses; they are meaningful only when consistent with geological and petrological observations.

Trace elements

The following summary of trace element distribution behavior is taken from a discussion by Wood and Fraser (1978, pp. 195-224). Properties of many trace elements such as size, charge, and possible ligand field stabilization are quite different from those of the major constituents of the host phase. Small changes in the concentration of a trace component do not significantly affect the magmatic environment because of the low concentrations involved; the activities of trace components are directly proportional to their concentrations and are said to obey Henry's Law. The tendency for trace elements to be partitioned into crystalline phases or into melts during crystallization or melting processes may result in changes in concentration of these elements of several orders of magnitude. This tendency can be expressed in terms of a

"distribution coefficient" which is defined as the ratio of the concentration of an element in a specified solid phase to the concentration of that element in a liquid phase for a given set of temperature, pressure, and bulk composition conditions (see Appendix E). An understanding of the distribution behavior of trace elements permits their use as sensitive monitors of igneous evolution.

The Rayleigh (disequilibrium) fractionation law describes trace element distribution behavior during fractional crystallization when crystals fail to maintain equilibrium with the remaining melt, either because of slow diffusion in the crystal or because of crystal removal from the system. However, if crystals remain in contact with the melt, and if diffusion is sufficiently rapid for the interiors of the crystals to maintain equilibrium with the melt, then trace element distribution behavior is described by the equilibrium crystallization law.

The equations describing trace element distribution behavior during Rayleigh and equilibrium crystallization, and plots of changes in trace element concentrations against the extent of crystallization are shown in Figure 19. It can be seen from these plots that for a given degree of crystallization, Rayleigh fractionation is more efficient in changing trace element concentrations than is equilibrium fractionation and so represents a limiting case. In evaluating the role of

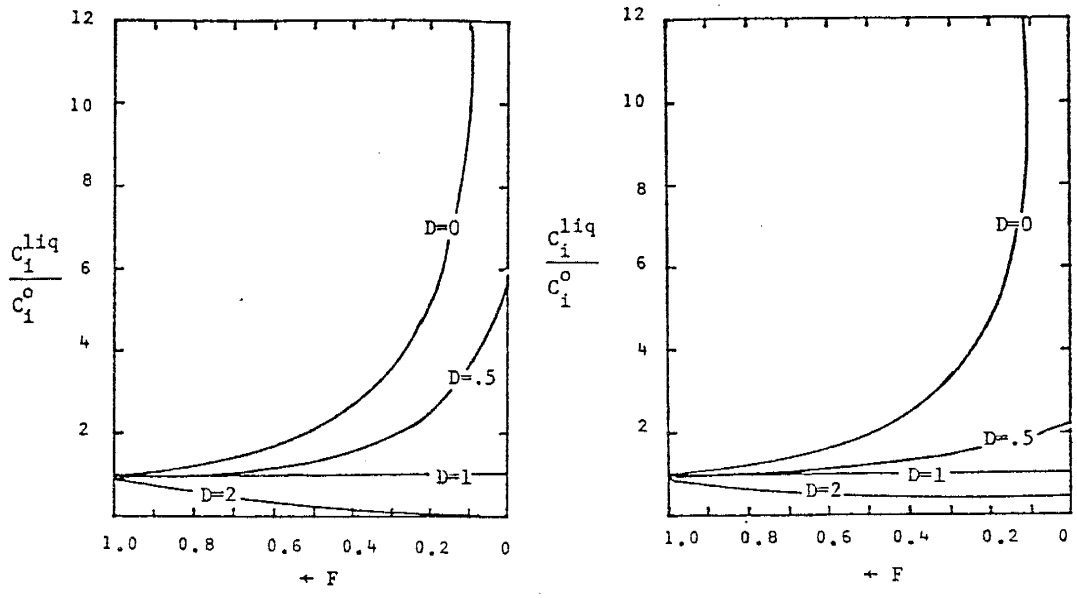

For Rayleigh fractionation:

$$C_i^{liq}/C_i^o = F^{D-1}$$

For Equilibrium fractionation:

$$C_i^{liq}/C_i^o = \frac{1}{D(1-F) + F}$$

where:

C_i^{liq} = concentration of trace element i in the daughter liquid

C_i^o = concentration of trace element i in the parent liquid

F = fraction of parent liquid remaining

D = (bulk) distribution coefficient for crystallizing mineral phases

Figure 19. Trace element distribution behavior during Rayleigh and equilibrium crystallization.

fractional crysallization in the production of the lavas of the Carrizozo Basalt Field, only the case of Rayleigh fractionation is considered because in this study, it is necessary to evaluate the maximum levels of enrichment or depletion of trace element concentrations possible by fractional crystallization; also, zoned plagioclase phenocrysts and corroded and embayed edges of olivine and plagioclase phenocrysts are observed, indicating that a disequilibrium condition between crystals and magma has existed.

For the partial melting process, four models of trace element distribution behavior are considered:

1) Equilibrium melting, where the melt is always in equilibrium with residual solid phases until it is removed;
2) Fractional melting, where the melt is removed as it is formed and is never in equilibrium with residual solid phases;
3) Fractional melting with collection of the melt, where:
   a. the melt is removed as it is formed and is collected in a mixing chamber where the composition of the melt in the chamber represents an average of all the increments collected;
   b. the melt is removed as it is formed and is collected in a magma chamber where no

mixing occurs and a compositionally-zoned chamber results.

Equations describing trace element distribution behavior with respect to these four cases, and plots of changes in trace element concentrations against the degree of partial melting are shown in Figure 20.

For the tests of partial melting models, it has been assumed that distribution coefficients remain constant throughout melting events, although evidence is accumulating which indicates that this is frequently not the case. This assumption has been made because knowledge about the quantitative dependence of distribution coefficients on temperature, pressure and the bulk composiion of solid and liquid phases is very fragmentary, making quantitative evaluation of these effects difficult. Also, this assumption is probably an acceptable approximation for models covering a small range of the degree of melting (Hertogan and Gijbels, 1976), as is the case in this study.

Appendix E contains the mineral distribution coefficients and the bulk distribution coefficients calculated from them which have been used in this study.

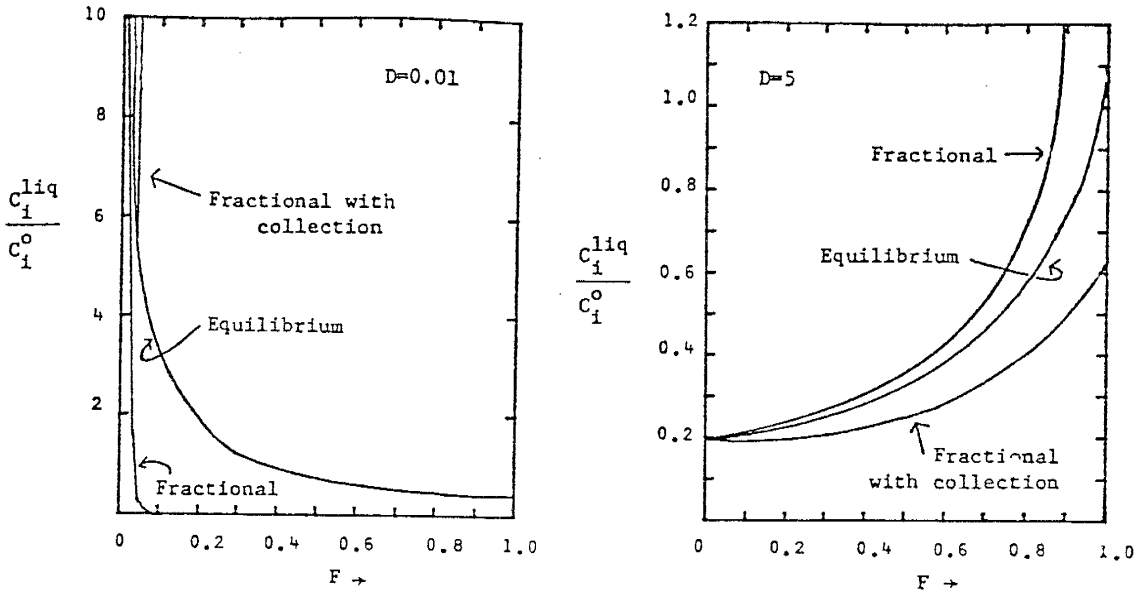

1. For Equilibrium Melting:

$$C_i^{liq}/C_i^o = \frac{1}{D + F(1-P)}$$

2. For Fractional Melting:

$$C_i^{liq}/C_i^o = \frac{1}{D}\left(1 - \frac{PF}{D}\right)^{(1/P - 1)}$$

3. For Fractional Melting with collection of the melt:

A. Collection in a chamber where mixing occurs:

$$C_i^{liq}/C_i^o = \frac{1}{F}\left[1 - \left(1 - \frac{PF}{D}\right)^{1/P}\right]$$

B. Collection in a chamber where little or no mixing occurs:

The equation describing fractional melting (Eq. 2 above) applies.

where:

C_i^{liq} = concentration of trace element i in the daughter liquid

C_i^o = concentration of trace element i in the parent mineral assemblage

F = fraction of melting

D = (bulk) distribution coefficient of the parent rock, weighted according to the modal proportions of the minerals involved

P = (bulk) distribution coefficient of the parent rock, weighted according to the eutectic melting proportions of the minerals involved

Figure 20. Trace element distribution behavior during partial melting.

Evaluation of the Dominant Process Involved

Fractional crystallization

Evidence for Differentiation

Various indices have been proposed as parameters to quantify the degree of differentiation of basaltic magmas. This differentiation broadly involves the fractional crystallization of two mineral groups: the mafic group (olivine, pyroxene, amphibole, and biotite) and the felsic group (chiefly feldspars) (Simpson, 1954). Indices discussed below include the Solidification Index (Kuno, 1957), the Crystallization Index (Poldervaart and Parker, 1964), and the Felsic and Mafic Indices (Simpson, 1954). values of these indices for the basalts in this study are given in Table 15.

The Solidification Index

Renault (1970) evaluated evidence for differentiation in the Carrizozo Basalt Field by means of the Solidification Index (SI). It was proposed by Kuno (1957) and is defined as

$$SI = (MgO \times 100) / (MgO + FeO + Na_2O + K_2O)$$

TABLE 15. Values of various differentiation parameters.

Broken Back Crater Flow

	SI	CI	FI	MI
CAR-12	32.40	44.10	38.52	58.60
CAR-13	35.09	46.04	36.60	55.90
CAR-14	30.09	44.53	38.39	61.21
MEAN	32.53	44.89	37.84	58.57
STD DEV	2.50	0.72	1.07	2.66

lower Carrizozo Flow

	SI	CI	FI	MI
CAR-15	29.27	43.63	36.10	62.79
CAR-16	32.76	47.69	34.13	59.59
CAR-17	32.39	45.25	36.29	59.37
CAR-18	31.58	45.45	36.10	60.43
CAR-19	30.42	44.70	35.76	61.87
CAR-21	32.76	46.81	34.83	58.60
CAR-22	32.90	45.29	35.14	59.08
CAR-24	33.74	45.88	35.74	57.71
CAR-25	31.45	42.87	37.96	59.62
CAR-26	33.82	45.64	35.37	57.87
CAR-27	33.24	45.56	36.95	57.94
MEAN	32.21	45.34	35.85	59.53
STD DEV	1.41	1.21	1.04	1.63

upper Carrizozo Flow

	SI	CI	FI	MI
CAR- 5	33.72	45.40	38.17	56.67
CAR- 6	30.46	42.90	38.27	60.89
CAR- 7	29.23	43.20	38.39	62.50
CAR- 8	28.83	42.51	36.64	63.56
CAR- 9	32.03	45.32	36.07	59.33
CAR-10	27.69	39.89	38.25	64.64
CAR-11	30.16	43.00	37.37	61.86
MEAN	30.30	43.02	37.67	61.35
STD DEV	2.04	1.65	0.80	2.69

SI = Solidification Index
CI = Crystallization Index
FI = Felsic Index
MI = Mafic Index

where the oxides are expressed in weight percents and the total iron concentration is expressed as FeO. The SI may be thought of as the percentage of MgO in an AFM diagram. SI values less than 35 imply that the sample is a product of differentiation of basic magma within the crust; values from 35-40 imply that the sample represents basic magma which has undergone little or no differentiation. SI values greater than 40 imply that the sample represents an olivine-rich residue. Values of the SI for the basalts under study are less than 35 (Table 15). At the 95% confidence level, the mean SI for the upper Carrizozo Flow is lower than the mean SI for the lower Carrizozo Flow. A plot showing the location of the Broken Back Crater, lower, and upper Carrizozo Flows on an AFM diagram is shown in Figure 21.

The Crystallization Index

Poldervaart and Parker (1964) propose the use of a parameter called the Crystallization Index (CI) to measure the progression of a system from the primitive system anorthite-diopside- forsterite:

$$CI = An + Di' + Fo' + Sp'$$

where:

Figure 21. AFM diagram (modified from Renault, 1970).

BB = Broken Back Crater Flow
LC = lower Carrizozo Flow
UC = upper Carrizozo Flow

Interpretation of SI values is from Kuno (1957).

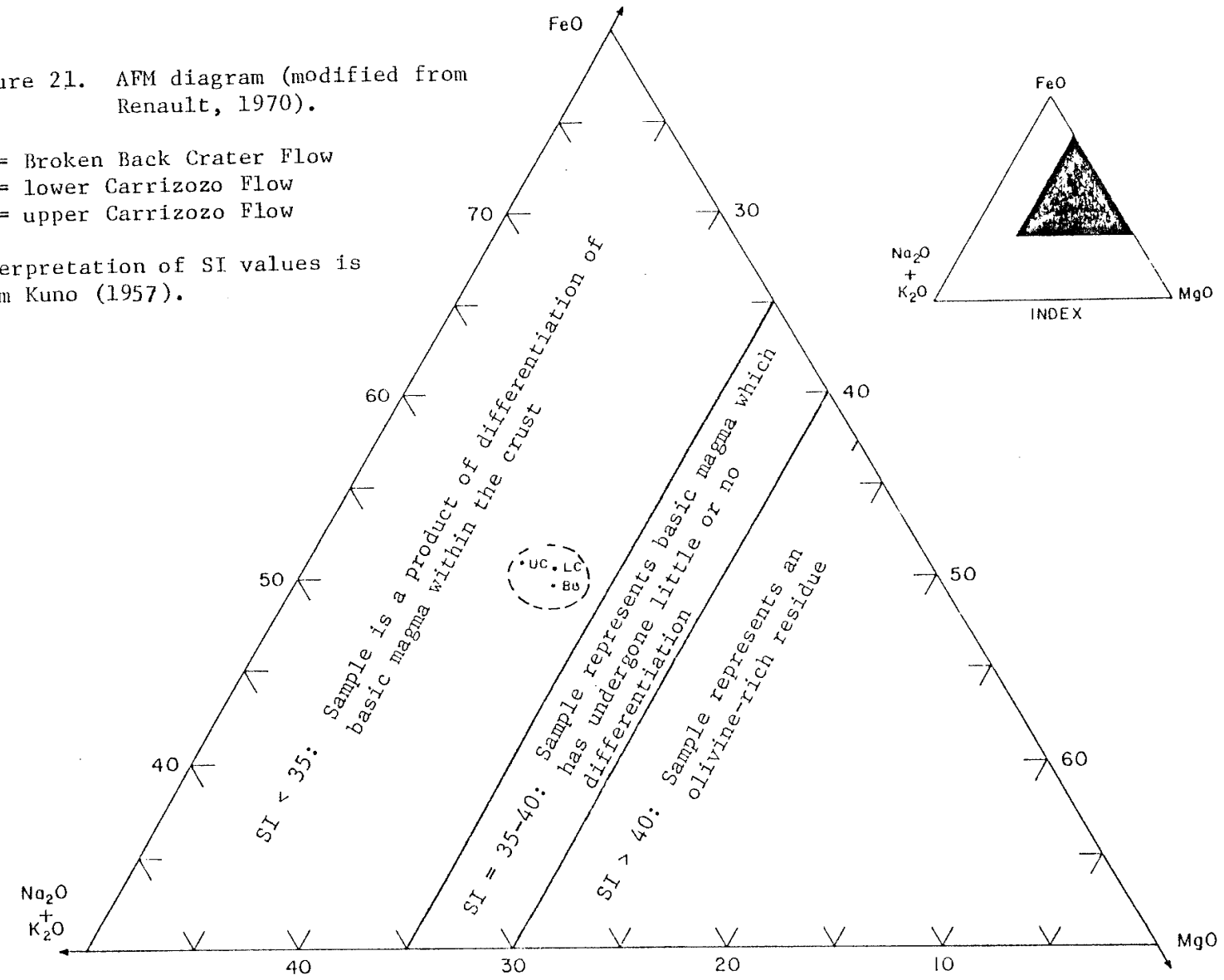

An = weight percent normative anorthite

Di′ = weight percent normative magnesian diopside

Fo′ = weight percent forsterite + normative enstatite converted to forsterite

Sp′ = weight percent magnesian spinel

Anorthite, diopside, forsterite, and spinel are thought to be the earliest phases of magmatic crystallization. The CI includes an expression for the fractionation of both the felsic and mafic reaction series and gives an indication of how far a magma has evolved from some initial composition. A decreasing trend of CI values implies an increasing degree of differentation of a basic magma. At the 95% confidence level, the mean CI for the upper Carrizozo Flow is lower than that of the lower Carrizozo Flow (Table 15). Plots of the CI against major oxide concentrations are shown in Figure 22.

The Felsic and Mafic Indices

The relative influence of the felsic and mafic mineral groups on the differentiation trend of basic magma can be evaluated by the Felsic Index (FI) and the Mafic Index (MI) defined by Simpson (1954) as:

$$FI = (Na_2O + K_2O) \times 100 / (CaO + Na_2O + K_2O)$$

$$MI = (FeO + Fe_2O_3) \times 100 / (MgO + FeO + Fe_2O_3)$$

Figure 22. Crystallization index (CI) vs. major oxide weight percentages.

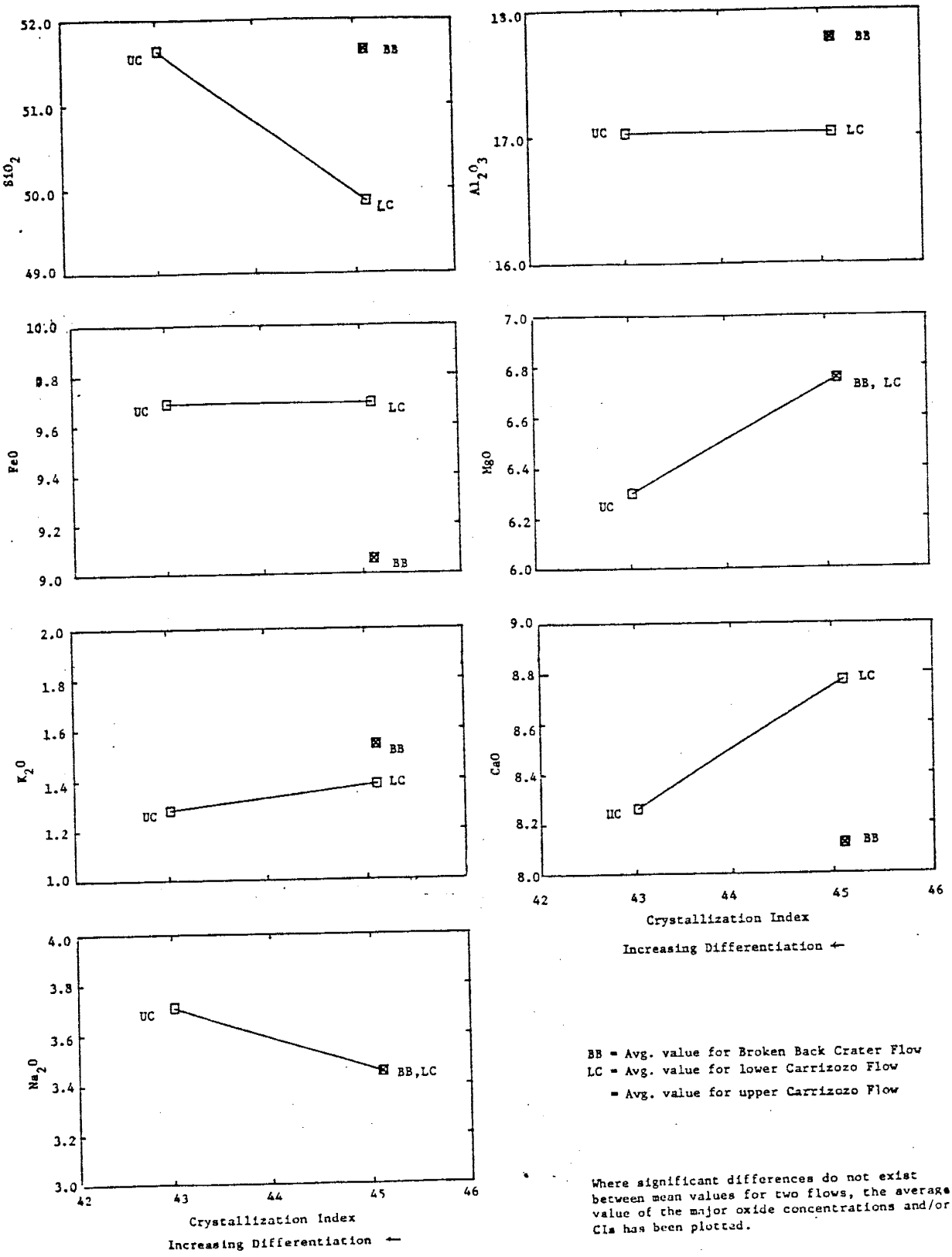

BB = Avg. value for Broken Back Crater Flow
LC = Avg. value for lower Carrizozo Flow
= Avg. value for upper Carrizozo Flow

Where significant differences do not exist between mean values for two flows, the average value of the major oxide concentrations and/or CIs has been plotted.

where the oxides are expressed in weight percents. An increasing trend of FI and MI values implies an increasing degree of differentiation of a basic magma. At the 95% confidence level, the mean MI for the upper Carrizozo Flow is greater than that of the lower Carrizozo Flow (Table 15). Plots of the MI against major element oxide concentrations are shown in Figure 23. When the effects of felsic and mafic mineral group fractionation are balanced, the rock series developed will be represented by a straight line at a 45 degree angle to the abscissa on a FI vs. MI plot. It can be seen from Figure 24 that the basalts of this study plot in the field where fractionation would be dominated by minerals of the mafic series.

Summary

Before considering evidence for differentiation provided by these indices, it should be noted that the observed decrease in K_2O concentration with decreasing age of the flows is not consistent with a simple differentiation model, as K_2O would not be effectively removed from a magma until the crystallization of orthoclase. Therefore, some other process, other than or dominating fractional crystallization, must be called upon to produce the observed trend of K_2O concentrations. The expressions to evaluate the Solidification and Felsic Indices include potassium, and therefore evidence for differentiation in the Carrizozo Basalt Field provided by these indices may not be valid.

Figure 23. Mafic index (MI) vs. major oxide weight percentages.

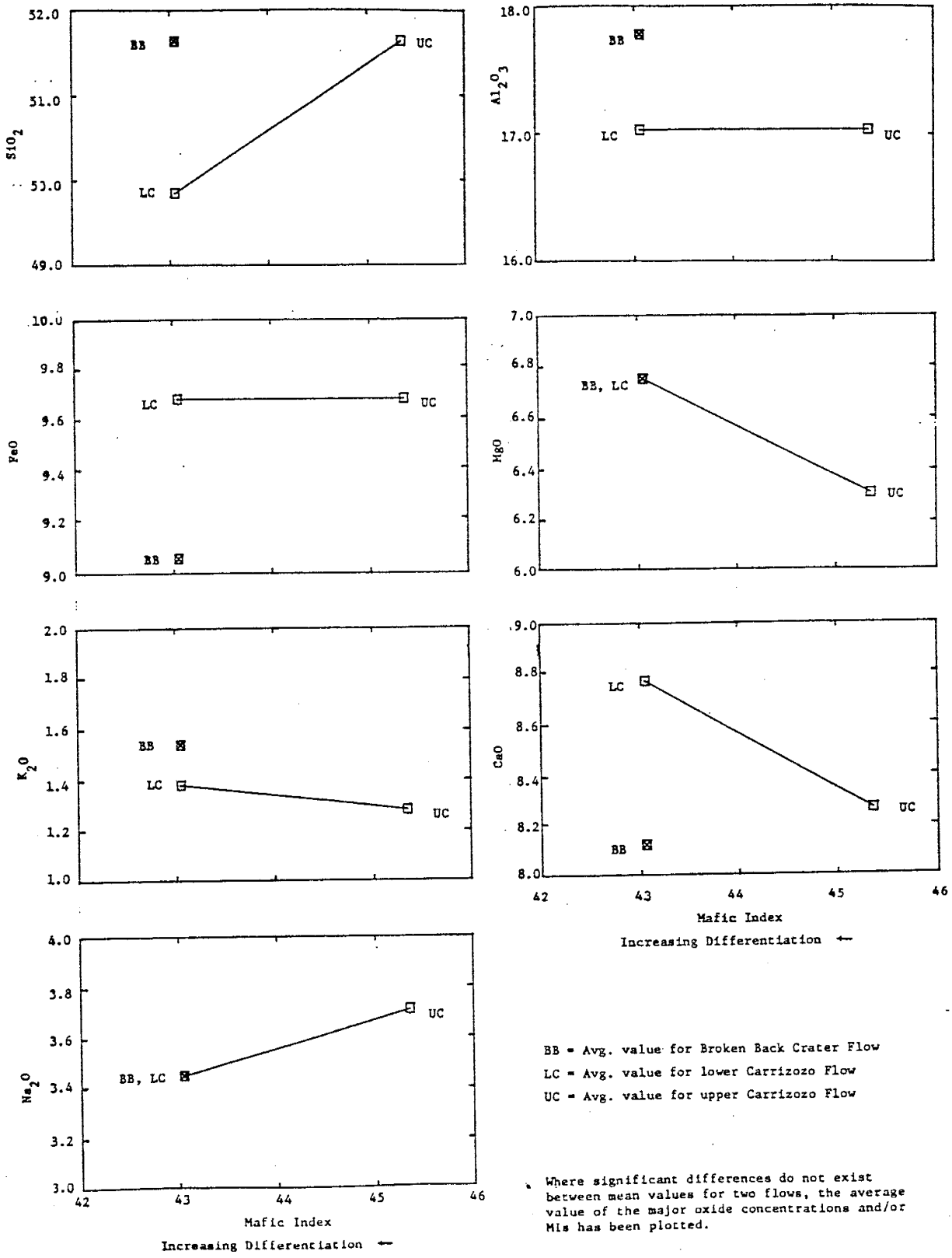

BB = Avg. value for Broken Back Crater Flow
LC = Avg. value for lower Carrizozo Flow
UC = Avg. value for upper Carrizozo Flow

* Where significant differences do not exist between mean values for two flows, the average value of the major oxide concentrations and/or MIs has been plotted.

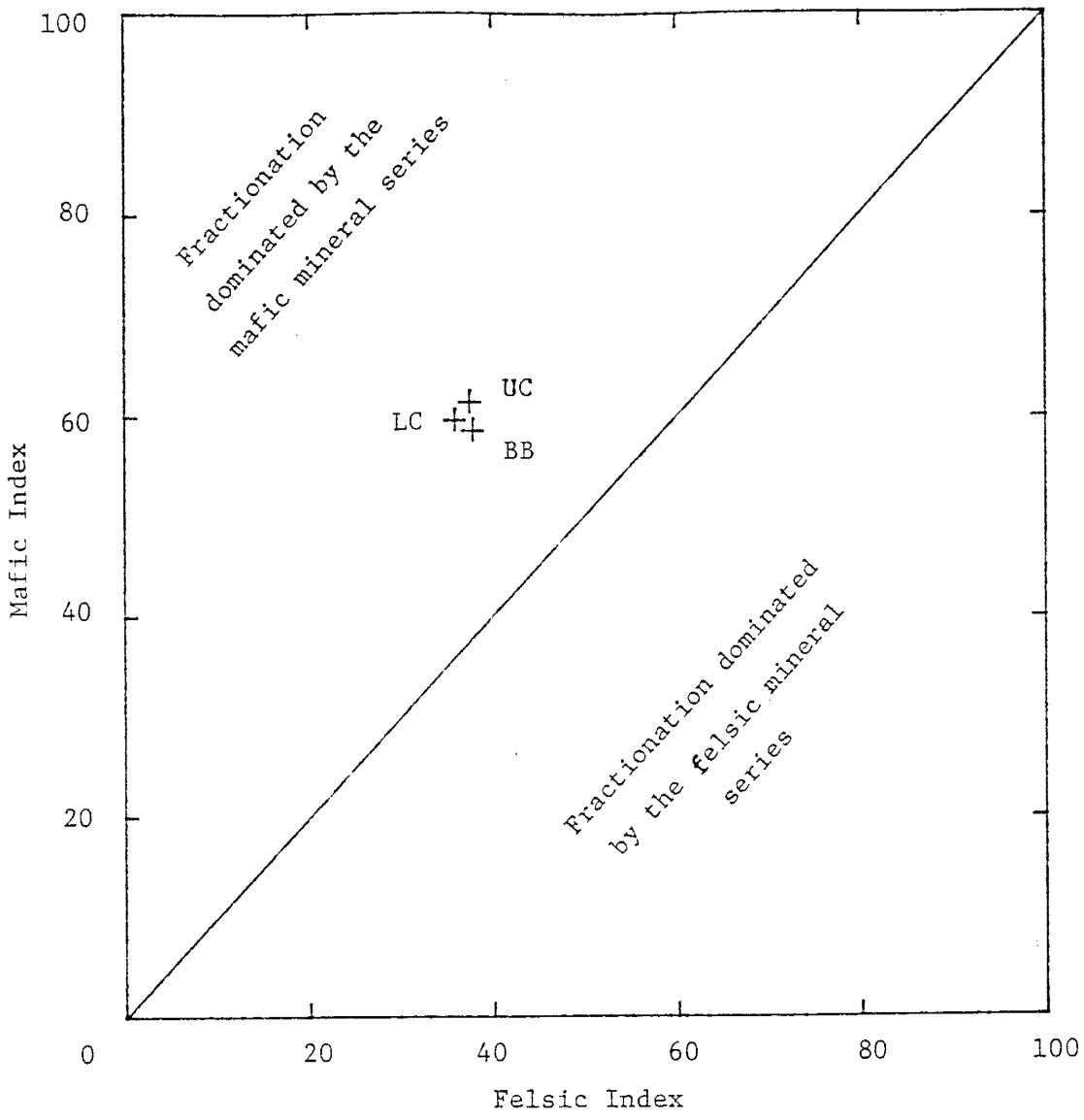

Figure 24. Felsic Index (FI) vs. Mafic Index (MI).

Samples from the Carrizozo Basalt Field plot in the field where fractionation would be dominated by minerals of the mafic series (Simpson, 1954).

If chemical variations within the flows of this study are to be interpreted as differentiation trends, then evidence provided by the Crystallization and Mafic Indices may be examined. Differences in the average values of the CI and MI between the lower and upper Carrizozo Flows exist at the 95% confidence level, and indicate that the upper Carrizozo flow may be more differentiated than the older lower Carrizozo Flow. No statistically significant differences exist between the Broken Back Crater and lower Carrizozo Flows, which may indicate that the lower Carrizozo Flow is not more differentiated than the older Broken Back Crater Flow. If fractional crystallization has occurred, then minerals of the mafic series may have been involved (Figure 24).

Results of Major and Trace Element Tests

Green and Ringwood (1967) propose that basaltic magmas with significant LIL element enrichment can be derived by fractional crystallization of a parent magma produced by partial melting of a mantle source. For various petrographic and chemical reasons, they chose an olivine tholeiite as the composition of this parent magma. In addition to the composition of Green and Ringwood's (1967) proposed olivine tholeiite, the compositions of average continental rift tholeiites and average island tholeiites (Condie, 1976a and 1976b) were tested as possible parent magmas of the lower Carrizozo Flow.

The effects of fractionation at various depths based on experimental results by Green and Ringwood (1967) are summarized in Table 16 and indicate that high-alumina olivine tholeiites are produced by fractionation of olivine, ortho- and clinopyroxene at depths of 15-35 km, and that olivine-rich alkalic basalts are produced by fractionation dominated by the separation of Al-rich orthopyroxene, or orthopyroxene and subcalcic augite, at depths of 35-70 km. Because the basalts of this study are compositionally transitional between olivine tholeiites and alkalic basalts, models 2 and 3 (Table 16) were tested. The chemical analyses of proposed parent magmas and minerals involved in fractionation, and the results of major element least-squares fits are given in Appendix F. Of the parent magmas tested, only the average continental rift tholeiite composition is reasonably compatible with a fractional crystallization model to produce the lower Carrizozo Flow as less than 12% fractional crystallization is required for all models tested (compared with up to 92% fractional crystallization required for the other proposed parents) and computed sensitivites (errors) are significantly lower for this proposed parent composition. A summary of major element least-squares fits assuming an average continental rift tholeiite parent composition is given in Table 17. Models 2c and 3a are preferred as no minerals expected to be involved in fractionation based on experimental results are prohibited by linear programming (Table 17).

Table 16 . Experimentally determined liquidus phases and fractionation trends for olivine tholeiite.

	Model 1: Fractionation at 15 km	Model 2: Fractionation at 15-35 km	Model 3: Fractionation at 35-70 km
Pressure (kb)	4.5	9	13.5 and 18
Fractionation trend	to Fe-enriched quartz tholeiites (normal alumina contents)	to-high alumina olivine tholeiites	to olivine-rich alkalic basalts
Liquidus phases	A) ol,plag, and cpx at < 1220°C B) ol and plag at 1220-1260°C C) ol at 1260-1340°C	A) ol; opx, and cpx at < 1230°C B) ol and opx at 1230-1250°C C) ol at 1250-1290°C	at temperatures in the range of 1350-1400°C, fractionation is dominated by the separation of A) Al-rich opx or B) opx and sub-calcic augite

from Green and Ringwood, 1967

Table 17. Summary of major element least squares fit results for a fractional crystallization model assuming a parent liquid of average continental rift tholeiite[1] composition.

Model	Depth (km)	Temperature	Expected residual minerals[2]	Production of the lower Carrizozo flow requires the removal of:	"Prohibited" residual minerals	"Sensitivity"
2a	15-35	<1230°C	ol, opx, cpx	∿12% cpx (F = 0.88)	ol, opx	≤1.78
2b	15-35	1230-1250°C	ol, opx	∿ 7% opx (F = 0.93)	ol	≤1.88
2c	15-35	1250-1290°C	ol	∿ 3% ol (F = 0.97)	-	≤1.51
3a	35-70	1350-1400°C	opx	∿ 6% opx (F = 0.94)	-	≤1.98
3b	35-70	1350-1400°C	opx, cpx	∿12% cpx (F = 0.88)	opx	≤1.91

1. Condie, 1976, p. 148.
2. Based on the experimental results of Green and Ringwood, 1967.

F = the weight % of melt remaining

All five models listed in Table 17 were tested in terms of trace elements assuming an average continental rift tholeiite parent composition; the results are summarized in Table 18. None of the models can provide the levels of enrichment of LIL elements such as K, Sr, Ba, U, and Th that are observed in the lower Carrizozo Flow. According to the Rayleigh fractionation law, enrichment factors increase as the distribution coefficient approaches zero. Even when the distribution coefficient is assumed to equal zero, 25-50% fractional crystallization would be required to produce the observed enrichment factors for K, Sr, and Ba; even greater degrees of fractional crystallization would be required in the cases of U and Th.

With the fractional crystallization of mafic minerals such as olivine, and ortho- and clinopyroxene, the concentrations of transition metals such as Cr, Co, and Ni would be expected to show concentration decreases in the daughter liquid relative to the parent liquid. An opposite trend is noted here (Table 13 and Appendix F-1).

REE were not quantitatively tested in terms of a fractional crystallization model as the suggested concentrations in the parent liquid (Appendix F-1) are higher than those in the proposed daughter liquid (Table 10) and an opposite relation would be expected. This observation indicates that although a parent liquid of average continental rift tholeiite composition might be acceptable

Table 18. Summary of trace element results for a Rayleigh fractionation model assuming a parent of average continental rift tholeiite (CRT)* composition.

	EF_{obs}	$EF_{2a,3b}$	EF_{2b}	EF_{2c}	EF_{3a}	Required % fractional crystallization to produce EF_{obs} assuming D = 0
K	2.1	1.1	1.1	1.0	1.1	∿50
Sr	1.3	1.1	1.1	1.0	1.1	∿25
Ba	2.0	1.1	1.1	1.0	1.1	∿45
U	3.4	1.1	1.1	1.0	1.1	∿70
Th	2.2	1.1	≠	1.0	≠	∿55
Cr	1.7	1.0-0.3 (D = 1-10)	0.9-0.2 (D = 2-8)	1.0	0.9-0.2 (D = 2-8)	
Co	1.2	1.1-0.8 (D = 0.5-3)	1.0-0.7 (D = 1-5)	1.0-0.7 (D = 1-10)	1.0-0.7 (D = 1-5)	
Ni	1.5	1.0-0.3 (D = 1-10)	1.0-0.5 (D = 1-10)	1.0-0.2 (D = 1-50)	1.0-0.6 (D = 1-10)	

EF = enrichment factor: ratio of the concentration of an element in the daughter liquid to the concentration of an element in the parent

EF_{obs} = "observed" enrichment factor assuming the average composition of the lower Carrizozo flow as a daughter liquid (see Tables 1, 11, 13, and 15)

$EF_{2a}(etc)$ = "calculated" enrichment factors based on the Rayleigh fractionation law and F values suggested by major element least squares fits (see Table 21)

* See Appendix G and Condie, 1976a, p. 148
≠ no value of D available for Th in orthopyroxene

in terms of major element least-squares fit results, it is not acceptable in terms of REE data.

If fractional crystallization was the dominant process operating to produce the basalts of this study, then additional processes such as wall-rock reaction (Green and Ringwood, 1967), volatile transfer (Engel, 1965), or crustal contamination must be called upon to produce the observed levels of LIL element enrichment. However, Gast (1968) has shown that wall-rock reaction is not a reasonable explanation, and that volatile transfer would not be expected to enrich Ba, La, U, and Th to the degrees observed. Within the Rio Grande rift, $^{87}Sr/^{86}Sr$ ratios are low (0.703 to 0.704; Stinnett, 1976) and vertical fracturing is extensive (Reiter and others, 1979), thus crustal contamination is not likely to have altered the composition of these basalts to any great extent. Also, if fractional crystallization was the dominant process operating in the production of these basalts, then K_2O concentrations would be expected to show an increase with decreasing age of the flows as K_2O is not effectively removed from a magma until the crystallization of orthoclase. An opposite trend is noted in the flows of the Carrizozo Basalt Field.

In light of these observations, the process of fractional crystallization is considered to have been of minor importance in the evolution of the basalts of this study.

Partial melting

Composition of the Parent Rock

In a partial melting model, any mineral assemblage which is to be considered as a possible parent for the basalts of this study must be able, upon melting, to directly yield a liquid similar in composition to these basalts, or to yield a liquid from which a liquid similar in composition to these basalts could be derived at or near the earth's surface. Many workers (Kushiro and Kuno, 1963; Gast, 1968; Ringwood, 1975; Yoder, 1976) believe that basalts represent partial melting products of upper mantle mineral assemblages. Peridotite and eclogite are the two mineral assemblages which are in the range of upper mantle densities and p-wave velocities; both rock types occur in the upper mantle as is evidenced by their appearances as zenoliths in kimberlite and nephelinite diatremes (Carmichael and others, 1974, p. 340).

Eclogite

There is abundant evidence to indicate that eclogite is present in the uppermost mantle (Anderson, 1979). Geophysical evidence cannot rule out models of a coarsely heterogeneous eclogite-peridotite mantle, or of regular or random lithologic variations within a large-scale

homogeneous mantle (Carmichael and others, 1974, p. 341). However, eclogite is not considered to be a likely source for the basalts of this study and was not tested quantitatively as such for two reasons. First, in a hypothetical eclogite-peridotite portion of the mantle, at certain depths eclogite would be expected to melt at a higher temperature than would peridotite (Yoder, 1976, p. 20). Secondly, O'Nions and Clark (1972) considered the partial melting of lherzolite with 5% garnet, and computed La/Yb ratios that fall from 20 to 6 over a 5-10% melting interval; partial melting of eclogite, which would contain a greater percentage of garnet, would show an even greater range of La/Yb ratios. La/Yb ratios in the basalts of this study range from ~8 to 6 over this assumed melting interval.

Peridotite

There is abundant evidence to indicate that peridotite is an important phase in the uppermost mantle:

1) It has appropriate densities and seismic velocities (Yoder, 1976, p. 43);
2) Anhydrous peridotite mineral assemblages are experimentally stable over the entire possible temperature-pressure regimes of the upper mantle (Carmichael and others, 1974, p. 340);
3) At high pressures, partial melts of natural

samples have basaltic compositions (Yoder, 1976, p. 34);

4) If a heterogeneous eclogite-peridotite upper mantle exists, then peridotite would tend to become concentrated upward towards the Moho, as its density is lower than that of eclogite, and it has an experimentally demonstrated capacity for plastic flow in the solid state (Carmichael and others, 1974, p. 341).

The peridotite mineral assemblage is composed chiefly of olivines and pyroxenes, but also may include accessory minerals such as plagioclase, spinel, and garnet. The type of accessory mineral present is of course dependent on the existing temperature and pressure conditions at depth. Aluminum not accommodated by pyroxene is accounted for by anorthite at depths less than 30 km (9 kb), by spinel at depths of 30-50 km (9-16 kb), and by garnet at depths greater than 50 km (16 kb) (Yoder, 1976, p. 28), as is shown in Figure 25.

Plagioclase peridotite is not considered to be a likely parent rock for the basalts of this study as the crust-mantle boundary is at a depth of about 35 km (10 kb) under the Rio Grande rift, hence plagioclase peridotite is probably not present (Baldridge, 1979). Also, partial melting of assumed plagioclase peridotite sources would not produce, even at very small degrees melting, the levels of Sr enrichment observed in the lavas of this study.

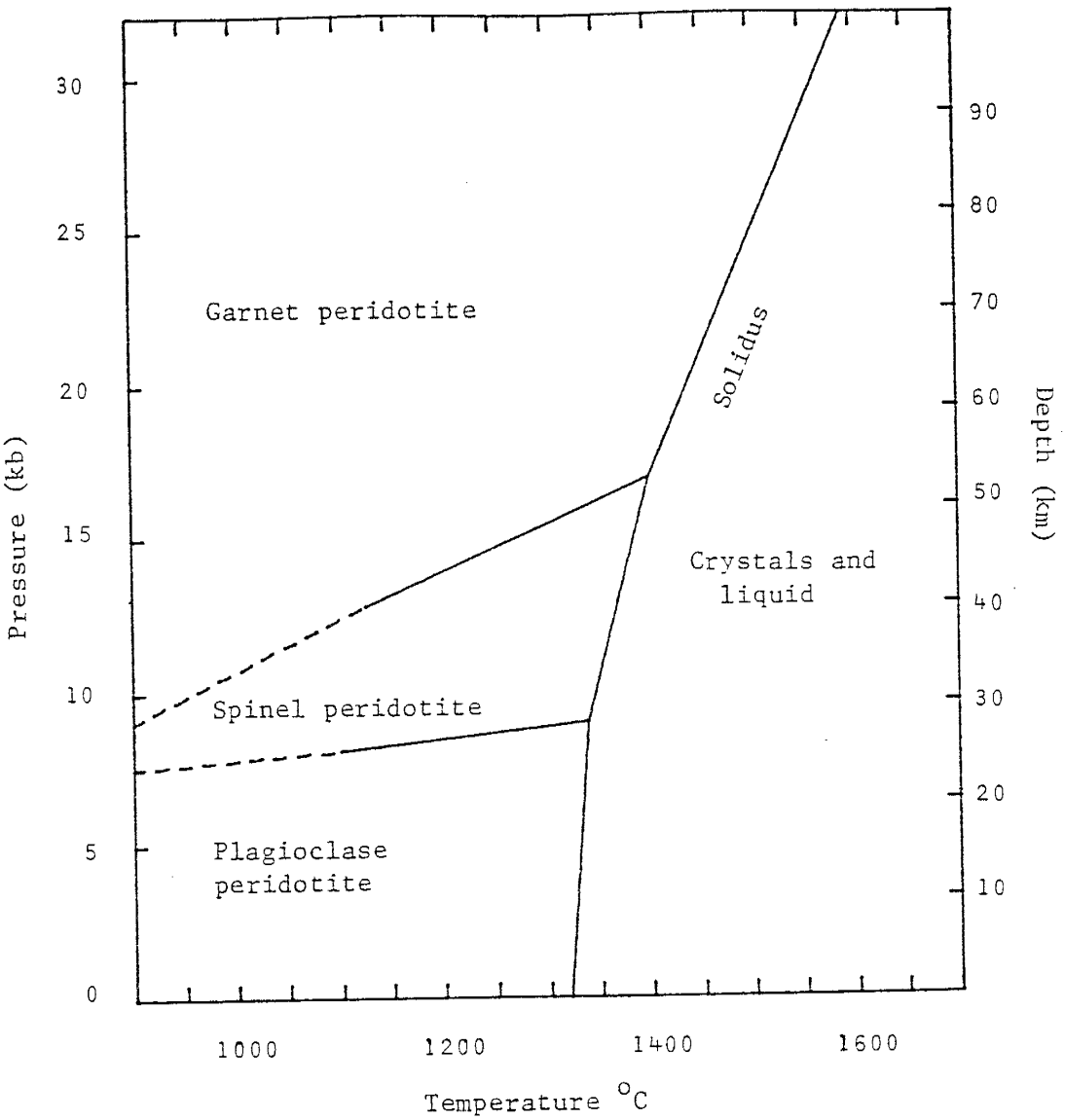

Figure 25. Generalized assemblage diagram for various peridotites based on experimental data. Depth scale is based on an average density of 3.2 g/cm^3. Modified from Yoder (1976, p. 28).

The degree of fractionation of light from heavy REE can be used to make a distinction between a possible spinel or garnet peridotite parent. Upon partial melting, both assemblages produce liquids in which concentrations of light REE are enriched with respect to heavy REE. However, this enrichment is more pronounced in liquids produced by melting of a garnet- bearing assemblage than by a spinel-bearing assemblage, due to the large distribution coefficient values of heavy REE in garnet. The calculated La/Yb enrichment factors that result from melting spinel and garnet peridotite are shown in Figure 26. If the parent rock for the basalts of this study was enriched in REE with respect to chondrites, then the La/Yb ratios of these basalts would be less than 5X the La/Yb ratios of the parent. Figure 26 shows that the degree of La/Yb fractionation in the lavas of the Carrizozo Basalt Field is much more consistent with < 10% melting of spinel peridotite than it is with melting of a garnet peridotite parent. Gast (1968) made similar comparisons between calculated and observed REE ratios in basalts, and suggested that alkali and undersaturated basalts are not derived from garnet peridotites. Other results, based on major element data, argue against garnet peridotite acting as a source for the basalts of this study. For example, for some assumed compositions of garnet peridotite, less than 1% melting would be required to produce these lavas (Table 19).

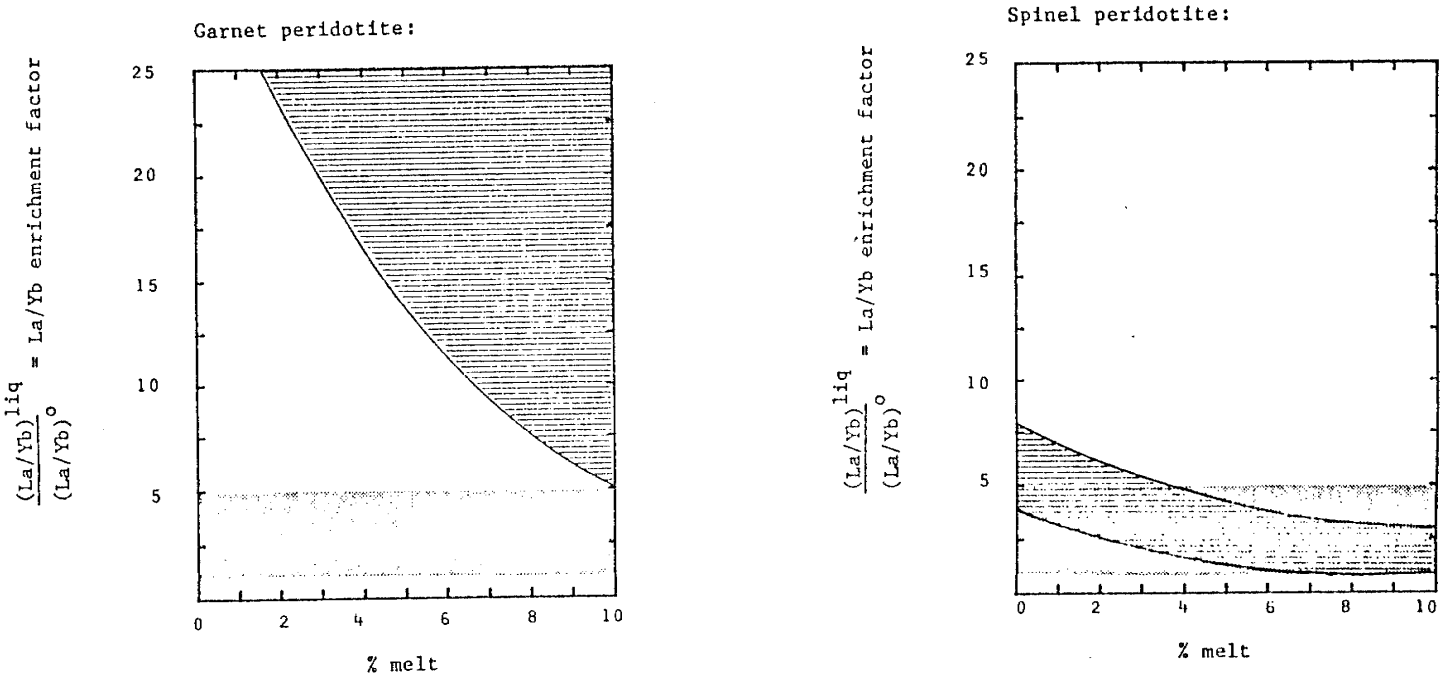

Calculations are based on the removal and collection of melt model (see Figure 21). The bulk distribution coefficients used in the calculations are given in Appendix E-4.

For garnet peridotite: Lower boundary of predicted range calculated assuming the modal and eutectic composition of GPER-B (see Appendix G-3); upper boundary is not shown.

For spinel peridotite: Lower boundary of predicted range calculated assuming the modal and eutectic composition of SPER-A (see Appendix G-3); upper boundary calculated assuming the modal and eutectic composition of SPER-B (see Appendix G-3).

Figure 26. Fractionation of La and Yb during partial melting of garnet and spinel peridotite.

Table 19. Summary of major element least-squares fits for a partial melting model.

Proposed Parent	Proposed residual minerals	Calculated % melting required to produce lower Carrizozo Flow	Calculated "prohibited" residual minerals	Calculated composition of residue based on least-squares fit	Calculated composition of residue based on eutectic melting proportion assumptions*
Pyrolite[1]	ol opx cpx[4]	15	-	59% ol 36% opx 5% cpx	67% ol 25% opx 8% cpx
Plagioclase peridotite (pyrolite)[1]:	ol opx cpx[4] plag[5]	15	plag	59% ol 36% opx 5% cpx 0% plag	58% ol 18% opx 15% cpx 9% plag
Spinel peridotite: pyrolite[1]	ol opx cpx[4] spin[4]	15	spinel	59% ol 36% opx 5% cpx 0% spin	74% ol 24% opx 0% cpx 2% spin
average spinel peridotite[2]	ol opx cpx[4] spin[6]	7	-	77% ol 16% opx 6% cpx 1% spin	70% ol 24% opx 4% cpx 2% spin
Garnet peridotite: pyrolite[1]	ol[3] opx[7] cpx[4] gar phlog	15	gar phlog	56% ol 36% opx 7% cpx	67% ol 32% opx 0% cpx
garnet peridotite[3]	ol[3] opx[7] cpx[4] gar phlog[3]	<1%	-	44% ol 46% opx 7% cpx 1% gar 2% phlog	63% ol 30% opx 2% cpx 5% gar <1% phlog

1. Ringwood, 1975, p. 188.
2. Maaloe and Aoki, 1977.
3. Carswell and Dawson, 1970.
4. Ernst and Piccardo, 1979.
5. Deer and others, 1966, p. 324.
6. Deer and others, 1963, v. 5, p. 65.
7. Deer and others, 1963, v. 2, p. 17.

ol = olivine
opx = orthopyroxene
cpx = clinopyroxene
gar = garnet
phlog = phlogopite

Compositions of proposed parents and residual minerals are tabulated in Appendix G.

* Eutectic melting proportion assumptions are given in Appendix G.

Results are calculated by the method of Wright & Doherty (1970) using the program "MIXING" in the New Mexico Tech Computer Library.

Major element least-squares fit results show that some of the spinel peridotite compositions tested are not likely to have served as parent rocks for the flows of the Carrizozo Basalt Field (Table 19 and Appendix G). However, Table 20 shows that 4-6% melting of upper mantle spinel peridotite (Maaloe and Aoki, 1977; see Appendix G-1) may well have been able to do so. These results correlate with Baldridge's (1978, 1979) suggestions that spinel peridotite inclusions from various locations along the Rio Grande rift (Kilbourne Hole, NM: Carter, 1970 and Reid, 1978; Elephant Butte: Baldridge, 1978) represent fragments of mantle country rock and that ~10% partial melting of spinel pyrolite at depths of 50-70 km would produce the alkali olivine basalts and basanites of the central Rio Grande rift. In light of the above discussion, spinel peridotite is considered to be the most likely parent rock for the lavas of the Carrizozo Basalt Field.

Kay and Gast (1973) indicate that unlike the parents of mid-ocean ridge basalts, the peridotitic parent rocks of alkali-rich basalts have not been previously depleted in LIL elements; in fact, these rocks have probably been enriched in LIL elements with respect to chondrite abundances. If the parent rock of the basalts of this study is assumed to have the REE abundances of chondrites, and if the most favorable melting model is evaluated (fractional melting with collection of melt; Figure 20), less than

Table 20. Summary of major element least-square fits for the production of the flows of the Carrizozo Basalt Field by partial melting of spinel peridotite.[1]

PARENT ROCK: Spinel peridotite DAUGHTER LIQUID: Broken Back Crater Flow

	Input data		Calculated Data					
	sper[1]	BB[2]	sper	BB	ol	opx	cpx	spnl
SIO2	44.20	51.70	44.57	51.60	39.67	54.77	50.38	0.00
TIO2	0.13	1.76	0.13	1.76	0.00	0.26	0.56	0.00
AL2O	2.05	17.80	2.07	17.76	0.00	3.31	6.69	83.96
FE2O3	0.00	0.00	0.00	0.00	0.00	6.26	0.00	0.00
FEO	8.20	9.06	8.27	9.04	9.80	0.00	3.52	12.43
MNO	0.13	0.15	0.13	0.15	0.14	0.16	0.13	0.15
MGO	42.20	6.67	42.56	6.66	50.35	32.26	16.32	3.46
CAO	1.92	8.12	1.94	8.10	0.04	2.95	22.20	0.00
NA2O	0.27	3.40	0.27	3.39	0.00	0.03	0.21	0.00
K2O	0.06	1.54	0.06	1.54	0.00	0.00	0.00	0.00
			SOLUTIONS ARE	4.80%	81.99%	5.80%	6.64%	0.78%
			SENSITIVITY	- 2.42	0.14	- 1.57	- 1.97	1.11

PARENT ROCK: Spinel peridotite DAUGHTER LIQUID: lower Carrizozo Flow

	Input data		Calculated Data					
	sper[1]	LC[2]	sper	LC	ol	opx	cpx	spnl
SIO2	44.20	49.90	44.57	50.50	39.67	54.77	50.38	0.00
TIO2	0.13	1.75	0.13	1.77	0.00	0.26	0.56	0.00
AL2O	2.05	16.80	2.07	17.00	0.00	3.31	6.69	83.96
FE2O3	0.00	0.00	0.00	0.00	0.00	6.26	0.00	0.00
FEO	8.20	9.71	8.27	9.83	9.80	0.00	3.52	12.43
MNO	0.13	0.16	0.13	0.16	0.14	0.16	0.13	0.15
MGO	42.20	6.83	42.56	6.91	50.35	32.26	16.32	3.46
CAO	1.92	8.77	1.94	8.88	0.04	2.95	22.20	0.00
NA2O	0.27	3.51	0.27	3.55	0.00	0.03	0.21	0.00
K2O	0.06	1.38	0.06	1.40	0.00	0.00	0.00	0.00
			SOLUTIONS ARE	5.21%	82.95%	4.61%	6.42%	0.81%
			SENSITIVITY	- 2.53	0.10	- 1.76	- 2.16	1.18

PARENT ROCK: spinel peridotite DAUGHTER LIQUID: upper Carrizozo Flow

	Input data		Calculated Data					
	sper[1]	UC[2]	sper	UC	ol	opx	cpx	spnl
SIO2	44.20	51.60	44.57	51.67	39.67	54.77	50.38	0.00
TIO2	0.13	1.71	0.13	1.71	0.00	0.26	0.56	0.00
AL2O	2.05	17.20	2.07	17.22	0.00	3.31	6.69	83.96
FE2O3	0.00	0.00	0.00	0.00	0.00	6.26	0.00	0.00
FEO	8.20	9.66	8.27	9.67	9.80	0.00	3.52	12.43
MNO	0.13	0.15	0.13	0.15	0.14	0.16	0.13	0.15
MGO	42.20	6.30	42.56	6.31	50.35	32.26	16.32	3.46
CAO	1.92	8.26	1.94	8.27	0.04	2.95	22.20	0.00
NA2O	0.27	3.71	0.27	3.71	0.00	0.03	0.21	0.00
K2O	0.06	1.28	0.06	1.28	0.00	0.00	0.00	0.00
			SOLUTIONS ARE	5.54%	83.28%	3.98%	6.45%	0.76%
			SENSITIVITY	- 2.59	0.09	- 1.76	- 2.15	1.19

Input data also included the following compositions of these assumed residual minerals:

	ol[3]	opx[3]	cpx[3]	spnl[4]
SIO2	39.40	54.50	49.70	0.00
TIO2	0.00	0.26	0.55	0.00
AL2O	0.00	3.29	6.60	57.70
FE2O3	0.00	6.23	0.00	0.00
FEO	9.73	0.00	3.47	8.54
MNO	0.14	0.16	0.13	0.10
MGO	50.00	32.10	16.10	2.38
CAO	0.04	2.94	21.90	0.00
NA2O	0.00	0.03	0.21	0.00
K2O	0.00	0.00	0.00	0.00

1. Maaloe and Aoki's (1977) suggested composition for the composition of the upper mantle.
2. Renault (1970).
3. Ernst and Piccardo (1979).
4. Deer and others (1966, p. 324).

0.01% melting would be required to produce the observed REE concentrations in the basalts of this study. It is unlikely that such a small amount of magma would separate from the residual, unmelted rock. It is therefore proposed that the parent rock of the lavas of the Carrizozo Basalt Field was enriched in REE with respect to chondrite values.

History of the Parent Rock

Although the primary sources of mafic magmas are considered to be ultramafic mantle rocks, it is neither necessary nor likely that recently erupted magma has been generated in a single cycle; rather it is likely that young basalts have mantle or deep crustal sources which are themselves products of partial melting (Carmichael and others, 1974, p. 648). Yoder suggests that the mantle may have undergone several periods of remelting, as is implied by evidence for mantle heterogeneity. Early in the earth's history, when the heat flow was probably much greater than it is today, rising diapirs may have been terminated at moderate depths upon contact with the base of a depleted, less dense, and cooler layer. If these diapirs can be considered daughter liquids of partial melting events, then they would be enriched in LIL elements relative to a more primitive, perhaps "chondritic" parent. They could also be sources of magma released on a later cycle of reheating (Yoder, 1976, p. 42).

In the previous section, it was proposed that the parent rock of the lavas of the Carrizozo Basalt Field was enriched in REE with respect to chondrites. The parent rock may therefore represent a daughter liquid which was produced by one or more partial melting events. Major element least-squares fits indicate that 60-70% melting of garnet peridotite could produce a liquid of Maaloe and Aoki's (1977) suggested upper mantle composition (Appendix G-4). If this liquid were to rise as a diapir and solidify within the stability field of spinel peridotite, subsequent melting in the range of 4-6% could produce the lavas of the Carrizozo Basalt Field (Table 20).

An iterative argument involving observed REE concentrations serves to support and refine this model. The average observed REE concentrations in the samples from the Carrizozo Basalt Field could be produced by ~5% melting of a spinel peridotite parent with the following REE enrichment factors relative to chondrites:

La : 4X

Ce : 3X

Sm : 1.7X

Eu, Tb, Yb, Lu : 1.6X

These proposed parent concentrations correlate with Kay and Gast's (1973) suggestion that the REE content of the mantle ranges from 1.9 to 5.1 X chondrite values;

Gast (1968) reached a similiar conclusion in his study of the REE content of ocean-ridge basalts. This parent rock, more enriched in light than heavy REE could represent a daughter liquid produced by 60-70% melting of a garnet peridotite with the following REE enrichment factors relative to chondrites:

La : 2.5X

Ce: 2X

Sm, Eu, Tb, Yb, Lu : 1X

The possible genetic relationship between the lavas of the Carrizozo Basalt Field, a spinel peridotite parent, and a garnet peridotite "source" in terms of REE is shown in Figure 27 and agrees with the proposals by Haskin and others (1966) that:

1) The upper mantle is more enriched in light than heavy REE;
2) The partitioning of light and heavy REE is accompanied by an increase in the absolute concentration of REE;
3) The mantle becomes less fractionated and more depleted with depth.

The fact that the model requires the garnet peridotite "source" to be enriched in La and Ce with respect to chondrite values indicates that perhaps the garnet

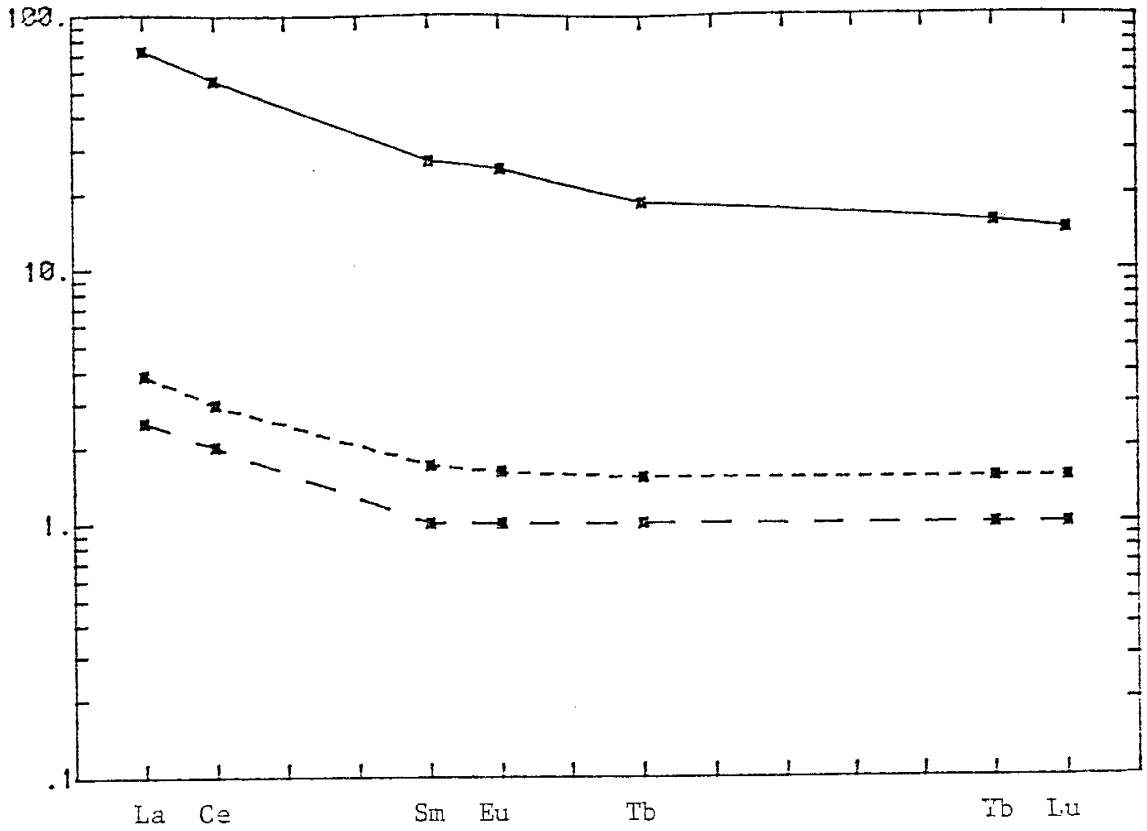

——— Average REE abundances in the flows of the Carrizozo Basalt Field. Both major element (see Table 24) and REE data are consistent with their formation by ∿5% melting of the proposed spinel peridotite parent.

----- REE abundances in the proposed spinel peridotite parent. Both major element (see Appendix G-4) and REE data are consistent with their formation by 60-70% melting of the proposed garnet peridotite source.

— — REE abundances in the proposed garnet peridotite source. Only La and Ce show enrichments relative to chondrites.

Figure 27. Chondrite-normalized REE patterns showing possible genetic relationships between the flows of the Carrizozo Basalt Field, the proposed spinel peridotite parent, and the proposed garnet peridotite source.

peridotite has also been generated by a partial melting event.

Other workers have found evidence that the parent material of Rio Grande rift basalts may represent a daughter liquid produced by partial melting. As a result of Rb-Sr and Sm-Nd isotopic studies, Williams and Murthy (1978) conclude that basalts and andesites of the Taos plateau are derived from a source region which has suffered prior light REE enrichment relative to chondrites. Based on major and trace element data for a suite of spinel lherzolite and harzburgite inclusions from Kilbourne Hole, New Mexico, Reid (1978) argues that the southern portion of the Rio Grande rift is underlain by a piece of oceanic lithosphere which has seen one or perhaps several episodes of partial melting.

Type of Partial Melting Involved

The effects of the three types of partial melting (equilibrium melting, fractional melting, and fractional melting with collection of the melt) on the concentrations of trace elements in a daughter liquid are shown in Figures 20 and 28. In further discussions concerning the role of partial melting in the evolution of the basalts of this study, only the fractional melting with collection of melt model will be considered because:

1) This model provides an upper limit on the degree of partial melting involved;

2) Based on geophysical evidence, Shankland (1978) proposes a model for the mantle underlying the Rio Grande rift in which an anomalous zone of partial melting exists at a depth of 45 km; data are consistent with the melt existing in a dike or sill complex, rather than as a film of melt surrounding crystal grains. His proposal would favor the fractional melting and collection of melt model, with a collection zone at 45 km;

3) Consideration of transition metal data in a following section leads to the hypothesis that the process of fractional crystallization has been involved to a minor extent in the production of the basalts of this study; therefore, a holding chamber in which crystal settling may have occurred, may also have been involved.

Constraints on the Degree of Partial Melting

Results of major element least-squares fits summarized in Table 20 indicate that the three flows of the Carrizozo Basalt Field could have been produced by 4-6% melting of an upper mantle spinel peridotite parent. The consideration of potassium concentrations is also useful in placing constraints on the degree of partial melting involved. A good estimate of the potassium concentration of

the proposed parent rock and accurate values for the concentrations in the proposed daughter liquids are known. Although potassium can be considered a major element, it can also be used in trace element modeling studies, because estimates of its distribution behavior between solid and liquid phases are available. The progressive enrichment of potassium in a daughter liquid produced by various melting processes is shown in Figure 28. If the potassium content of the parent is assumed to be that of Maaloe and Aoki's (1977) upper mantle spinel peridotite (Appendix G), then the production of the observed concentrations of potassium in the Carrizozo Basalt Field is consistent with 4-5% melting of this parent (Figure 28).

Sr and Ba are also useful in placing constraints on the degree of melting involved, as significant enrichment in these elements in daughter liquids is provided by small degrees of melting. Figure 29 shows the calculated enrichment factors in daughter liquids for Sr and Ba as functions of the degree of melting. Assuming Gast's (1968) estimates of Sr and Ba abundances in the mantle (Appendix G), the average concentrations of Sr and Ba in the lavas of the Carrizozo Basalt Field could be produced by less than 10% melting of a spinel peridotite assemblage.

Zr is a LIL transition metal whose bulk distribution coefficient is less than 1 for spinel peridotite (Appendix E). The average observed abundance of

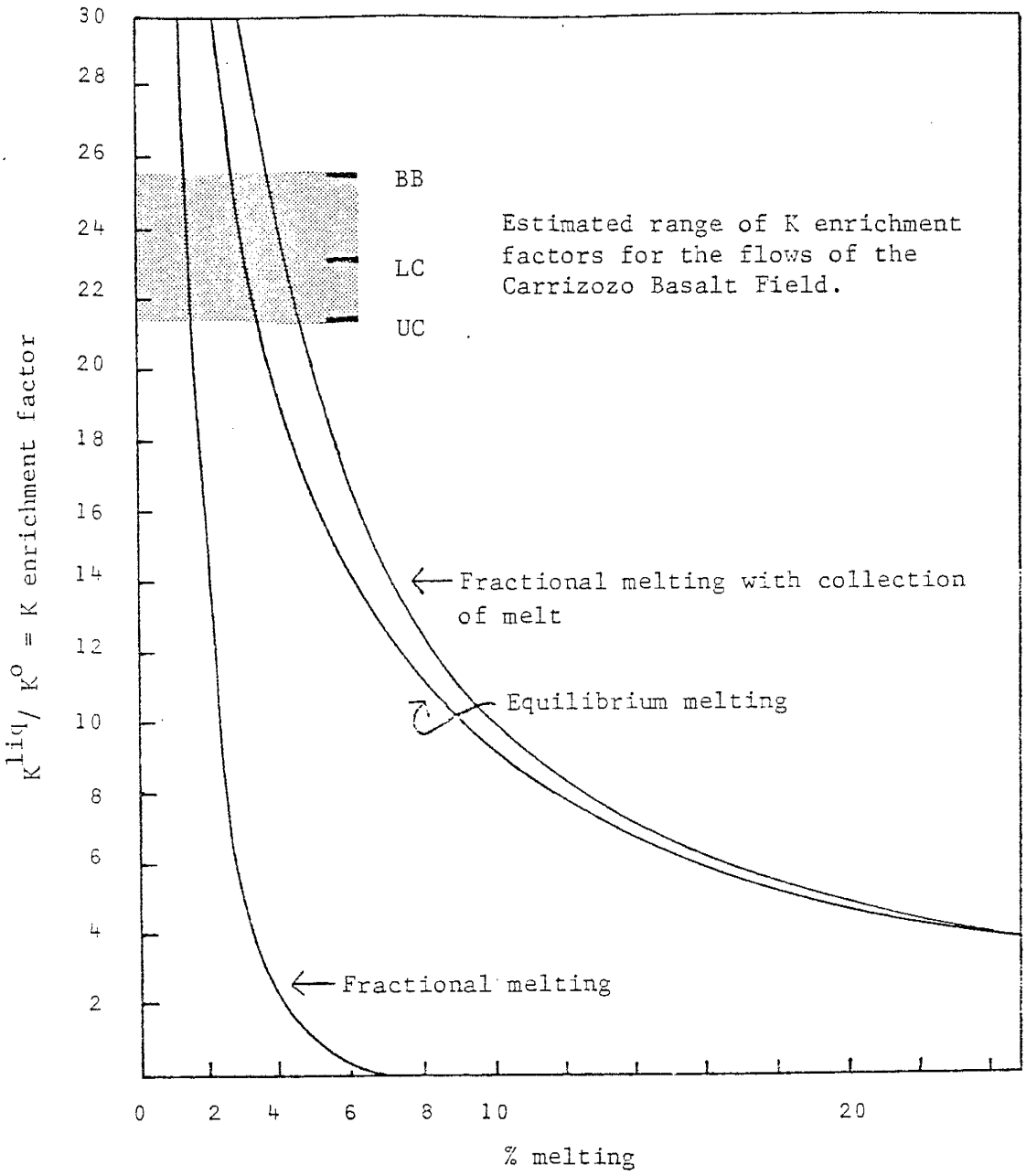

The fractional melting with collection of melt model suggests an upper limit for the degree of melting involved in the range of 4-5%.

Figure 28. Fractionation of K during partial melting of upper mantle spinel peridotite (composition of Maaloe and Aoki, 1977; see Appendix G-1).

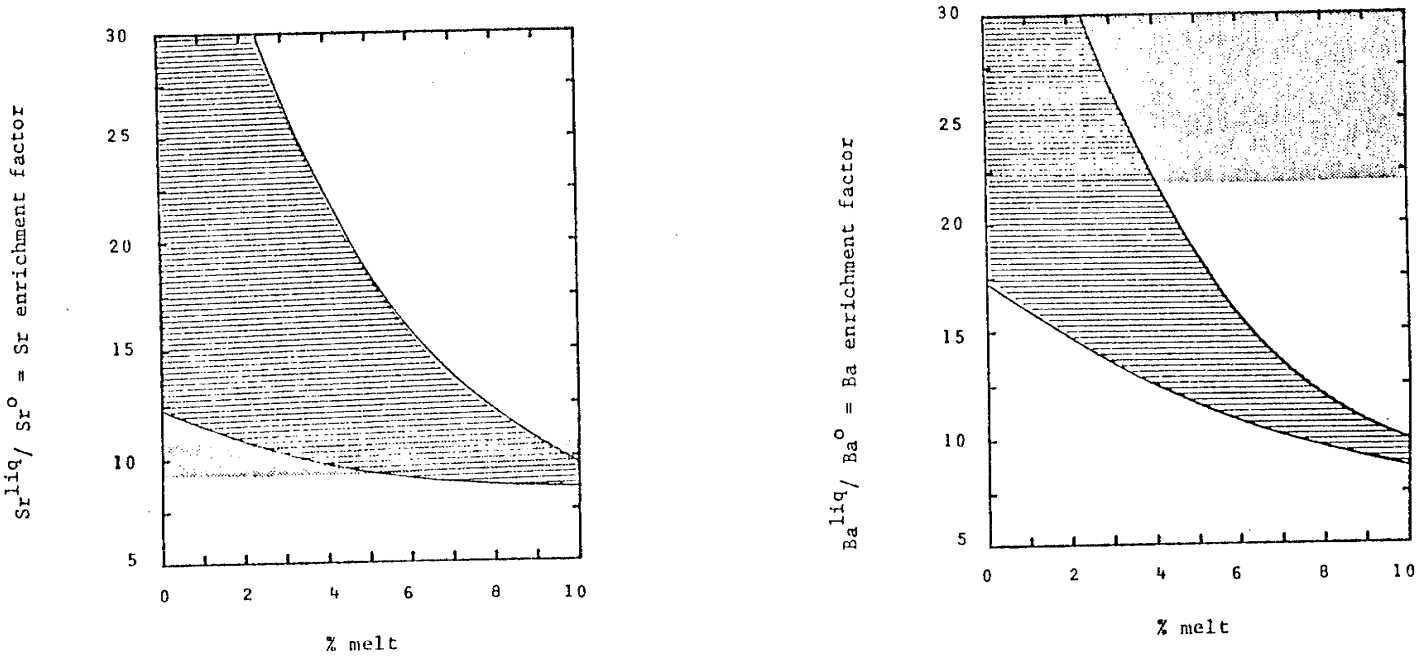

predicted range of enrichment factors produced upon melting of spinel peridotite

estimated range of enrichment factors for samples from the Carrizozo Basalt Field (using Gast's (1968) estimates of Sr and Ba in the mantle (see Appendix G-1))

Calculations are based on the removal and collection of melt model (see Figure 21). The bulk distribution coefficients used in the calculations are given in Appendix E-4.

Lower boundaries of predicted ranges calculated assuming the modal and eutectic composition of SPER-C (see Appendix G-3); upper boundaries calculated assuming the modal and eutectic composition of SPER-A (see Appendix G-3).

Figure 29. Fractionation of Sr and Ba during partial melting of spinel peridotite.

Zr in the flows of the Carrizozo Basalt Field (Table 13) is consistent with their generation by 5-8% partial melting of spinel peridotite.

Many workers (Gast, 1968; Kushiro and Kuno, 1963; Ringwood, 1975) agree that alkaline basaltic magmas can be generated by 2-9% melting of upper mantle assemblages. Baldridge (1979) concludes that alkali olivine basalts from the central Rio Grande rift could be derived from ~10% melting of spinel pyrolite at depths of 50-70 km. Based on electrical conductivity and seismic velocity data, Shankland (1978) proposes a model for mantle conditions beneath the Rio Grande rift which includes a zone of ~7% melting at a depth of 45 km.

REE data cannot provide as much information about possible degrees of melting as can K, Sr, Ba, and Zr because concentrations of these elements in the parent rock are difficult to estimate. Spinel lherzolites containing 41-47% MgO have REE concentrations similiar to chondrites as well as higher and lower concentrations (Maaloe and Aoki, 1977). However, Kay and Gast (1973) suggest that the REE content of the mantle ranges from ~2-5X chondrite values, and this concentration range has also been proposed for the parent rock of the lavas of the Carrizozo Basalt Field (see section titled "History of the Parent Rock"). The suggested parent concentrations were calculated so that upon ~5% partial melting, a spinel peridotite parent could give rise to the

basalt series under study (Figure 27). It is interesting to note that REE and major element data are consistent with a model whereby the assumed upper mantle spinel peridotite is produced by 60-70% melting of a garnet peridotite assemblage. This result may justify the use of the proposed parent REE concentrations, with their "built-in" capacity to give rise to the basalts of this study within the same melting intervals as are suggested by other LIL element data and major element least-squares fits.

Fractional Crystallization as a Minor Process

Although the process of fractional crystallization does not appear to have played a dominant role, transition metal data indicate that this process may have been involved to a minor extent in the evolution of the basalts of this study. Basalts which are produced by partial melting of the upper mantle and erupted without further modification are called "primitive" and have molar Mg/(Mg + Fe) ratios (Mg-values) of 0.68-0.72 (Ringwood, 1975, p. 165). Mg-values are 0.66, 0.64, and 0.62 for the Broken Back Crater, lower, and upper Carrizozo Basalt Flows, respectively. Baldridge (1974) states that since none of the mafic lavas from the Central Rio Grande rift have Mg-values greater than about 0.65, none are genuinely "primitive" in composition.

Two trends have been previously identified with respect to trace transition metal concentrations (see Tables 13 and 14 and the section titled "Transition metals"). The first trend is an increase in average transition metal concentrations from the Broken Back Crater to the lower Carrizozo Flow. Although this trend is only significant at the 95% confidence level for Ni and Cu, it is also noticed for Sc, Mn, Co, Hf, and Ta. Sc, Cr, Ni, and Co have bulk distribution coefficients which are greater than 1 for spinel peridotite (Appendix E). If evaluated in terms of a removal with collection of melt model, these elements would

be expected to show increasing enrichment in daughter liquids with increasing degrees of melting. Although distribution coefficients are strongly temperature dependent for these elements in olivine and pyroxene (Appendix E), progressive melting with time in the range of 4-6% could produce this observed trend of transition metal concentrations.

The second identified trend is a decrease in average transition metal concentrations from the lower to the upper Carrizozo Flow. This trend is significant at the 95% confidence level for Sc, Co, Ni, and Cu, but also noticeable for Cr, Hf, and Ta. Increasing degrees of melting in the range of 4-6% would not significantly increase Sc, Co, Ni, and Cu concentrations. Thus, to a first approximation, concentrations of transition metals in the lower Carrizozo Flow can be used as estimates of parent liquid concentrations from which mineral phases may have crystallized and separated to produce a "differentiated" upper Carrizozo Flow. Transition metals such as Cr, Co, and Ni have distribution coefficients which are generally greater than 1 for olivines and pyroxenes (Appendix E); these elements strongly "prefer" to enter these crystalline phases than to remain in the melt upon cooling. Crystallization of one or more of these minerals and their removal from the system would be the best way to explain the second identified trend.

Ni and Co data indicate that from 2-5% crystallization and removal of olivine would account for the average concentration decreases of these elements from the lower to the upper Carrizozo Flows. Distribution coefficients for Sc in olivine are estimated at less than 1 (Appendix E); therefore an additional crystallizing phase such as pyroxene may be necessary to account for the observed Sc decrease in this interval. The 14% decrease in Cr between the lower and upper Carrizozo Flows is not significant at the 95% confidence level, but may also require pyroxene to be an additional crystallizing phase. Alternatively, the decrease in Cr concentrations in this interval could be explained by the development of spinel inclusions in crystallizing olivine.

The average concentration of Mn is essentially the same in all three flows of the Carrizozo Basalt Field. This can be explained by the distribution behavior of Mn in mafic liquids. Duke (1976) has determined the distribution coefficients for Mn in olivine and clinopyroxene to be 1.25 and 0.63, respectively. Because these values are near 1, and because only moderate variations occur with changes in temperature (Duke, 1976), the concentration of Mn in a daughter liquid would not be expected to vary considerably with partial melting or fractional crystallization processes.

Depth of Origin

Based on laboratory behavior of crystal-melt equilibria in basaltic systems at high pressures and the occurrence of xenocrysts of high-pressure minerals and lherzolite xenoliths, the sources of alkali basalt are generally considered to exist at depths of 40-100 km (Carmichael and others, 1974, p. 487). MacGregor (1968) suggested depths up to 50 km as depths of formation for subalkaline basalts. Leeman and Rogers (1970) indicate that for the Basin and Range Province, calculated geothermal gradients intersect pyrolite solidus curves at 50-60 km; however, even a small amount of water present in the mantle would depress the solidus curves and allow partial melting at depths as shallow as 40 km. Therefore the suggested depth of origin for Basin and Range basalts is at 40-60 km, in the upper mantle near the Moho (Leeman and Rogers, 1970).

Geotherms for the Rio Grande rift in southern New Mexico calculated from accidental lherzolite xenoliths in basalts are shown in Figure 30; these generally represent minimum values and intersect the 5% and 10% melt curves at ~40-50 km for pyrolite containing 0.1% water (Seager and Morgan, 1979). Studies cited by Seager and Morgan (1979) and Baldridge (1979) indicate that basanitic lavas of the Rio Grande rift formed along an isotherm in the 50-70 km depth range; the subalkaline basalts of this study might be expected to originate at lesser depths. The anomolously

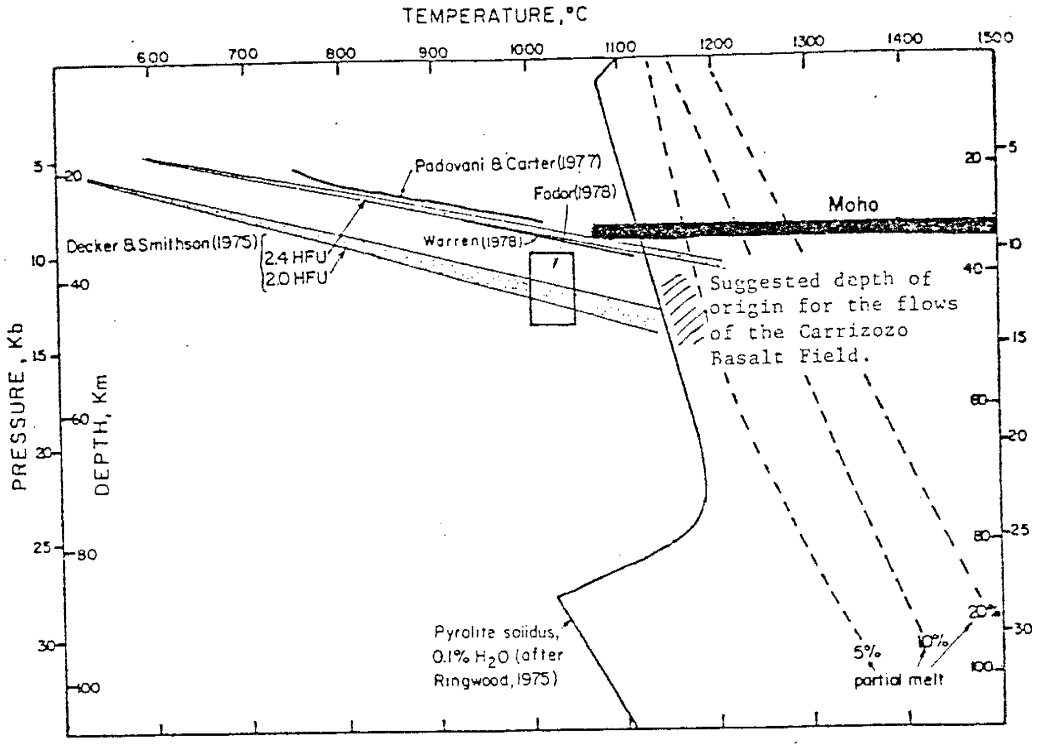

Figure 30. Calculated geotherm segments for the southern portion of the Rio Grande rift and depth of origin for the lavas of the Carrizozo Basalt Field (modified after Seager and Morgan, 1979).

high electrical conductivity and low seismic velocities of the mantle under the rift indicate the presence of partial melt in an anomalous zone at a depth of 45 km (Shankland, 1978).

Kushiro and Kuno (1963) suggest that the production of various basaltic magmas from a single peridotite is possible if various components of peridotitic minerals enter into the liquid fraction in different proportions depending on the temperature and pressure of melting. The basalt classification scheme they propose is based on major element chemical analyses and is used to place constraints on the temperature and pressure conditions at which basaltic magmas form. Samples from the Carrizozo Basalt Field belong to a compositional group, which according to Kushiro and Kuno (1963), can only be formed by the incongruent melting of orthopyroxene. Experimental data indicate that this incongruent melting vanishes at some high pressure, in the range of 6-15 kb (20-45 km). Based on this approach, and on the information discussed above, the basalts of this study might be expected to originate at depths of 40-50 km, within the stability field of spinel.

Comparison with Other Types of Basalts

Condie (1976a) suggests that the three principal magma series (tholeiite, calc-alkaline, and alkali) have distinct distributions when considered in terms of their plate tectonic settings. A summary of these relationships is given in Table 21 and the average compositions of various types of basalts and samples from the Carrizozo Basalt Field are given in Table 22.

Generally, it can be said that the basalts of this study are compositionally transitional between the average continental rift tholeiite and the average continental rift alkali basalt compositions. The average SiO_2 content of samples from the Carrizozo Basalt Field matches well with the average given for continental rift tholeiites. Elements whose concentrations in the basalts of this study are transitional between these two groups, but closer to the continental rift tholeiite category include Sr, Ba, Zr, Cr, and Co; those closer to the continental rift alkali basalt category include Ni, Yb, and Th.

Also, it is interesting to note that several major oxides (FeO, CaO, and Na_2O) and the suite of light REE (La, Ce, Sm, and Eu) (Figure 31) have average concentrations in the basalts of this study which closely resemble those of Condie's (1976a and 1976b) average oceanic alkali basalt, an average of Hawaiian alkali basalt compositions. Frey and others (1968) note that subalkaline to alkaline continental

Table 21. Plate tectonic classification of magmas. (after Condie, 1976a)

PLATE SETTING	PLATE MARGIN		INTRAPLATE			
			OCEANIC		CONTINENTAL	
	Converging (Subduction Zone)	Diverging (Oceanic Rise)	Marginal-Sea Basin	Large Ocean Basin	Rift System	Cratonic Area
MAGMA SERIES	Calc-Alkaline → Arc-Tholeiite, Calc-Alkaline (Low-K, High-K), Shoshonite	Tholeiite (Low-K)	Tholeiite (Low-K)	Alkali Tholeiite	Tholeiite Alkali (Sometimes Bimodal)	Alkali

(after Condie, 1976a)

Table 22. Compositions of average basalts from various plate tectonic settings.

	Low-K Tholeiite		Continental Rift Tholeiite	Island Tholeiite	High-Al Tholeiite	Oceanic Alkali Basalt	Cont. Rift Alkali Basalt	Carrizozo Basalt Field
	Rise	Arc						
SiO_2	49.8	51.1	50.3	49.4	51.7	47.4	47.8	50.64
TiO_2	1.5	0.83	2.2	2.5	1.0	2.9	2.2	1.74
Al_2O_3	16.0	16.1	14.3	13.9	16.9	18.0	15.3	17.08
FeO_T	9.0	10.6	12.2	11.2	10.4	9.5	11.2	9.59
MgO	7.5	5.1	5.9	8.4	6.5	4.8	7.0	6.62
CaO	11.2	10.8	9.7	10.3	11.0	8.7	9.0	8.50
Na_2O	2.8	2.0	2.5	2.13	3.10	3.99	2.85	3.56
K_2O	0.14	0.30	0.8	0.38	0.40	1.66	1.31	1.37
Cr	300	50	100	250	40	67	400	237
Co	32	20	40	30	50	25	60	42
Ni	100	25	100	150	25	50	100	111
Cu	70	80	100					50
Rb	1	5	30	5	10	33	200	
Sr	135	225	350	350	330	800	1500	451
Cs	0.02	0.05	1	0.1	0.3	2	>3	
Ba	11	60	200	100	115	500	700	363
Zr	100	60	200	125	100	330	800	188
La	3.5	3.9	27	7.2	10	17	54	22
Ce	12	7		26	19	50	95	46
Sm	3.9	2.2	8.2	4.6	4.0	5.5	9.7	5.7
Eu	1.5	0.9	2	1.6	1.3	1.9	3.0	1.6
Gd	5.8	4.0	8.1	5.0	4.0	6.0	8.2	
Tb	1.2	0.4	1.1	0.82	0.80	0.81		0.9
Yb	3	2	2.5	1.7	2.7	1.5	1.7	2.6
Lu	0.3	0.3	0.4					0.45
U	0.10	0.15	0.4	0.18	0.2	0.75	0.5	1.3
Th	0.18	0.5	1.5	0.67	1.1	4.5	4.0	3.3
Th/U	1.8	3.3	3.8	3.7	5.9	6.0	8.0	2.5
K/Ba	105	66	32	32	12	28	16	
K/Rb	1160	660	176	630	344	420	55	
Rb/Sr	0.007	0.022	0.089	0.014	0.029	0.045	0.13	
La/Yb	1.2	2	10	4.2	3.7	11	32	8.5

(modified after Condie, 1976a and 1976b)

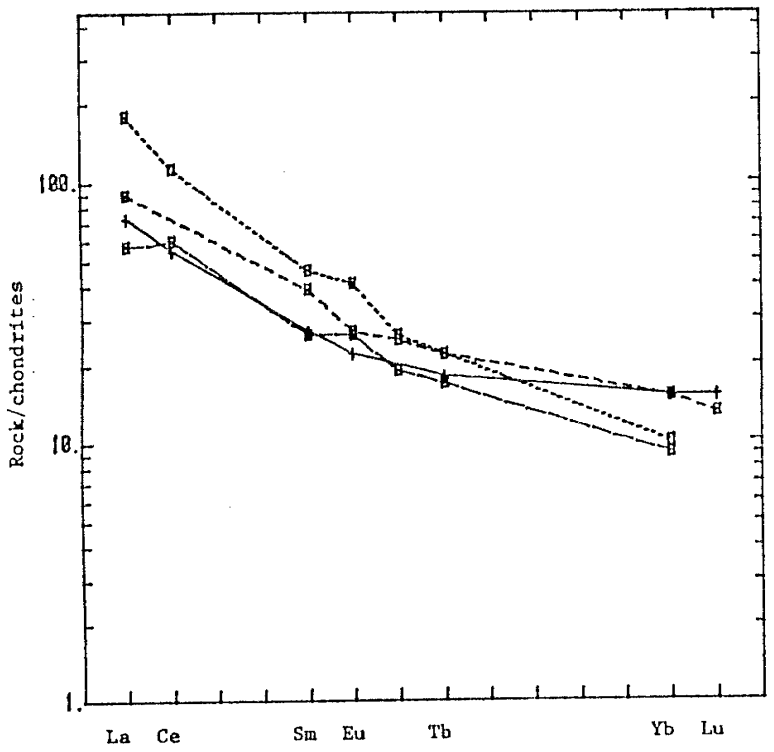

Average continental rift alkali basalt

Average continental rift tholeiite

Average oceanic alkali basalt

Average of the samples from the Carrizozo Basalt Field

The REE pattern for the basalts of this study closely resembles the pattern for average oceanic alkali basalts.

Figure 31. Comparison of chondrite-normalized REE patterns for average basalts from various plate tectonic settings (Condie,1976a and 1976b) and the Carrizozo Basalt Field (Table 10)

and oceanic island basalts are characterized by an enrichment of light REE with respect to heavy REE and that there are no obvious gross differences in terms of REE distributions between subalkaline to alkaline continental and oceanic basalts. Based on their Pb isotopic properties and alkaline chemistries, Everson and Silver (1978) conclude that the alkaline basalt magmas between Socorro and Las Cruces have source regions which resemble those of alkaline ocean island basalts.

Summary and Conclusions

Because the three flows of the Carrizozo Basalt Field are closely related in terms of spatial distribution, age, and composition, it is proposed that these basalts were derived from a common source by a common mechanism: to a first approximation, the three flows of the Carrizozo Basalt Field may represent three major eruptive phases from a compositionally-zoned magma chamber. Major element, alkali and alkaline earth trace element, and light REE data are consistent with the hypothesis that all three flows were generated from a spinel peridotite parent by increasing degrees of partial melting with time. Results of major element least-squares fits indicate that the Broken Back Crater, lower, and upper Carrizozo Flows require 4.8, 5.2, and 5.5% melting of spinel peridotite, respectively, for their formations (Table 20). Statistically, these figures

are virtually identical, but they do vary in the right direction to support the model. Observed concentrations of K, Sr, Ba, and light REE show trends of decreasing average concentrations with decreasing age of the flows, which is consistent with a model of progressive increases in the degree of melting with time in the range of 4-6 %. These effects are shown in Figures 9 and 28 for K, Figures 10 and 29 for Sr, Figure 29 for Ba, and Figures 12 and 27 for the light REE. Potassium and the light REE appear to be fractionated between the three flows of this study and show a pattern which constitutes good evidence that a continuing, evolutionary partial melting process was involved. The model of progressive tapping of a compositionally-zoned magma chamber can best account for these observations.

In a study of Quaternary basalts from the Mohave Desert area, California, Wise (1969) noted a series with increasing SiO_2 and decreasing K, Rb, and Sr concentrations, and a decreasing Mg/(Mg + Fe) ratio with time, a trend which generally exists for the lavas of the Carrizozo Basalt Field. He believes that this series may represent a succession of magmas tapped from a zone of continuing partial melting in the mantle.

If some assumptions are made as to how a compositionally-zoned chamber forms and how magma is erupted and flows from it, then the compositional variations of the lavas of this study can be related to the compositional

stratification which may have existed in the proposed holding chamber.

Melting of the mantle may be initiated by a local increase in temperature, by tensional faulting and consequent pressure release, or by influx of mobile constituents such as water which have the effect of depressing the melting point of the solid (Cox and others, 1979, p. 5). Magma formed within the mantle is less dense than the surrounding country rock and has a tendency to move upward.

In a simple "removal with collection of melt" model, a conduit and/or holding chamber must be available for magma storage. It is assumed that the first increments of melt which separate from the parent rock and collect in the chamber would be less dense than later extracts, so that magmas having compositions representing smaller degrees of melting would be concentrated toward the top of the chamber.

A somewhat more complicated model for the production of a compositionally-stratified zone of partial melting is suggested by Harris (1957) and Kushiro (1968). They also call upon the mechanism of continuing partial melting to explain trends in basalt compositions, but their model does not require a pre-existing void space for magma collection. It is proposed that melting begins at or near the isobaric invariant points of systems including the components of upper mantle materials; compositions of

magmas produced by partial melting are closely related to the composition of these invariant points. Melting is expected to take place more rapidly at the ceiling of a molten zone, since crystals are more soluble at the top where the total pressure is lower, and since the temperature of complete melting is greater than the temperature of partial melting. Magma formed at this ceiling would have a composition at or close to the invariant point corresponding to the pressure at which melting is occurring, and its composition would change with ascent of the melting zone. The final composition of the magma would be determined by the composition of the invariant point at the depth pressure at which the ascent ceases. A compositionally-zoned magma chamber would result since the compositions of invariant points are pressure-dependent and would be different between the top and bottom of the melting zone.

It is assumed that the earliest parts of an erupted sequence come from the upper part of a storage chamber and that successive products come from deeper levels (Cox and others, 1979, p. 272). It is possible that the magma erupted from the upper part of a chamber would travel farthest from the vent, as it would contain more volatiles and so be less viscous than magma from the lower part of the chamber.

Pahoehoe flows are believed to advance in the following manner (McDonald, 1972). Very soon after

eruption, the upper few inches of the flow cool quickly to produce a semi-solid, plastic crust; however, beneath this crust, a liquid interior exists. Continuing addition of liquid stretches the plastic crust at the flow margin until rupturing occurs to allow a stream of liquid to push ahead to form a lava "toe". Margins of pahoehoe flows are thought to advance by the protrusion of one toe after another.

Based on the assumptions that a compositionally-zoned magma chamber was involved where magma representing the smallest degrees of partial melting was concentrated toward the top, a simplified model for the eruptive history of the Carrizozo Basalt Field is shown schematically in Figure 32. The tapping of Zone 1 would produce the Broken Back Crater Flow; later eruption of Zones 2 and 3 would produce the lower and upper Carrizozo Flows, respectively.

Although it is suggested that partial melting was the dominant process operating to produce the lavas of the Carrizozo Basalt Field, a previous discussion of trace transition metal data indicates that up to 5% fractional crystallization of olivine and possibly pyroxene may also have been involved (see section titled "Fractional crystallization as a minor process"). Assuming that some partial melting process can establish trace transition metal concentration gradients in a holding chamber, that magmas representing the smallest degrees of melting are

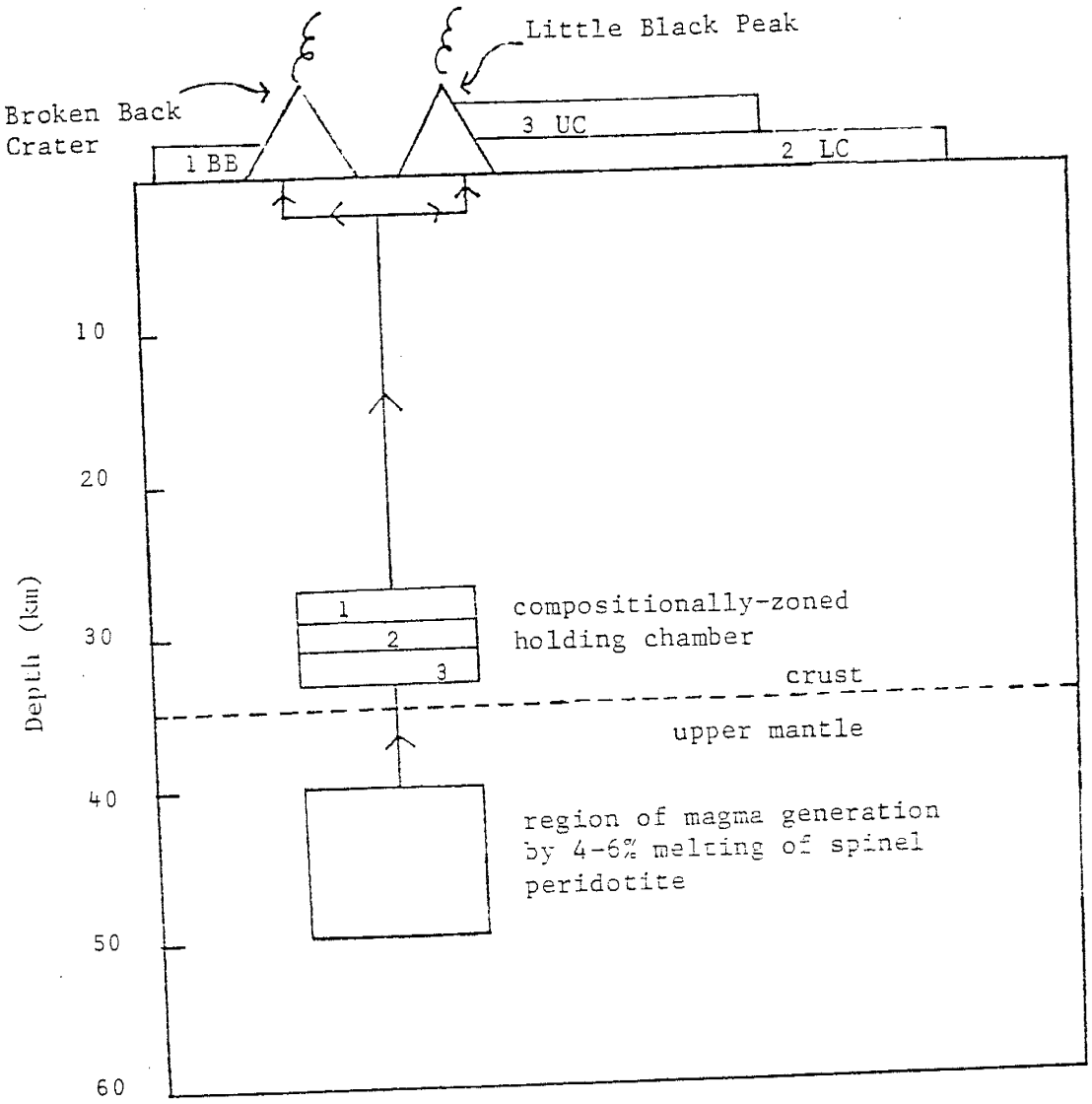

Figure 32. Schematic diagram for the eruptive history of the Carrizozo Basalt Field.

concentrated near the top of the chamber, and that the zones are erupted sequentially from top to bottom, an increase in average concentrations with decreasing age of the flows would be expected for such elements as Cr, Co, Ni, and Cu which have distribution coefficients greater than 1 for mafic minerals (Appendix E).

However, decreases in the average concentrations of these elements from the lower to the upper Carrizozo Flow is observed. The transition metal concentration pattern produced by fractional crystallization may be superimposed upon the pattern produced by partial melting here. It is proposed that, at some time after the eruption of the Broken Back Crater Flow (the uppermost zone), crystallization of olivine and possibly pyroxene begins in the remaining part of the chamber, which has on a large scale retained the compositional zonation set up by partial melting (Figure 33). If these crystals can be removed from the system by gravitational settling, more crystals might be expected to be removed from Zone 3 rather than Zone 2, as Zone 3 has a longer subsurface residence time and also borders on the system (Zones 1-3 of the magma chamber) boundary. In this case, the average concentration of a trace transition metal such as Ni, Co, or Cr would be greater in Zone 2 (representing the lower Carrizozo Flow) than in Zone 3 (representing the upper Carrizozo Flow). However, within each of these zones, an increase in Ni, Co, and Cr

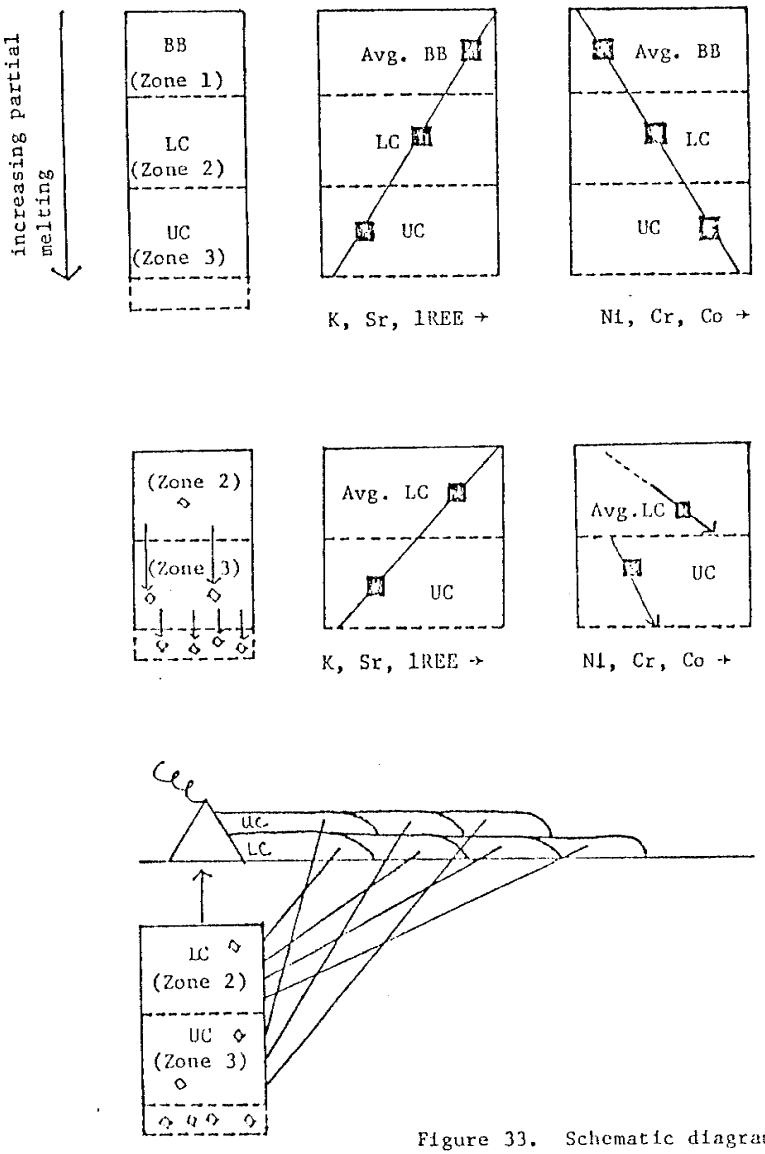

1. A compositionally-zoned magma chamber is created by progressive partial melting of spinel peridotite in the range of 4-6%. Magma representing the smallest degree of partial melting is concentrated towards the top of the chamber. The resulting trace element compositional trends are shown.

2. Zone 1 is erupted to produce the Broken Back Crater Flow. Subsequently, crystallization of olivine ± pyroxene and gravitational settling of these crystals begins. If more crystals settle from Zone 3 out of the system than settle from Zone 2 to Zone 3, then the average concentration of trace transition metals such as Ni, Co, and Cr would be greater in Zone 2 than Zone 3. However, within each of these zones, increasing concentrations of these elements with depth would exist due to the effects of partial melting and gravitational settling. The concentrations of LIL elements are unaffected by this fractional crystallization.

3. Zones 2 and 3 are erupted sequentially to produce the lower and upper Carrizozo Flows, respectively. Within each flow, the depth from which magma was erupted from the holding chamber increases with distance from the vent.

Figure 33. Schematic diagram summarizing the proposed model.

concentrations with depth would be seen due to the effects of both partial melting and gravitational settling processes. The concentrations of LIL elements would be essentially unaffected by this fractional crystallization. Because pahoehoe flows are believed to advance by protrusion of lava "toes" (McDonald, 1972), lava at the distal ends of the lower and upper Carrizozo Flows may represent magma which was erupted last, from the deepest portions of the respective compositional zones (Figure 33); within the lower and upper Carrizozo Flows, the depth from which magma was erupted from the conduit or holding chamber is believed to increase with distance from the vent. The model for the manner of lava advance is consistent with the model developed for a compositionally-zoned magma chamber in that within the upper and lower Carrizozo Flows, the observed concentrations of trace transition metals tend to increase with distance from the vent (Figures 13-17).

The model heretofore proposed is a simplified one, based primarily on the average compositions of the Broken Back Crater, lower, and upper Carrizozo Flows. The distribution of trace elements within the individual flows indicates that a more complex model is required to account for the natural situation. For example, different ways of grouping samples according to compositional relationships are suggested by the distributions of different trace elements. In the cases of K, Sr, Ni, and possibly Cu,

sample groups representing the lower and upper Carrizozo Flows could be different than those defined by Renault (1970): if four samples from the narrow neck area of the lower Carrizozo Flow (CAR-15, CAR-16, CAR-17, and CAR-27) are grouped with the samples from the upper Carrizozo Flow, then two reasonably well-defined linear trends are observed (see sections titled "Alkali and alkaline earth elements" and "Transition metals").

In order to offer some explanation for these irregularities, it must first be remembered that the simplified model is based on a number of assumptions which are somewhat idealized. It has been assumed that:

1) A compositionally-zoned magma chamber can be created in some manner by partial melting;
2) Such a chamber can retain its compositional stratification for some period of time (convection in the chamber is prohibited);
3) In such a chamber, magma is erupted in an orderly manner from the upper zones downwards; eruption does not disturb the compositional gradients of the zones;
4) Erupted magma flows in an orderly direction.

Cox and others (1979, p. 36) state that variation diagrams for volcanic rock suites showing reasonable coherence illustrate the chemical evolution of liquids,

whether formed by progressive partial melting or by fractional crystallization, but that it is perhaps too much to expect of a complex natural system that the reproducibility of the fractionation process, or indeed the duplication of the parental magma supplied at different times should be exact. They suggest further that the simple idea that a parental magma fractionates progressively to give rise to the members of the series may be replaced by the idea of a fractionation process which is reproducible at different times. Thus each of the three sample groups of Renault (1970) may represent a series of related compositions which are derived from a commmon source, even though the effects of the fractionation process(es) involved are not continuous nor exactly reproduced in the three flows of this study. It is also not surprising that variation diagrams for different elements suggest different ways of grouping samples or that they define linear trends of varying slopes.

Some of the observed inter- and intraflow compositional variation may also be due to the porphyritic nature of these basalts, complex flow patterns, or to the effects of "flowage differentiation", in which solid particles tend to concentrate in the center of a flowing liquid (Cox and others, 1979).

References

Aoki, K., and Kudo, A.M., 1976, Major element variations of later Cenozoic basalts of New Mexico, in Elston, W.E., and Northrop, S.A., eds., Cenozoic volcanism in southwestern New Mexico: New Mexico Geological Society, Special Publication 5, p. 82-88.

Allen, J.E., 1951, The Carrizozo Malpais: Roswell Geological Society, Guidebook 5th field conference, p. 9-11.

American Geological Institute, 1972, Glossary of geology: Washington D.C., American Geological Institute, 805 p.

Anderson, D.L., 1979, The upper mantle transition region: eclogite? : Geophysical Research Letters, v. 6, p. 433-436.

Augustithis, S.S., 1978, Atlas of the textural patterns of basalts and their genetic significance: Amsterdam, Elsevier Scientific Publishing Co., 323 p.

Baird, A.K., 1961, A pressed-specimen die for the Norelco vacuum x-ray spectrograph: Norelco Reporter, v. 8, no. 6, p. 108-109.

Baldridge, W.S., 1978, Mafic and ultramafic inclusions from the Rio Grande rift and their bearing on the composition and the thermal state of the lithosphere (abs.), in 1978 International symposium on the Rio Grande rift, Santa Fe, program and abstracts: Los Alamos Scientific Laboratory, p. 15-16.

---------- 1979, Petrology and petrogenesis of Plio-Pleistocene basaltic rocks from the central Rio Grande rift, New Mexico, and their relation to rift structure, in Reicker, R.E., ed., Rio Grande rift: tectonics and magmatism: Washington, D.C., American Geophysical Union, p. 323-354.

Bhattacharyya, G.K., and Johnson, R.A., 1977, Statistical concepts and methods: New York, John Wiley and Sons, 639 p.

Bingler, E.C., Trexler, D.T., Kemp, W.R., and Bonham, H.F., 1976, A BASIC language program for petrologic calculations: Nevada Bureau of Mines and Geology, Report 28, 27 p.

Bowden, P., and Luena, G., 1966, The use of T-1 as a geochemical standard: Geochimica et Cosmochimica Acta, v. 30, p. 361.

Bryan, W.B., Finger, L.W., and Chayes, F., 1968, Estimating proportions in petrographic mixing equations by least squares approximation: Science, v. 163, p. 926-927.

Carmichael, I.S., Turner, F.J., 1974, and Verhoogan, J., 1974, Igneous petrology: New York, McGraw-Hill, 739 p.

Carswell, D.A., and Dawson, J.B., 1970, Garnet peridotite xenoliths in South African kimberlite pipes and their petrogenesis: Contributions to Mineralogy and Petrology, v. 25, p. 163-184.

Carter, J.L., 1970, Mineralogy and chemistry of the earth's upper mantle based on the partial fusion - partial crystallization model: Geological Society of America Bulletin, v. 81, p. 2021-2034.

Chapin, C.E., 1979, Evolution of the Rio Grande rift: a summary, in Riecker, R.E., ed., Rio Grande rift: tectonics and magmatism: Washington, D.C., American Geophysical Union, p. 1-5.

Chapin, C.E., and Seager, W.R., 1975, Evolution of the Rio Grande rift in the Socorro and Las Cruces areas: New Mexico Geological Society, Guidebook 26th field conference, p. 297-322.

Chapin, C.E., Chamberlin, R.M., Osburn, G.R., and White, D.W., 1978, Exploration framework of the Socorro geothermal area, in Field guide to selected cauldrons and mining districts of the Datil-Mogollon volcanic field, New Mexico: New Mexico Geological Society, Special Publication 7, p. 115-130.

Chayes, F., 1966, Alkaline and subalkaline basalts: American Journal of Science, v. 264, p. 28-145.

Cook, F.A., McMullar, D.B., Decker, E.R., and Smithson, S.B., 1979, Crustal structure and evolution of the Rio Grande rift, in Riecker, R.E., ed., Rio Grande rift: tectonics and magmatism: Washington, D.C., American Geophysical Union, p. 195-208.

Condie, K.C., 1976a, Plate tectonics and crustal evolution: New York, Pergamon Press, 288 p.

---------- 1976b, Trace element geochemistry of Archaen greenstone belts: Earth Science Reviews, v. 12, p. 393-417.

Cordell, L., 1978a, Regional geophysical setting of the Rio Grande rift: Geological Society of America Bulletin, v. 89, p. 1073-1090.

---------- 1978b, Overview of geophysical studies in the Rio rift (abs.), in 1978 International symposium on the Rio Grande rift, Santa Fe, program and abstracts: Los Alamos Scientific Laboratory, p. 28-29.

Cox, K.G., Bell, J.P., and Pankhurst, R.J., 1979, The interpretation of igneous rocks: London, George Allen and Unwin, 450 p.

Dane, C.H., and Bachman, G.O., 1958, Preliminary geologic map of the southeastern part of New Mexico: U.S. Geological Survey, Miscellaneous Geologic Investigations Map I-256.

---------- 1961, Preliminary geologic map of the southwestern part of New Mexico: U.S. Geological Survey, Miscellaneous Geologic Investigations Map I-344.

---------- 1965, compilers, Geologic map of New Mexico: U.S. Geological Survey, scale 1:500,000.

Decker, E.R., and Smithson, S.B., 1975, Heat flow and gravity interpretation across the Rio Grande rift in southern New Mexico and west Texas: Journal of Geophysical Research, v. 80, no. 17, p. 2542-2552.

Deer, W.A., Howie, R.A., and Zussman, J., 1967, Rock formimg minerals: London, Longman Group Ltd., v. 5, 379 p.

---------- 1975, An introduction to the rock forming minerals: London, Longman Group Ltd, 528 p.

Drake, M.J., 1976, Evolution of major mineral compositions and trace element abundances during fractional crystallization of a model lunar composition: Geochimica and Cosmochimica Acta, v. 40, p. 401-411.

Duke, J.M., 1976, Distribution of the period four transition elements among olivine, calcic clinopyroxene, and mafic silicate liquid: experimental results: Journal of Petrology, v. 17, p. 499-521.

Eaton, G.P., 1978, A plate-tectonic model for late Cenozoic uplift and crustal spreading in the western United States (abs.), in 1978 International symposium on the Rio Grande rift, Santa Fe, program and abstracts: Los Alamos Scientific Laboratory, p. 31-32.

Engel, A.E., Engel, C.G., and Havens, R.G., 1965, Chemical characteristics of oceanic basalts and the upper mantle: Geological Society of America Bulletin, v. 76, p. 719-734.

Ernst, W.G., and Piccardo, G.B., 1979, Petrogenesis of some Ligurian peridotites - I. Mineral and bulk rock chemistry: Geochimica et Cosmochimica Acta, v. 43, p. 219-237.

Evans, S.H., 1979, and Nash, W.P., 1979, Petrogenesis of xenolith-bearing basalts from southeastern Arizona: American Mineralogist, v. 64, p. 249-267.

Everson, J.E., and Silver, L.T., 1978, Lead systematics of the late Cenozoic basalts from the Rio Grande rift (abs.), in 1978 International symposium on the Rio Grande rift, Santa Fe, program and abstracts: Los Alamos Scientific Laboratory, p. 36-37.

Flanigan, F.J., 1976, 1972 compilation of data on USGS standards, in Flanigan, F.J., ed., Descriptions and analyses of eight new U.S.G.S. rock standards: U.S. Geological Survey Professional Paper 840, p. 131-183.

Fodor, R.V., 1978, Ultramafic and mafic inclusions and megacrysts in Pliocene basalt, Black Range, New Mexico: Geological Society of America Bulletin, v. 89, p. 451.

Frey, F.A., Haskin, M.A., Poetz, J.A., and Haskin, L.A., 1968, Rare earth abundances in some basic rocks: Journal of Geophysical Research, v. 73, p. 6085-6098.

Foster, R.W., and Stipp, T.F., 1961, Preliminary geologic relief map of the Precambrian rocks of New Mexico: New Mexico Bureau of Mines and Mineral Resources, Circular 57, 37 p.

Gast, P.W., 1968, Trace element fractionation and the origin of tholeiitic and alkaline magma types: Geochimica et Cosmochimica Acta, v. 32, p. 1057-1086.

Geological Survey Division, Tanganyikan Ministry of Commerce and Industry, 1963, Standard geochemical sample T-1 Msusule tonalite: Supplement 1.

Gordon, G.E., Rle, K., Goles, G.G., Corliss, J.B., Beeson, M.H., and Oxley, S.S., 1968, Instrumental activation analysis of standard rocks with high resolution gamma-ray detectors: Geochimica et Cosmochimica Acta, v. 32, p. 369-396.

Green, D.H., 1971, Composition of basaltic magmas as indicators of conditions of origin: application to oceanic volcanism: Royal Society of London Philosophical Transactions, v. 268, p. 707-722.

Green, D.H., and Ringwood, A.E., 1967, The genesis of basaltic magma: Contributions to Mineralogy and Petrology, v. 15, p. 104-190.

Gurney, J.J., 1978, personal communication to K.C. Condie.

Harris, P.G., 1957, Zone refining and the origin of potassic basalts: Geochimica et Cosmochimica Acta, v. 12, p. 195-208.

Haskin, L.A., Frey, F., Schmitt, R., and Smith, R., 1966, Meteoritic, solar, and terrestrial rare earth distributions, in Ahrens, L.H., ed., Physics and Chemistry of the Earth: Oxford, Pergamon Press, v. 7, p. 167-321.

Hermance, J.F., and Pedersen, J., 1978, Deep structure of the Rio Grande rift: a magnetotelluric interpretation (abs.), in 1978 International symposium on the Rio Grande rift, Santa Fe, program and abstracts: Los Alamos Scientific Laboratory, p. 41-42.

Hertogan, J., and Gijbels, R., 1976, Calculation of trace element fractionation during partial melting: Geochimica et Cosmochimica Acta, v. 40, p. 313-322.

Irvine, T.N., and Barager, W.R., 1971, A guide to the chemical classification of common volcanic rocks: Canadian Journal of Earth Sciences, v. 8, p. 523-548.

Irving, A.J., 1978, A review of experimental studies of crystal/ liquid trace element partitioning: Geochimica et Cosmochimica Acta, v. 42, p. 743-779.

Jenkins, R., 1976, An introduction to x-ray spectrometry (2nd ed.): London, Heyden and Son, 163 p.

Jenkins, R., and DeVries, J.L., 1967, Practical x-ray spectrometry: New York, Springer-Verlag, 182 p.

Jiracek, G.R., Ander, M.E., and Reddy, I.K., 1978, Magnetotelluric profiling across the Rio Grande rift COCORP study area in New Mexico (abs.), in 1978 International symposium on the Rio Grande rift, Santa Fe, program and abstracts: Los Alamos Scientific Laboratory, p. 46-47.

Jiracek, G.R., Ander, M.E., and Holcombe, H.T., 1979, Magnetotelluric soundings of crustal conductive zones in major continental rifts, in Riecker, R.E., ed., Rio Grande rift: tectonics and magmatism: Washington, D.C., American Geophysical Union, p. 209-222.

Kay, R.W., and Gast, P.W., 1973, The rare earth content and origin of alkali-rich basalts: Journal of Geology, v. 81, p. 653-682.

Keller, G.R., Braile, L.W., and Schlue, J.W, 1978, Regional crustal structure of the Rio Grande rift from surface wave dispersion measurements (abs.), in 1978 International symposium on the Rio Grande rift, Santa Fe, program and abstracts: Los Alamos Scientific Laboratory, p. 47-48.

Kelley, V.C., and Thompson, T.B., 1964, Tectonics and general geology of the Ruidoso-Carrizozo region, central New Mexico: New Mexico Geological Society, Guidebook 15th field conference, p. 110-121.

Kerr, P.F., 1959, Optical mineralogy (3rd ed.): New York, McGraw-Hill, 442 p.

Krumbein, W.C, and Graybill, F.A., 1965, An introduction to statistical models in geology: New York, Mcgraw-Hill, 475 p.

Kuno, H., 1968, Differentiation of basalt magmas, in Hess, H.H., and Poldervaart, A., eds., Basalts: New York, 1978 Interscience Publishers, v. 2, p. 623-688.

Kuno, H., and others, 1957, Differentiation of Hawaiian magmas: Japanese Journal of Geology and Geography, v. 28, p. 179-218.

Kushiro, I., 1968, Compositions of magmas formed by partial melting of the earth's upper mantle: Journal of Geophysical Research, v. 73, p. 619-634.

---------- 1972, Effect of water on the composition of magmas formed at high pressures: Journal of Petrology, v. 13, p. 311-334.

Kushiro, I., and Kuno, H., 1963, Origin of primary basalt magmas and classification of basaltic rocks: Journal of Petrology, v. 4, p. 75-89.

Leeman, W.P., and Rogers, J.W., 1970, Late Cenozoic alkali-olivine basalts of the Basin and Range province, USA: Contributions to Mineralogy and Petrology, v. 25, p. 1-24.

Lehmann. E.L., 1975, Nonparametrics: statistical methods based on ranks: San Francisco, Holden-Day, 457 p.

Lipman, P.W., 1969, Alkalic and tholeiitic basaltic volcanism related to the Rio Grande depression, southern Colorado and northern New Mexico: Geological Society of America Bulletin, v. 80, p. 1343-1354.

Lowder, G.G., 1973, Late Cenozoic transitional alkali olivine - tholeiitic basalt and andesite from the margin of the Great Basin, southwest Utah: Geological Society of America Bulletin, V. 84, p. 2993-3012.

Maaloe, S., and Aoki, K., 1977, The major element composition of the upper mantle estimated from the composition of lherzolites: Contributions to Mineralogy and Petrology, v. 63, p. 161-173.

MacDonald, G.A., 1972, Volcanoes: Englewood Cliffs, Prentice- Hall, 510 p.

MacDonald, G.A, and Katsura, T., 1964, Chemical composition of Hawaiian lavas: Journal of Petrology, v.5, p. 82-133.

Manson, V. , 1967, Geochemistry of basaltic rocks: major elements, in Hess, H.H., and Poldervaart, A., (eds.), Basalts: New York, 1978 Interscience Publishers, v. 1, p. 215-269.

Mayo, E.B., 1958, Lineament tectonics and some ore districts of the southwest: Mining Engineering, v. 10, p. 1169-1175.

Nockolds, S.R., Knox, R.W., and Chinner, G.A., 1978, Petrology for students: Cambridge, Cambridge University Press, 435 p.

O'Hara, M.J., and Yoder, H.S., 1967, Formation and fractionation of basic magmas at high pressures: Scottish Journal of Geology, v. 3, p. 67-117.

O'Nions, R.K., and Clarke, D.B., 1972, Comparative trace element geochemistry of Tertiary basalts from Baffin Bay: Earth and Planetary Science Letters, v. 15, p. 436-446.

Padovani, E.R., 1978, Deep crustal evolution beneath south-central New Mexico: constraints on the geothermal gradient from xenolithic assemblages (abs.), in 1978 International symposium on the Rio Grande rift, Santa Fe, program and abstracts: Los Alamos Scientific Laboratory, p. 66.

Padovani, E.R., and Carter, J.L., 1977, Aspects of the deep crustal evolution beneath south central New Mexico, in Heacock, J.G., ed., The earth's crust: American Geophysical Union, Geophysical Monograph 20, p. 754.

Poldervaart, A., 1964, Chemical definition of alkali basalt and tholeiite: Geological Society of America Bulletin, v. 75, p. 229-232.

Poldervaart, A., and Parker, A.B., 1964, The crystallization index as a parameter of igneous differentiation in binary variation diagrams: American Journal of Science, v. 262, p. 281-289.

Reid, J.B., 1978, (abs.), in 1978 International symposium on the Rio Grande rift, Santa Fe, program and abstracts: Los Alamos Scientific Laboratory, p. 72.

Reiter, M., Mansure, A.J., and Shearer, C., 1979, Geothermal characteristics of the the Rio Grande rift within the southern Rocky Mountain complex, in Riecker, R.E., ed., Rio Grande rift: Tectonics and Magmatism: Washington, D.C., American Geophysical Union, p. 253-268.

Rinehart, E.J., Sanford, A.R., and Ward, R.M., 1979, Geographic extent and shape of an extensive magma body at mid-crustal depths in the Rio Grande rift near Socorro, New Mexico, in Riecker, R.E., ed., Rio Grande rift: tectonics and magmatism: Washington, D.C., American Geophysical Union, p. 237-252.

Renault, J.R., 1970, Major element variations in the Potrillo, Carrizozo and Upper McCartys basalt fields, New Mexico: New Mexico Bureau of Mines and Mineral Resources, Circular 113, 22 p.

---------- 1978, Overview of the Rio Grande basalts with special reference to TiO2 variation, in Guidebook to the Rio Grande rift in New Mexico and Colorado: New Mexico Bureau of Mines and Mineral Resources, Circular 163, p. 230-233.

Ringwood, A.E., 1975, Composition and petrology of the earth's mantle: New York, McGraw-Hill, 618 p.

Roeder, P.L., and Emslie, R.F., 1970, Olivine-liquid equilibrium: Contributions to Mineralogy and Petrology, v. 29, p. 275-289.

Sanford, A.R., Alptekin, O.S., and Toppozada, T.R., 1973, Use of reflection phases on microearthquake seismograms to map an unusual discontinuity beneath the Rio Grande rift: Bulletin of the Seismological Society of America, v. 63, p. 2021-2034.

Schilling, J.G., 1975, Rare earth variations across "normal segments" of the Reykanes ridge: Journal of Geophysical Research, v. 80, p. 1459-1473.

Schmucker, U., 1964, Anomalies of geomagnetic variations in the southwestern United States: Journal of Geomagnetism and Geoelectricity, v. 15, p. 193-221.

Seager, W.R., amd Morgan, P., 1979, Rio Grande rift in southern New Mexico, west Texas, and northern Chihuahua, in Riecker, R.E., ed., Rio Grande rift: tectonics and magmatism: Washington, D.C., American Geophysical Union, p. 87-106.

Shankland, T.J., 1978, Simultaneous consideration of electrical and elastic anomalies in rift zones (abs.), in 1978 International symposium on the Rio Grande rift, Santa Fe, program and abstracts: Los Alamos Scientific Laboratory, p. 89.

Shaw, D.M., 1970, Trace element fractionation during anatexis: Geochimica et Cosmochimica Acta, v. 34, p. 237-243.

Simpson, E.S., 1954, On the graphical representation of differentation trends in igneous rocks: Geology Magazine, v. 91, p. 238-244.

Smith, C.T., 1964, Reconnaissance geology of the Little Black Peak quadrangle, Lincoln and Socorro counties, New Mexico: New Mexico Geological Society, Guidebook 15th field conference, p. 92-99.

Smith, C.T., and Budding, A.J., 1959, Reconnaissance geologic map of the Little Black Peak fifteen-minute quadrangle : New Mexico Bureau of Mines and Mineral Resources, Geologic Map 11.

Stinnett, J.W., 1976, A strontium isotopic and geochemical study of volcanic series from the Datil-Mogollon field, southwestern New Mexico (abs.) : Geological Society of America abstracts with programs, v. 8, no. 5, p. 636.

Sun, S., and Nesbitt, R.W., 1977, Chemical heterogeneity of the Archean mantle, composition of the earth, and mantle evolution: Earth and Planetary Science Letters, v. 35, p. 429-448.

Ulvog, C. and Thompson, S., 1964, Road log from Carrizozo to Malpais: New Mexico Geological Society, Guidebook 15th field conference, p. 22.

U.S. Geological Survey, 1978, Index to topographic maps of New Mexico: U.S. Geological Survey.

Victoreen, J.A., 1949, The calculation of x-ray mass absorption coefficients: Journal of Applied Physics, v. 20, p. 1141-1147.

Volborth, A., 1963, Total instrumental analysis of rocks: Nevada Bureau of Mines, Report 6, 72 p.

Warren, R.G., 1978, Characterization of the lower crust - upper mantle of the Engle Basin, Rio Grande rift, from a petrochemical and field geologic study of basalts and their inclusions: unpublished Ph.D. thesis, University of New Mexico, Albuquerque, NM, 156 p.

Warren, R.G., Kudo, A.M., and Keil, K., 1979, Geochemistry of lithic and single-crystal inclusions in basalt and a characterization of the upper mantle - lower crust in the Engle Basin, Rio Grande rift, New Mexico, in Riecker, R.E., ed., Rio Grande rift: tectonics and magmatism: Washington, D.C., American Geophysical Union, p. 393-415.

Weber, R.H., 1964, Geology of the Carrizozo quadrangle, New Mexico: New Mexico Geological Society, Guidebook 15th field conference, p. 100-109.

White, W.M., and Schilling, J.G., 1978, The nature and origin of geochemical variation in mid-Atlantic ridge basalts from the central north Atlantic: Geochimica et Cosmochimica Acta, v. 42, p. 1501-1516.

Wood, B.J., and Fraser, D.G., 1978, Elementary thermodynamics for geologists: Oxford, Oxford University Press, 303 p.

Woodward, L.A., Callender, J.F., Seager, W.R., Chapin, C.E., Shaffer, W.L., and Zilinski, R.E., 1978, Tectonic map of the Rio Grande rift region in New Mexico, Chihuahua, and Texas: New Mexico Bureau of Mines and Mineral Resources, Circular 163, sheet 2.

Woolard, G.P., and Joesting, H.R., 1964, Bouguer gravity map of the United States: American Geophysical Union and the U.S. Geological Survey, scale 1:2,500,000.

Wright, T.L., and Doherty, P.C. 1970, A linear programming and least squares computer method for solving petrologic mixing problems: Geological Society of America Bulletin, v. 81, p. 1995-2008.

Yoder, H.S., 1976, Generation of basaltic magma: Washington D.C., National Academy of Sciences, 265 p.

Yoder, H.S., and Tilley, C.E., 1962, Origin of basaltic magmas: an experimental study of natural and synthetic rock systems: Journal of Petrology, v. 3, p. 342-532.

Appendix A. Definition and Discussion of Statistical Parameters (from Johnson and Bhattachcryya, 1977, unless otherwise noted)

1. Coefficient of Variation (CV):

(Relative Standard Deviation)

$$CV = (s/M) \times 100$$

where:

s = sample standard deviation

M = mean composition of samples (Renault, 1970)

2. Confidence Interval (CI):

For small sample size ($n<30$), if the population distribution is normal and if σ (population standard deviation) is unknown, the 100 $(1-\alpha)$% confidence interval for μ (population mean) is

$$\bar{X} \pm t_{\alpha/2} \frac{s}{n}$$

where:

$\bar{X}$ = sample mean

$t_{\alpha/2}$ = upper $\alpha/2$ point of the t-distribution with n-1 degrees of freedom

s = sample standard deviation

n = number of samples

3. Correlation Coefficient (r):

$$r = \frac{\sum_{i=1}^{n} (X_i-\bar{X})\ (Y_i-\bar{Y})}{\sqrt{\left[\sum_{i=1}^{n} (X_i-\bar{X})^2\right]\left[\sum_{i=1}^{n} (Y_i-\bar{Y})^2\right]}}$$

where:

$(X_1,Y_1),\ldots,(X_n,Y_n)$ are the n pairs of observations

4. % Counting Error (CE):

$$CE = \frac{100}{N^{\frac{1}{2}}}$$

where:

N = number of counts

5. Lower Limit of Detection (LLD):

$$LLD \simeq \frac{3}{m}\left(\frac{I_b}{T_b}\right)^{\frac{1}{2}}$$

where:

m = number of counts/sec per % of element

I_b = number of backround counts

T_b = backround counting time (sec)

6. Sample Mean ($\bar{X}$):

$$\bar{X} = \frac{1}{n}\sum_{i=1}^{n} X_i$$

where:

n = number of samples

X_i = value of the i^{th} sample

7. % Relative RMS Error:

$$\% \text{ RMS} = \sqrt{\frac{\sum\left(\frac{C_i - M_i}{M_i}\right)^2}{n}} \times 100$$

where:

C_i = concentration of element in i^{th} standard calculated from calibration curve

M_i = assumed concentration of element i^{th} standard used to construct calibration curve

n = number of standard points used to construct calibration curve

8. Sample Size Determination (n):

Assuming a normal population distribution, the number of samples required for the mean value of these samples to be within a given tolerance range at the 100(1-α)% confidence level is given by

$$n = \left(\frac{t_{\alpha/2} \cdot s}{d} \right)^2$$

where:

$t_{\alpha/2}$ = the tabulated value of the t-distribution for probability $\alpha/2$ with M-1 degrees of freedom

m = number of samples from which sample standard deviation was calculated

s = sample standard deviation

d = specified tolerance level

(Krumbein & Graybill, 1965)

9. Sample Standard Deviation (s):

$$s = \sqrt{\frac{\sum_{i=1}^{n} (X_i - \bar{X})^2}{n-1}}$$

where:

n = number of samples

X_i = value of the i^{th} sample

$\bar{X}$ = mean value of the samples

10. Standard Error (SE):

$$SE = \frac{s}{\sqrt{n}}$$

where:

s = sample standard deviation

n = number of samples

11. Wilcoxon Rank-Sum Test to Compare 2 Populations:

The 2-sided Wilcoxon rank-sum test is a non-parmetric inference procedure and is used to compare 2 populations based on independent, random samples and to detect statistically significant differences between them. This procedure does not require modeling of a population in terms of a specific parametric form of density curves, such as a normal distribution; it instead uses simple aspects of sample data (in this case, order relationships) to calculate a "test-statistic". The Wilcoxon rank sum test is appropriate for the small sample sizes that are involved in this study.

The following is a description of the procedure used to detect major and trace element concentration differences between the Broken Back Crater, lower and upper Carrizozo Flows, based on a discussion by Lehmann (1975, p. 23-29):

1) Let $a_1, \ldots, a_m$ and $b_1, \ldots, b_n$ be independent random samples from continuous populations A and B, respectively.

2) Rank the combined sample of $N = m + n$ observations in increasing order of magnitude.

3) Compute W_B, the sum of the ranks of samples from population B in the combined sample ranking.

4) $B > A$ if $W_B \geq \frac{1}{2} n (N + 1) + C$;

$A > B$ if $W_B \leq \frac{1}{2} n (N + 1) + C$;

suspend judgment if $|W_B - \frac{1}{2} n (N + 1)| < C$.

The constant C is determined by specifying α, the maximum tolerable error probability, and solving the equation:

$$\alpha = P\left[W_B \leq \tfrac{1}{2} n (N + 1) - C\right] = P\left[W_B \geq \tfrac{1}{2} n (N + 1) + C\right]$$

Appendix B. Mass absorption coefficient values at various analytical wavelengths.

K_α (Å)	Cr 2.291	Mn 2.103	Ni 1.659	Cu 1.542	Rb 0.927	Sr 0.877	Zr 0.788
Samples							
CAR-12	188.36	148.44	76.74	62.64	15.24	13.06	9.71
CAR-13	185.96	146.54	75.78	61.83	15.04	12.89	9.58
CAR-14	188.83	148.80	76.93	62.77	15.26	13.09	9.72
CAR-15	190.73	150.34	77.81	63.51	15.47	13.27	9.86
CAR-16	192.01	151.37	78.36	63.97	15.60	13.37	9.94
CAR-17	189.68	149.50	77.35	63.13	15.37	13.18	9.80
CAR-18	191.66	151.08	78.18	63.82	15.55	13.33	9.91
CAR-19	192.38	151.65	78.49	64.07	15.61	13.39	9.95
CAR-21	191.45	150.95	78.11	63.76	15.53	13.32	9.90
CAR-22	193.16	152.27	78.81	64.33	15.68	13.44	9.99
CAR-24	189.71	149.55	77.40	63.18	15.40	13.21	9.81
CAR-25	190.15	149.87	77.54	63.29	15.41	13.22	9.82
CAR-26	193.31	152.38	78.86	64.37	15.69	13.45	10.00
CAR-27	191.41	150.88	78.08	63.73	15.53	13.31	9.90
CAR-5	188.54	148.57	76.83	62.69	14.98	13.07	9.71
CAR-6	191.55	150.97	78.10	63.74	15.52	13.31	9.89
CAR-7	190.66	150.29	77.77	63.47	15.46	13.26	9.85
CAR-8	190.24	149.96	77.60	63.34	15.21	13.04	9.69
CAR-9	187.61	148.05	76.57	62.49	15.21	13.04	9.69
CAR-10	192.56	151.79	78.54	64.11	15.62	13.39	9.95
CAR-11	193.11	151.20	78.73	64.26	15.64	13.41	9.97
Standards							
PCC-1		111.83		37.30	11.30	9.68	7.18
BCR-1	204.12	160.98	83.44	68.13	16.65	14.29	10.63
AGV-1	161.45	127.04	65.43	53.33	12.86	11.02	8.17
GSP-1		116.69	59.88	48.74	11.66	9.98	
BLCR	169.94		69.05		13.63		
BR	212.91		87.26				
T-1	153.09						

Mass absorption coefficients calculated by means of a computer program (CHEM2 by J.R. Renault) using major element analyses (Renault, 1970) and Victoreen (1949) parameters.

Appendix C. Chemical analyses for non-USGS rock standards.

	BCLR	BR	T-1
SiO_2	53.5	38.20	62.65
Al_2O_3	18.1	10.20	16.52
Fe_2O_3 T	7.62	12.88	6.03
MgO	4.85	13.28	1.89
CaO	8.39	13.80	5.19
Na_2O	3.57	3.05	4.39
K_2O	1.32	1.40	1.23
TiO_2	0.89	2.60	0.59
Total	98.24	95.41	98.49
Ba	370	1050	680
Ce	28		
Co	30	50	13
Cr	130	420	24
Cs	2.5		
Cu	9	70	47
Eu	1.28		
Ga	15		
Ho	1.1		
Hf	4.3		
La	12	85	
Lu	0.55		
Mn	1090		850
Nd	15		
Ni	100	270	10
Pb	26		37
Rb	37	45	30
Sc	32		
Sm	4.0		
Sr	234	1350	680
Ta	0.48		
Tb	0.8		
Th	4.0		
V		240	96
Y	37	27	25
Yb	3.5		
Zn	57	160	190
Zr	188	240	200

BCLR and BR are New Mexico Tech standard basalts (Condie, unpublished data, 1978).

T-1 is a standard tonalite (Tanganyikan Geological Survey, 1963).

Major elements concentrations are given in oxide weight percent; trace element concentrations are given in ppm.

Appendix D. Rare earth element chondrite values (ppm).

La	0.30 ± 0.06
Ce	0.84 ± 0.18
Pr	0.12 ± 0.02
Nd	0.58 ± 0.13
Sm	0.21 ± 0.04
Eu	0.074 ± 0.015
Gd	0.32 ± 0.07
Tb	0.049 ± 0.010
Dy	0.31 ± 0.07
Ho	0.073 ± 0.014
Er	0.21 ± 0.04
Tm	0.333 ± 0.007
Yb	0.17 ± 0.03
Lu	0.031 ± 0.005

Values are taken from Haskin and others (1966).

Appendix E. Distribution coefficients for mafic-andesitic mineral and rock compositions

Definitions

If trace elements are assumed to obey Henry's Law, simple activity-composition relationships may be used to describe the distribution of trace elements between different phases (Wood and Fraser, 1978):

Nernst distribution coefficient (K_D):

$$K_D = \frac{C_i^{min}}{C_i^{melt}}$$

where:

K_D = Nernst (mineral) distribution coefficient

C_i^{min} = concentration of element i in the mineral phase

C_i^{melt} = concentration of element i in the melt phase

Bulk distribution coefficient D:

$$D_i = x^1 K_D{}^1 + x^2 K_D{}^2 + \ldots x^n K_D{}^n$$

where:

D_i = bulk distribution coefficient for the parent rock for element i

x^n = initial weight fraction of mineral n in parent rock

$K_D{}^n$ = Nernst distribution coefficient for mineral n and element i

Bulk distribution coefficient P:

$$P_i = P^1 K_D{}^1 + P^2 K_D{}^2 + \ldots P^n K_D{}^n$$

where:

P_i = bulk distribution coefficient for the parent rock for element i

P^n = the weight fraction of melt contributed by mineral n

$K_D{}^n$ = Nernst distribution coefficient for mineral n and element i

Mineral distribution coefficients (K_D) values used

	Olivine	Ortho-pyroxene	Clino-pyroxene	Spinel	Garnet	Plagioclase
K	≈0.01	0.01	0.02		0.03	0.2
Sr	≈0.01	≈0.02	0.05		0.02	1.8
Ba	≈0.01	0.02	0.05		0.03	0.2
La	0.01	0.02	0.1	0.02	0.05	0.10
Ce	0.01	0.02	0.1	0.02	0.1	0.10
Sm	0.01	0.02	0.3	0.03	0.4	0.07
Eu*	0.01	0.03	0.3	0.05	0.5	0.07
Tb	0.02	0.05	0.4	0.08	2	0.05
Yb	0.03	0.1	0.5	0.10	7	0.04
Lu	0.03	0.1	0.5	0.10	7	0.04
Sc	0.4	0.5-1.5	1-8	≈0.05	10-30	0
Cr	≈0.8	2-8	1-10	50-500	10-20	0
Co	1-10	1-5	0.5-3	2-3	3-5	0
Ni	1-50	1-10	1-10	5-10	0.5-5	0
Zr	<0.01	≈0.05	0.1		≲0.5	≲0.01
U	<0.01	≈0.01	≈0.002			
Th	<0.01		≈0.003			

* At 20-30 kb

from Drake, 1976 and Irving, 1978

Bulk distribution coefficients used

	for < 25% melting		for > 29% melting	
	Garnet	Peridotite	Garnet	Peridotite
	D	P	D	P
K	0.01	0.02		
Sr	0.02	0.03	0.01	0.02
Ba	0.02	0.04	0.01	0.02
La	0.03	0.07	0.01	0.02
Ce	0.04	0.09	0.01	0.02
Sm	0.10	0.33	0.03	0.04
Eu	0.12	0.38	0.05	0.07
Tb	0.35	1.13		
Yb	1.07	3.53		
Lu	1.07	3.53		

	Spinel	Peridotite	Plagioclase	Peridotite
	D	P	D	P
K	0.01	0.02	0.04	0.11
Sr	0.02	0.03	0.29	0.92
Ba	0.02	0.03	0.05	0.12
La	0.02	0.06	0.04	0.08
Ce	0.02	0.06	0.04	0.08
Sm	0.04	0.17	0.07	0.12
Eu	0.04	0.17	0.07	0.12
Tb	0.06	0.24	0.09	0.14
Yb	0.08	0.30	0.12	0.17
Lu	0.08	0.30	0.12	0.17
Sc	0.54	1.88		
Cr	2-12	2-7.5		
Co	1-8	0.75-5		
Ni	1-36	1-20		
Zr	0.03	0.07		

Calculated from mineral distribution coefficients (see Appendix E-3) and modal and eutectic minerals proportions (see Appendix G-3).

Appendix F. Fractional crystallization model

Compositions of proposed parent magmas

	OT[1]	IT[2]	CRT[3]
SiO_2	46.95	49.4	50.3
TiO_2	2.02	2.5	2.2
Al_2O_3	13.10	13.9	14.3
$*Fe_2O_3$	3.51	4.00	3.70
*FeO	7.94	8.81	10.18
MnO	0.15	NG	NG
MgO	14.55	8.4	5.9
CaO	10.16	10.3	9.7
Na_2O	1.73	2.12	2.5
K_2O	0.08	0.38	0.66

ppm	IT[2]	CRT[3]
Sr	350	350
Ba	100	170
La	7.2	33
Ce	26	98
Sm	4.6	8.2
Eu	1.6	2.3
Tb	0.82	1.1
Yb	1.7	4.4
Cr	250	160
Co	30	38
Ni	150	85
Zr	125	200
U	0.18	0.4
Th	0.67	1.5

Compositions of proposed residual minerals[4]

	9kb 1230°C ol	9kb 1250°C ol	9kb 1290°C ol	9kb 1250°C opx	15kb 1400°C opx	13.5 kb 1350°C cpx
SiO_2	39.8	39.9	40.3	52.9	53.4	49.3
Al_2O_3	ND	ND	ND	6.9	7.3	11.3
FeO	14.7	14.0	12.3	9.1	6.4	8.3
MgO	45.2	45.8	47.1	28.5	30.4	21.2
CaO	0.3	0.3	0.3	2.6	2.5	9.9

NG = not given
ND = not detected

* has been recalculated from FeO_T

1. Olivine tholeiite: Green & Ringwood, 1967.
2. Average island tholeiite: Condie, 1976, p. 148.
3. Average continental rift tholeiite: Condie, 1976, p. 148.
4. Green & Ringwood, 1967.

Results of major element least-squares fits to a fractional crystallization model

Fractionation at 15-35 km (<1230°C)

Model 2a (see Table 20)

INPUT DATA ACCEPTED

OXIDE	WEIGHT	CPT	LCAR	ol	opx	cpx
SIO2	1.0	50.30	50.20	39.80	52.90	49.30
TIO2	1.0	2.20	1.72	0.00	0.00	0.00
AL2O	1.0	14.30	16.90	0.00	6.90	11.30
FE2O	1.0	3.70	3.21	0.00	0.00	0.00
FEO	1.0	10.20	6.63	14.70	9.10	8.30
MNO	1.0	0.15	0.16	0.00	0.00	0.00
MGO	1.0	5.90	6.56	45.20	28.50	21.20
CAO	1.0	9.70	8.42	0.30	2.60	9.90
NA2O	1.0	2.50	3.53	0.00	0.00	0.00
K2O	1.0	0.66	1.36	0.00	0.00	0.00
TOTAL		99.61	98.69	100.00	100.00	100.00

SUM= 0.9021, SOLUTIONS= 0.71554 0.00102 -0.31481 0.50065

HAVE PROHIBITED SOLUTIONS FOR : opx (1) REPEAT WITHOUT : opx

SUM= 0.9378, SOLUTIONS= 0.71138 -0.12930 0.35577

*REPEAT AGAIN WITHOUT : ol

SUM= 0.8523, SOLUTIONS= 0.74959 0.10276

CALCULATED DATA

OXIDE	WEIGHT	CALC	DIFF	CRT	LCAR	ol	opx	cpx
SIO2	1.0	50.68	0.4%	50.50	50.87	39.80	52.90	49.30
TIO2	1.0	1.53	-30.6%	2.21	1.74	0.00	0.00	0.00
AL2O	1.0	16.42	14.4%	11.36	17.12	0.00	6.90	11.30
FE2O	1.0	2.86	-23.0%	3.71	3.25	0.00	0.00	0.00
FEO	1.0	6.91	-32.5%	10.24	6.72	14.70	9.10	8.30
MNO	1.0	0.14	-5.3%	0.15	0.16	0.00	0.00	0.00
MGO	1.0	8.40	41.8%	5.92	6.65	45.20	28.50	21.20
CAO	1.0	8.70	-10.7%	9.74	8.53	0.30	2.60	9.90
NA2O	1.0	3.15	25.3%	2.51	3.58	0.00	0.00	0.00
K2O	1.0	1.21	82.9%	0.66	1.38	0.00	0.00	0.00
SOLUTIONS ARE					87.94%	0.00%	0.00%	12.06%
SENSITIVITY					0.88	1.78	1.60	1.25

Results of major element least-squares fits to a fractional crystallization model

Fractionation at 15-35 km (1230-1250°C)

Model 2b (see Table 20)

INPUT DATA ACCEPTED

OXIDE	WEIGHT	CRT	LCAR	+ ol	+ opx
SIO2	1.0	50.30	50.20	39.90	52.90
TIO2	1.0	2.20	1.72	0.00	0.00
AL2O	1.0	14.30	16.90	0.00	6.90
FE2O	1.0	3.70	3.21	0.00	0.00
FEO	1.0	10.20	6.63	14.00	9.10
MNO	1.0	0.15	0.16	0.00	0.00
MGO	1.0	5.90	6.56	45.80	28.50
CAO	1.0	9.70	8.42	0.30	2.60
NA2O	1.0	2.50	3.53	0.00	0.00
K2O	1.0	0.66	1.36	0.00	0.00
TOTAL		99.61	98.69	100.00	100.00

SUM= 0.9524, SOLUTIONS= 0.72906 -0.27906 0.50237

HAVE PROHIBITED SOLUTIONS FOR : ol

(1) REPEAT WITHOUT : ol

SUM= 0.8289, SOLUTIONS= 0.77215 0.05674

CALCULATED DATA

OXIDE	WEIGHT	CALC	DIFF	CRT	LCAR	ol	opx
SIO2	1.0	51.01	1.0%	50.50	50.87	39.90	52.90
TIO2	1.0	1.62	-26.5%	2.21	1.74	0.00	0.00
AL2O	1.0	16.42	14.4%	14.36	17.12	0.00	6.90
FE2O	1.0	3.03	-18.4%	3.71	3.25	0.00	0.00
FEO	1.0	6.88	-32.8%	10.24	6.72	14.00	9.10
MNO	1.0	0.15	0.3%	0.15	0.16	0.00	0.00
MGO	1.0	8.14	37.5%	5.92	6.65	45.80	28.50
CAO	1.0	8.13	-16.6%	9.74	8.53	0.30	2.60
NA2O	1.0	3.33	32.8%	2.51	3.58	0.00	0.00
K2O	1.0	1.28	93.7%	0.66	1.38	0.00	0.00
			SOLUTIONS ARE		93.15%	0.00%	6.85%
			SENSITIVITY		1.11	1.00	1.77

Results of major element least-squares fits to a fractional crystallization model

Fractionation at 15-35 km (1250-1290°C)

Model 2c (see Table 20)

INPUT DATA ACCEPTED

OXIDE	WEIGHT	CRT	LCAR	ol
SIO2	1.0	50.30	50.20	40.30
TIO2	1.0	2.20	1.72	0.00
AL2O	1.0	14.30	16.90	0.00
FE2O	1.0	3.70	3.21	0.00
FEO	1.0	10.20	6.63	12.30
MNO	1.0	0.15	0.16	0.00
MGO	1.0	5.90	6.56	47.10
CAO	1.0	9.70	8.42	0.30
NA2O	1.0	2.50	3.53	0.00
K2O	1.0	0.66	1.36	0.00
TOTAL		99.61	98.69	100.00

SUM= 0.8106, SOLUTIONS= 0.78437 0.02622

CALCULATED DATA

OXIDE	WEIGHT	CALC	DIFF	CRT	LCAR	ol
SIO2	1.0	50.52	0.1%	50.50	50.87	40.30
TIO2	1.0	1.69	-23.6%	2.21	1.74	0.00
AL2O	1.0	16.57	15.4%	14.36	17.12	0.00
FE2O	1.0	3.15	-15.3%	3.71	3.25	0.00
FEO	1.0	6.90	-32.6%	10.24	6.72	12.30
MNO	1.0	0.16	4.2%	0.15	0.16	0.00
MGO	1.0	7.96	34.3%	5.92	6.65	47.10
CAO	1.0	8.27	-15.1%	9.74	8.53	0.30
NA2O	1.0	3.46	37.9%	2.51	3.58	0.00
K2O	1.0	1.33	101.3%	0.66	1.38	0.00
			SOLUTIONS ARE		96.77%	3.23%
			SENSITIVITY		0.70	1.51

Results of major element least-squares fits to a fractional crystallization model

Fractionation at 35-70 km:

Model 3a (see Table 20)

INPUT DATA ACCEPTED

OXIDE	WEIGHT	CRT	LCAR	opx
SIO2	1.0	50.30	50.20	53.40
TIO2	1.0	2.20	1.72	0.00
AL2O	1.0	14.30	16.90	7.30
FE2O	1.0	3.70	3.21	0.00
FEO	1.0	10.20	6.63	6.40
MNO	1.0	0.15	0.16	0.00
MGO	1.0	5.90	6.56	30.40
CAO	1.0	9.70	8.42	2.50
NA2O	1.0	2.50	3.53	0.00
K2O	1.0	0.66	1.36	0.00
TOTAL		99.61	98.69	100.00

SUM= 0.8237, SOLUTIONS= 0.77721 0.04652

CALCULATED DATA

OXIDE	WEIGHT	CALC	DIFF	CRT	LCAR	opx
SIO2	1.0	51.01	1.0%	50.50	50.87	53.40
TIO2	1.0	1.64	-25.5%	2.21	1.74	0.00
AL2O	1.0	16.57	15.4%	14.36	17.12	7.30
FE2O	1.0	3.07	-17.4%	3.71	3.25	0.00
FEO	1.0	6.70	-34.6%	10.24	6.72	6.40
MNO	1.0	0.15	1.6%	0.15	0.16	0.00
MGO	1.0	7.99	34.9%	5.92	6.65	30.40
CAO	1.0	8.19	-15.9%	9.74	8.53	2.50
NA2O	1.0	3.37	34.5%	2.51	3.58	0.00
K2O	1.0	1.30	96.2%	0.66	1.38	0.00
			SOLUTIONS ARE		94.35%	5.65%
			SENSITIVITY		1.14	1.98

Model 3b (see Table 20)

INPUT DATA ACCEPTED

OXIDE	WEIGHT	CRT	LCAR	opx	cpx
SIO2	1.0	50.30	50.20	53.40	49.30
TIO2	1.0	2.20	1.72	0.00	0.00
AL2O	1.0	14.30	16.90	7.30	11.30
FE2O	1.0	3.70	3.21	0.00	0.00
FEO	1.0	10.20	6.63	6.40	8.30
MNO	1.0	0.15	0.16	0.00	0.00
MGO	1.0	5.90	6.56	30.40	21.20
CAO	1.0	9.70	8.42	2.50	9.90
NA2O	1.0	2.50	3.53	0.00	0.00
K2O	1.0	0.66	1.36	0.00	0.00
TOTAL		99.61	98.69	100.00	100.00

SUM= 0.9249, SOLUTIONS= 0.70461 -0.34635 0.56659

HAVE PROHIBITED SOLUTIONS FOR : px

(1) REPEAT WITHOUT : px

SUM= 0.8523, SOLUTIONS= 0.74959 0.10276

CALCULATED DATA

OXIDE	WEIGHT	CALC	DIFF	CRT	LCAR	opx	cpx
SIO2	1.0	50.68	0.4%	50.50	50.87	53.40	49.30
TIO2	1.0	1.53	-30.6%	2.21	1.74	0.00	0.00
AL2O	1.0	16.42	14.4%	14.36	17.12	7.30	11.30
FE2O	1.0	2.86	-23.0%	3.71	3.25	0.00	0.00
FEO	1.0	6.91	-32.5%	10.24	6.72	6.40	8.30
MNO	1.0	0.14	-5.3%	0.15	0.16	0.00	0.00
MGO	1.0	8.40	41.8%	5.92	6.65	30.40	21.20
CAO	1.0	8.70	-10.7%	9.74	8.53	2.50	9.90
NA2O	1.0	3.15	25.3%	2.51	3.58	0.00	0.00
K2O	1.0	1.21	82.9%	0.66	1.38	0.00	0.00
			SOLUTIONS ARE		87.94%	0.00%	12.06%
			SENSITIVITY		0.88	1.91	1.25

Appendix G. Partial Melting Model

Compositions of proposed parent magmas

	PY[1]	SPER[2]	GPER[3]
SiO_2	45.16	44.20	46.60
TiO_2	0.71	0.13	0.09
Al_2O_3	3.54	2.05	1.77
Fe_2O_3	0.46	* 1.63	2.45
FeO	8.04	* 6.83	4.27
MnO	0.14	0.13	0.10
MgO	37.47	42.21	42.3
CaO	3.08	1.92	1.46
Na_2O	0.57	0.27	0.15
K_2O	0.13	0.06	0.13

	SPER[2]	SPER[4]	GLHZ[5]	ARCH[6]	UM[7]
Sr			49	19-26	30-60
Ba			120	∿7	10-20
Yb				0.33-0.51	
Sc				14-20	
Cr	2870	2400	5500	3000	
MnO	0.18	0.13	0.17	0.15	
Co			190	100	
Ni	2040	1900	2400	2000	
Cu			17		
Zr			14	10-13	

1. Pyrolite: Ringwood, 1975, p. 188.
2. Upper mantle spinel peridotite; Maaloe and Aoki, 1977.
3. Garnet peridotite: Carswell and Dawson, 1970.
4. Spinel peridotite: Ernst and Piccardo, 1979.
5. Fertile garnet lherzolite: Gurney, 1978.
6. Archaen mantle: Sun and Nesbitt, 1977.
7. Upper mantle: Gast, 1968.

Compositions of proposed residual minerals

	ol[3]	ol[4]	opx[4]	opx[10]	cpx[4]	cpx[4]	plag[8]	spin[4]	spin[9]	gar[3]	phlog[3]
SiO_2	40.8	39.40	54.53	55.0	49.73	50.17	58.1	0.03	NEG	42.0	41.0
TiO_2	0.00	NEG	0.26	0.12	0.55	0.37	*0.00	0.70	NEG	0.23	0.82
Al_2O_3	0.00	NEG	3.29	2.69	6.60	5.28	2.64	27.98	57.7	21.5	17.3
Fe_2O_3	0.00	NEG	NEG	1.81	NEG	NEG	0.00	5.25	NEG	1.23	0.43
FeO	5.72	9.73	6.23	7.18	3.47	3.14	0.00	18.3	8.54	5.67	2.38
MnO	0.04	0.14	0.16	0.19	0.13	0.13	0.00	0.30	.10	0.34	0.00
MgO	53.3	49.96	32.08	32.1	16.11	16.75	0.00	11.5	2.38	21.5	23.0
CaO	0.16	0.04	2.94	0.48	21.94	21.08	7.80	NEG	NEG	4.18	0.00
Na_2O	0.00	NEG	0.03	0.02	0.21	0.36	6.50	NEG	NEG	0.00	0.16
K_2O	0.00	NEG	NEG	0.01	NEG	NEG	1.10	NEG	NEG	0.00	9.80
Cr_2O_3			0.84		NEG	1.21		35.19			

1. Pyrolite: Ringwood, 1975, p. 188.
2. Upper mantle spinel peridotite: Maaloe and Aoki, 1977.
3. Garnet peridotite: Carswell and Dawson, 1970.
4. Spinel peridotite: Ernst and Piccardo, 1979.
5. Fertile garnet lherzolite: Gurney, 1978.
6. Archean mantle: Sun and Nesbitt, 1977.
7. Upper mantle: Gast, 1968.
8. Deer and others, 1966, p. 324.
9. Deer and others, 1963, v. 5, p. 65.
10. Deer and others, 1963, v. 2, p. 17.

ol = olivine
opx = orthopyroxene
cpx = clinopyroxene
plag = plagioclase
spin = spinel
gar = garnet
phlog = phlogopite

* Calculated from FeO_T

NEG = negligible

Major oxides given in weight percent; trace elements given in ppm.

Proposed modal compositions

	PY[1]	PPER[1]	SPER-A[2]	SPER-B[3]	SPER-C[3]	GPER-A[4]	GPER-B[1]
ol	60	51	66.70	65	35	62.6	57
opx	25	17	23.74	20	40	30	17
cpx	15	17	7.83	10	20	2	12
spin			1.73	5	5		
plag		15				5	14
gar						0.4	
phlog							

Proposed eutectic compositions

	PY[1]	PPER[1]	SPER-A[1]	SPER-B[3]	SPER-C[3]	GPER-A[5]	GPER-B[1]
ol	25	11	25	25	25	3	3
opx	20	11	20	25	25	3	3
cpx	55	28	55	50	50	42	47
spin							
plag		50				42	47
gar						10	
phlog							

PY = pyrolite
PPER = plagioclase peridotite
SPER = spinel peridotite
GPER = garnet peridotite

1. Schilling (1975)
2. Maaloe and Aoki (1977)
3. Gast (1968)
4. Carswell and Dawson (1970)
5. White and Schilling (1978)

Results of major element least-squares fit to a partial melting model

Major element data are consistent with the hypothesis that upper mantle mantle spinel peridotite (composition of Maaloe and Aoki, 1977; see Appendix G-1) can be generated by ∿ 70% melting of garnet peridotite (composition of Carswell and Dawson, 1970; see Appendix G-1). At this degree of melting, olivine and orthopyroxene are residual minerals, based on the eutectic melting proportions given in Appendix G-3).

INPUT DATA ACCEPTED

OXIDE	WEIGHT	GPEP			
SIO2	1.0	46.60	44.20	40.80	55.00
TIO2	1.0	0.09	0.13	0.00	0.12
AL2O	1.0	1.77	2.05	0.00	2.69
FEO	1.0	6.72	8.29	5.72	8.99
MNO	1.0	0.10	0.13	0.04	0.19
MGO	1.0	42.30	42.20	53.30	32.10
CAO	1.0	1.46	1.92	0.16	0.48
NA2O	1.0	0.15	0.27	0.00	0.02
K2O	1.0	0.13	0.06	0.00	0.01
TOTAL		99.32	99.25	100.02	99.60

SUM= 0.9492, SOLUTIONS= 0.66216 0.21329 0.07379

CALCULATED DATA

OXIDE	WEIGHT	CALC	DIFF	GPEP			
SIO2	1.0	44.52	-5.1%	46.92	44.53	40.79	55.22
TIO2	1.0	0.10	11.2%	0.09	0.13	0.00	0.12
AL2O	1.0	1.65	-7.4%	1.78	2.07	0.00	2.70
FEO	1.0	7.81	15.5%	6.77	8.35	5.72	9.03
MNO	1.0	0.12	14.4%	0.10	0.13	0.04	0.19
MGO	1.0	44.14	3.6%	42.59	42.52	53.29	32.23
CAO	1.0	1.42	-3.2%	1.47	1.93	0.16	0.48
NA2O	1.0	0.19	26.7%	0.15	0.27	0.00	0.02
K2O	1.0	0.04	-67.2%	0.13	0.06	0.00	0.01

SOLUTIONS ARE 69.76% 22.47% 7.77%

SENSITIVITY -0.26 0.27 -1.05